Experimental Study of a Façade-integrated Photovoltaic/thermal System with Unglazed Transpired Collector

James Bambara

A Thesis
in
The Department
of
Building, Civil and Environmental Engineering

Presented in Partial Fulfillment of the Requirements
for the Degree of Master of Applied Science (Building Engineering) at
Concordia University
Montreal, Quebec, Canada

August 2012

CONCORDIA UNIVERSITY
School of Graduate Studies

This is to certify that the thesis prepared

By: James Bambara

Entitled: Experimental Study of a Façade-integrated Photovoltaic/thermal System with Unglazed Transpired Collector

and submitted in partial fulfillment of the requirements for the degree of

Master of Applied Science (Building Engineering)

complies with the regulations of the University and meets the accepted standards with respect to originality and quality.

Signed by the final examining committee:

Dr. Radu Zmeureanu Chair

Dr. Pragasen Pillay Examiner

Dr. Liangzhu Wang Examiner

Dr. Andreas Athienitis Supervisor

Approved by _____
Chair of Department or Graduate Program Director

_____
Dean of Faculty

Date August 17, 2012

ABSTRACT

Experimental Study of a Façade-integrated Photovoltaic/thermal System
with Unglazed Transpired Collector

James Bambara

Building façades and roofs receive significant amounts of solar radiation that can be used to generate useful renewable energy onsite. Photovoltaic (PV) technology may be integrated into well-oriented building surfaces to convert up to 20% of incident solar energy into electricity. However, most of the solar energy not converted into electricity is turned into heat, which must be appropriately vented to the exterior to avoid overheating and reduced PV lifetime or delamination. Building-integrated photovoltaic/thermal (BIPV/T) systems recover the useful excess heat from the PV modules for use within the building, in addition to generating electricity. As the exterior cladding is replaced by the BIPV/T façade, costs associated with traditional building materials can be avoided through architectural integration.

This thesis presents an experimental study of a BIPV/T system made by mounting custom-designed PV modules over an unglazed transpired collector. Experimental testing of the prototype was performed in an outdoor testing facility at Concordia University and in a solar simulator - environmental chamber laboratory. The BIPV/T concept was applied to the façade (288 m²) of an institutional building in Montreal (45°N). Measured combined efficiency (thermal plus electrical) on the order of 50% shows the potential for BIPV/T technology to reduce the energy needs of the built environment while providing a durable building skin. Design correlations developed for predicting the performance of the BIPV/T system may be used for the design of similar systems in new buildings or for retrofit applications.

ACKNOWLEDGEMENTS

Thanks to my supervisor, Dr. Andreas Athienitis, for giving me the opportunity to work on this interesting project. I would like to acknowledge Dr. Panagiota Karava for providing me with the chance to study at Purdue University on a research exchange. In addition, I would like to thank Dr. Paul Fazio and Dr. Radu Zmeureanu for their kind advice, and all the other great people in the BCEE department. The scholarships awarded by Concordia University and the Natural Sciences and Engineering Research Council (NSERC) of Canada were very much appreciated and motivating.

In all the three research projects undertaken, there were many people and organisations involved at different stages. In particular, the researchers involved in the project would like to acknowledge the financial support of Natural Resources Canada, through its CanmetENERGY Laboratory, and the NSERC of Canada, through the Solar Buildings Research Network. Josef Ayoub of CanmetENERGY was instrumental in bringing together the partners for the demonstration project. The project engineer, Brendan O'Neill, and the Concordia facilities management did excellent work. Thanks to Lyne Dee, Meli Stylianou, Jacques Payer, Luc Demers, Jiwu Rao, Joe Hrib and Jaime Yeargans for their assistance with the projects. Last but not least, I would like to acknowledge the help of my co-researchers Costas Kapsis, Luis and Jose Candanedo, YiChao Chen, Ting Ting Yang, Diane Bastien, Johnathan Faille, Sam Sadighi, Scott Bucking, Niesz Koziol and Neetha Vasan as well as numerous others who also contributed to the experiments and data analysis.

I am also very grateful for my supportive family and friends!

CONTENTS

LIST OF FIGURES

LIST OF TABLES

NOMENCLATURE

AC	Alternating Current
BIPV	Building Integrated Photovoltaic
BIPV/T	Building Integrated Photovoltaic/Thermal
COP	Heat pump Coefficient of Performance
DC	Direct Current
EN	European Standard
HVAC	Heating, Ventilating, and Air Conditioning
ISO	International Organization for Standardization
JMSB	John Molson School of Business building
MHG	Metal Halide Global
MSDM	Monitored Site Data Manager
NOC	Normal Operating Conditions
NSERC	National Science and Engineering Research Council of Canada
PV	Photovoltaic
PV/T	Photovoltaic/Thermal
SBRN	Solar Buildings Research Network
SSEC	Solar Simulator - Environmental Chamber
STC	Standard Testing Conditions
USD	United States Dollar
UTC	Unglazed Transpired Collector
$A_{collector}$	Total surface area of the solar collector (m^2)
A_{PV}	Total surface area of PV (m^2)
c_{air_avg}	Specific heat of air (J/kg·ºC)
c_{fluid}	Specific heat of collector fluid (J/kg·ºC)

E_{PV}	Electrical power produced by PV (W)
E_{PV_theo}	Theoretical electrical power produced by PV (W)
I_{PV}	Electrical current through the PV (A)
I_{solar}	Incident solar irradiance (W/m²)
m_{air}	Air collection rate per unit area of collector (kg/hr·m²)
$m_{collector}$	Total air collection rate through the collector (kg/s)
m_{fluid}	Total mass flow rate of fluid through the collector (kg/s)
$Q_{thermal}$	Thermal energy absorbed in the collector fluid (W)
$T_{exterior}$	Temperature of exterior air (ºC)
T_{inlet}	Temperature of fluid at the collector inlet (ºC)
T_{outlet}	Temperature of fluid at the collector outlet (ºC)
$T_{outlet\_high\_wind}$	Temperature of air at the BIPV/T collector outlet for high winds (ºC)
$T_{outlet\_low\_wind}$	Temperature of air at the BIPV/T collector outlet for low winds (ºC)
$T_{PV\_high\_wind}$	Temperature of the PV on the BIPV/T collector for high winds (ºC)
$T_{PV\_low\_wind}$	Temperature of the PV on the BIPV/T collector for low winds (ºC)
T_{stc}	PV surface temperature under standard testing conditions (ºC)
$V_{airport}$	Wind speed measured at Montreal international airport (m/s)
$V_{anemometer}$	Wind speed at the anemometer height (m/s)
$V_{gradient}$	Wind speed at the atmospheric gradient height (m/s)
V_{PV}	Electrical voltage across the PV (V)
$Z_{airport}$	Height above ground for airport wind speed measurement (m)
$Z_{anemometer}$	Height above ground for anemometer wind speed measurement (m)
$Z_{gradient}$	Atmospheric gradient height (m)
α_{city}	Exponential coefficient for the city of Montreal
α_{flat_open}	Exponential coefficient for neutral air around flat open terrain

β_{PV}	PV module temperature coefficient (%/ºC)
$\eta_{BIPV/T}$	Combined efficiency (thermal plus electrical) of the BIPV/T collector (%)
$\eta_{PV/T}$	Combined efficiency (thermal plus electrical) of the BIPV/T collector (%)
$\eta_{thermal}$	Thermal efficiency of the solar collector (%)
$\eta_{thermal\_adjusted}$	Adjusted thermal efficiency of the BIPV/T collector (%)
$\eta_{thermal\_equivalent}$	Thermal equivalent efficiency of the PV/T collector (%)
η_{PV}	PV electrical efficiency (%)
η_{PV_theo}	Theoretical PV electrical efficiency (%)
η_{stc}	PV electrical efficiency under standard testing conditions (%)

1. INTRODUCTION

In Canada, buildings account for about 30% of energy consumption and about 50% of electricity consumption (NRCan-OEE, 2012). The emissions related to obtaining and consuming this energy are increasingly posing environmental and health concerns. At least half of the energy consumed by buildings is used for space heating, and nearly 10% for domestic hot water heating (Figure 1.1). Therefore, a small improvement in this sector could help reduce building energy consumption and its associated emissions. The oil crisis of the 1970s provided an impetus for much of the research and development in energy efficiency and renewable energy research performed thereafter and, as a result, buildings have improved their energy profile considerably in Canada. Government programs, such as R2000 for homes and the commercial buildings incentive program, which advocate and promote higher performance than the National Energy Building Code, have had a major positive impact on the design and construction of new buildings. However, population growth, economic development, and a rising standard of living have led to ever-increasing energy consumption, with resultant increases in emissions.

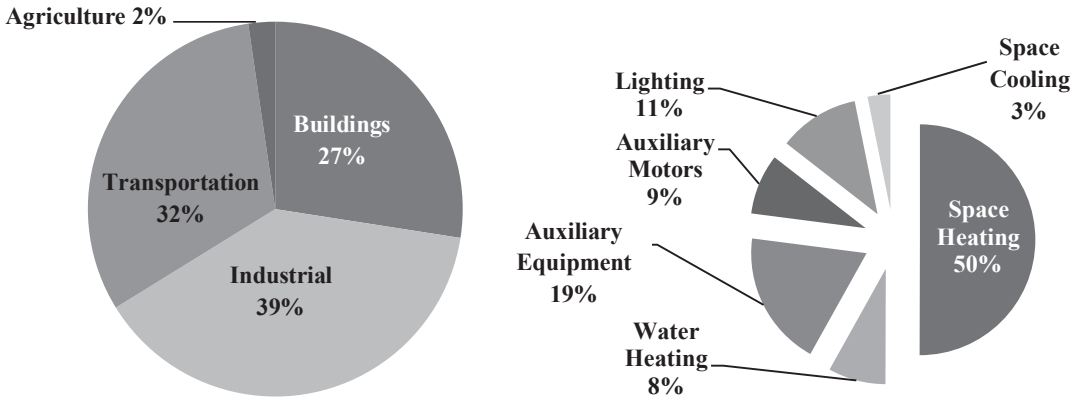

Figure 1.1: Secondary energy use, by sector, in Canada, 2009 (left). Percentage of energy consumption, by end use, for the institutional and commercial building sectors in Canada, 2009. (NRCan-OEE, 2012)

The sun is an abundant source of clean, renewable energy. In the urban environment, significant solar energy is received by well-oriented building façades and roofs. In mid-latitudes, the low winter sun provides peak annual irradiation to vertical façades, providing more energy when it is needed most. This incident solar energy can be converted into heat (solar thermal collector), electricity (photovoltaic system), or both (photovoltaic/thermal system). Solar thermal collectors transfer the absorbed solar heat to a working fluid, such as water or air. A well-known, highly efficient collector is the open-loop unglazed transpired collector (UTC), which consists of dark, porous cladding through which outdoor air is drawn and heated by absorbed solar radiation. This low-cost solar collector is capable of converting up to 70% of incident solar radiation into useful energy by pre-heated ambient exterior air by up to 40°C. The perforated cladding sheets can be installed in lieu of conventional cladding at little or no additional cost, while providing large amounts of renewable heat (Figure 1.2).

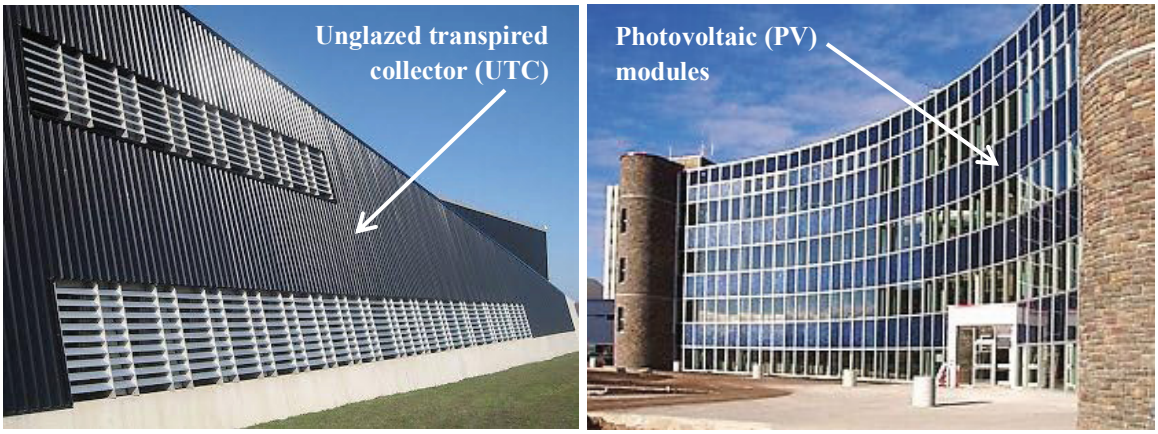

Figure 1.2: Building-integrated unglazed transpired solar collector in Canada (left) (SolarWall, 2012). Building-integrated photovoltaic system in Canada (right) (Visionwall, 2012).

The discovery of the photovoltaic (PV) effect allows for the conversion of direct sunlight into electricity, a more valuable type of energy compared to heat. Commercially available PV systems typically produce electricity with efficiencies up to about 20%. The portion of incident solar irradiance not converted to electricity (typically around 80%) is mainly converted into heat, increasing the photovoltaic surface temperature and lowering its efficiency. Properly designed PV systems usually have provisions to allow natural air circulation to cool the PV surface and avoid possible structural damage. As the efficiency of solar cell technology increases and the cost of PV technology decreases, a growing number of successful projects around the world demonstrate that conventional building cladding and roofing can be effectively replaced with electricity-generating PV materials. However, issues of overheating, low efficiency-to-cost ratios, and limited availability of building surface area create the need for innovative and more efficient building-integrated PV designs.

Building-integrated photovoltaic/thermal (BIPV/T) systems recover useful excess heat from the PV modules for use within the building, in addition to generating electricity. The resulting improved system benefits from both thermal and electrical energy production, which can yield a combined efficiency of up to about 70%. The heat may be used within the building for space heating, fed into an air source heat pump to preheat domestic hot water, and/or provide cooling using desiccants. Many different techniques have been developed to optimize the extraction of heat from the PV modules, and improvement continues as research brings new, more efficient and cost-effective solutions that can be readily integrated into the built environment.

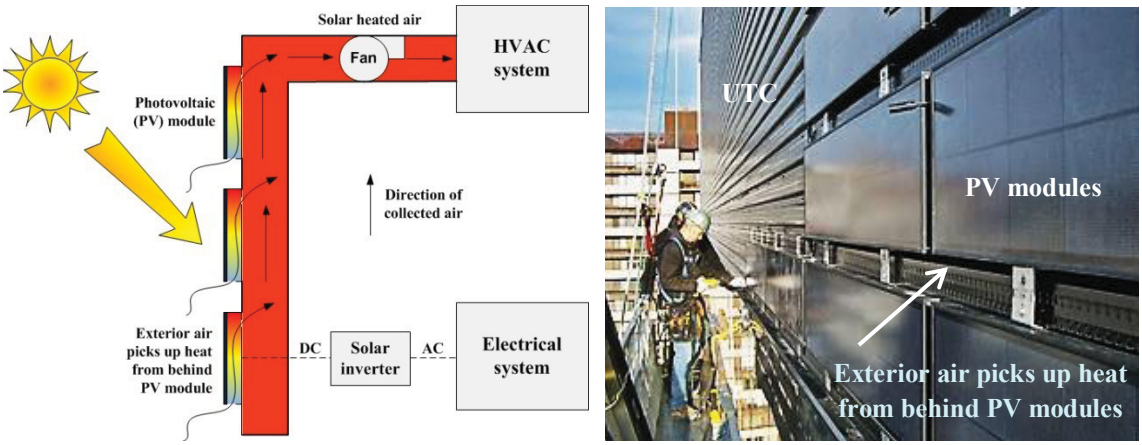

Figure 1.3: Schematic of a BIPV/T system (left). A BIPV/T system being installed at Concordia University (right).

The idea of replacing conventional building cladding with a BIPV/T system to provide electricity and heat is an area that, until recently, has received only limited attention. Although BIPV/T systems are not as prevalent as solar thermal collectors, the integration of PV and solar thermal collectors into the building envelope could provide a greater opportunity for the production of renewable solar energy onsite. The effective building integration of solar electric and thermal technologies is a hallmark of the approach to be undertaken. Innovative companies have made major strides in the production of PV modules for the roofs and façades of buildings, but there has been little work, in Canada or elsewhere, on the integration of PV/T systems into the heating, ventilation, and air conditioning (HVAC) systems of buildings. In doing this work, the local climate, the available solar energy, the existing energy infrastructure, and the existing building infrastructure need to be considered, as they all have profound effects on the system. Moreover, the potential energy savings from integrated and optimized solar technologies are significantly higher than the energy savings obtained from

applying the technologies separately. Retrofit applications are also possible, with a new active façade constructed over an existing one that may need to be renovated.

The present research aims to reduce the footprint of the built environment by turning static building skins into dynamic energy conversion systems. In 2005, the Natural Sciences and Engineering Research Council (NSERC) approved the creation of the Solar Buildings Research Network (SBRN). The SBRN's long-term goal was the development of the optimized solar building as an integrated, cost-effective technological system that approaches, under Canadian climatic conditions, net-zero annual total energy consumption. One of the major tasks was to develop a BIPV/T system that maximizes solar energy conversion and can easily be integrated onto well-oriented building façades. The SBRN's design team developed a novel BIPV/T system using custom-designed PV modules installed over UTC, with a suitable mounting system. Heat is collected as exterior air is drawn behind the PV modules and into the air cavity, resulting in cooler PV temperatures and maintained electrical efficiency (Figure 1.3). The main objective of this thesis is to investigate the performance of a BIPV/T system with UTC and its integration with the building's envelope and energy systems. The main steps undertaken for this research project and the contributions of the author are:

- Overview of the existing literature and technology (Chapter 2).
- Presentation of the design concept for a BIPV/T system with UTC developed by the NSERC SBRN design team (Chapter 3).
- Experimental testing of the prototype BIPV/T system in an outdoor research facility. The work of the author consists mainly of modifying and instrumenting

the experimental façade for testing of the prototype BIPV/T system. The BIPV/T system's performance was compared using two PV module configurations. Experimental data that was collected and analyzed is presented in Chapter 4.

- The developed BIPV/T design concept was applied to a Concordia building as a demonstration project. Measurements and analysis, using data from a full-scale system is presented in Chapter 5. During this BIPV/T research project, various participants were involved during the different stages. The author was involved particularly at the early stages of commissioning during the start-up of the system to ensure proper operation of all the BIPV/T data acquisition devices and the implementation of a database for the remote access of the measured data and public display. Large amounts of data have been collected since the construction of the demonstration project, and significant work has been done as part of this thesis to structure and organize the data into usable forms, in support of this thesis as well as the work of future researchers.

- Experimental testing of the BIPV/T system under controlled conditions in a new solar simulator - environmental chamber (SSEC) laboratory is covered in Chapter 6. The author participated in the commissioning of the new research laboratory and the instrumentation and setup of data acquisition devices for the analysis of the experimental data. Design correlations were developed to predict the performance of similar systems under low and high wind conditions. These correlations can aid the design of similar systems.

- Conclusion and recommendations for future work (Chapter 7).

2. LITERATURE AND TECHNOLOGY REVIEW

Renewable energy generation using radiation from the sun is most often carried out in two forms: thermal collection, for heating a fluid such as air or water, and electric generation, using the photovoltaic effect. Photovoltaic/thermal (PV/T) systems combine both thermal and electrical energy production from the same solar collector and benefit from a higher overall efficiency than both systems applied separately. Building integration of solar collector technology can be carried out during the early design stages to replace the need for conventional cladding. Fully integrated façade or roof systems provide the same protective features as conventional building skins (thermal insulation and moisture, wind, and water protection), while generating significant renewable energy throughout their service lives as part of the building.

2.1 Flat Plate Solar Thermal Collectors

2.1.1 Overview

A solar thermal collector is, essentially, a heat exchanger that transforms solar radiation into heat. Stationary solar collectors (without a tracking devices) are common for low and medium temperature (less than 100ºC) applications, whereas concentrating collectors with tracking systems are more often used for applications at medium to high temperatures (250–2500ºC). Flat-plate solar collectors provide appropriate temperatures for building applications, and they can be integrated into the roof and/or facade, where they can convert solar radiation (up to 1200 W/m²) into heat at efficiencies of nearly 80%. They use both direct beam and diffuse solar radiation (incident solar irradiance) to heat a working fluid, such as air or water, which is useful for various heating and cooling

applications. In a steady state, the performance of flat-plate thermal solar collectors is described by an energy balance that indicates the distribution of incident solar irradiance into useful energy gained by the fluid, thermal losses to the local environment, as well as optical losses, such as reflection from the collector's glass cover (Figure 2.1). The thermal energy lost to the surrounding environment includes conduction, convection, and infrared radiation (Duffie and Beckman, 2006).

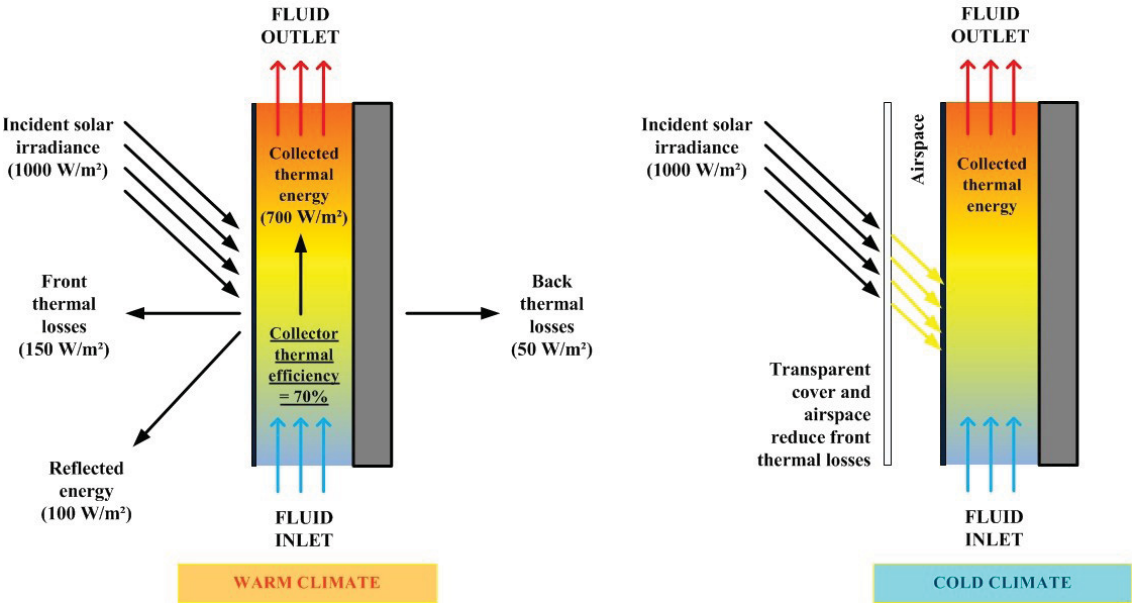

Figure 2.1: Schematics of the simplified energy balance of unglazed (left) and glazed (right) solar thermal collectors.

Flat-plate thermal collectors are available in either glazed or unglazed configurations (Figure 2.1). In unglazed solar collectors, a portion of radiant energy incident on a solar collector is typically either reflected or absorbed. Several advanced dark-coloured coatings have been developed to maximize the absorption of solar energy and minimize radiant losses. Glazed solar collectors have a transparent cover (typically low-iron glass or weather-resistant plastic sheet) placed in front of the absorber surface, with an airspace in between. The stagnant air inside the cavity reduces thermal losses at

the front and is beneficial in colder climates. However, the additional glazing increases the system's overall cost, and optical losses associated with the cover reduce the solar energy that is received by the absorber surface.

Various experiments have been conducted to evaluate the performance of solar thermal collectors. Thermal efficiency is defined as the portion of incident solar irradiance that is picked up as heat by a circulating fluid inside the solar collector. Most commercially available collectors undergo standard experimental testing to determine their thermal efficiency, such as the certification of performance and reliability defined by European standard EN 12975. The major unknown is the fluid's outlet temperature, T_{outlet} in ºC, which is experimentally measured and used to calculate the amount of solar heat, $Q_{thermal}$ in W, that is transferred to the moving fluid using

$$Q_{thermal} = m_{fluid} \cdot c_{fluid} \left(T_{outlet} - T_{inlet} \right) \tag{1}$$

where

m_{fluid}, in kg/s, is the mass flow rate of the collector fluid.
c_{fluid}, in J/kg·ºC, is specific heat of the collector fluid (1005 J/kg·ºC for air, 4120 J/kg·ºC for water).
T_{outlet}, in ºC, is the solar collector's fluid outlet temperature.
T_{inlet}, in ºC, is the solar collector's fluid inlet temperature.

The thermal efficiency of the solar thermal collector, $\eta_{thermal}$ in %, can then be determined

$$\eta_{thermal} = 100 \cdot \left[\frac{Q_{thermal}}{A_{collector} \cdot I_{solar}} \right] \tag{2}$$

where

$Q_{thermal}$, in W, is the thermal energy absorbed by the moving fluid.
$A_{collector}$, in m², is the total surface area of the solar collector.
I_{solar}, in W/m², is the incident solar irradiance on the solar collector.

A thermal model of a solar collector allows the designer to predict the performance of the system before it is built. The following equation is derived from a simplified energy balance. It can be used to calculate a solar thermal collector's fluid outlet temperature, knowing (or assuming) the collector's thermal efficiency, $\eta_{thermal}$ in %; the incident solar irradiance, I_{solar} in W/m²; and the fluid's inlet temperature, T_{inlet}, in ºC; as well as mass flow rate, m_{fluid} in kg/s, and specific heat, c_{fluid} in J/kg·ºC.

$$T_{outlet} = T_{inlet} + \frac{\eta_{thermal} \cdot A_{collector} \cdot I_{solar}}{100 \cdot m_{fluid} \cdot c_{fluid}} \tag{3}$$

Flat-plate thermal solar collectors transfer thermal energy to the working fluid, which is generally air, water or an antifreeze mixture. As the fluid is heated, the convective and radiative losses increase, and the amount of energy that can be effectively collected from the absorber surface diminishes. Therefore, for efficient heat transfer to occur, it is desirable to maintain the largest temperature differential between absorber surface and circulating fluid temperature. The working principle of a flat-plate solar thermal collector is similar for both liquid and solar air collectors. However, solar air collectors have some advantages over liquid collectors (Tiwari and Ghosal, 2005):

- The use of air as the heat transfer fluid avoids the need for special heat transfer fluids (oil or glycol) able to withstand freezing conditions.
- Corrosion and leakage through joints and ducts is less of a concern.
- High-pressure protection is not required.
- The device is more compact and lightweight, less complicated, and easy to install.

Nonetheless, the solar thermal air heater has some shortcomings relative to flat-plate liquid collectors. In particular, the heat transfer rate is relatively slow, due to lower thermal conductivity of air, and a greater volume of air per unit collector area is required to store the thermal energy, due to the lower specific heat capacity of air.

Most liquid solar collectors operate in a closed-loop configuration, where the fluid is recirculated from the collector to the heat delivery location within the building. Air solar collectors work with either closed-loop or open-loop configurations (Figure 2.2). Open-loop collectors continuously draw fresh exterior air through the collector, where it is preheated and used to provide thermal energy for one or more functions in the building before being exhausted to the exterior. This simple collector avoids the need for recirculating ducting and is a particularly suitable method for preheating ventilation air where all of the absorbed heat is useful. Because the inlet temperatures of open-loop collectors are lower than those of closed-loop systems, they normally operate with higher thermal efficiency, although lower outlet air temperatures are typically achieved.

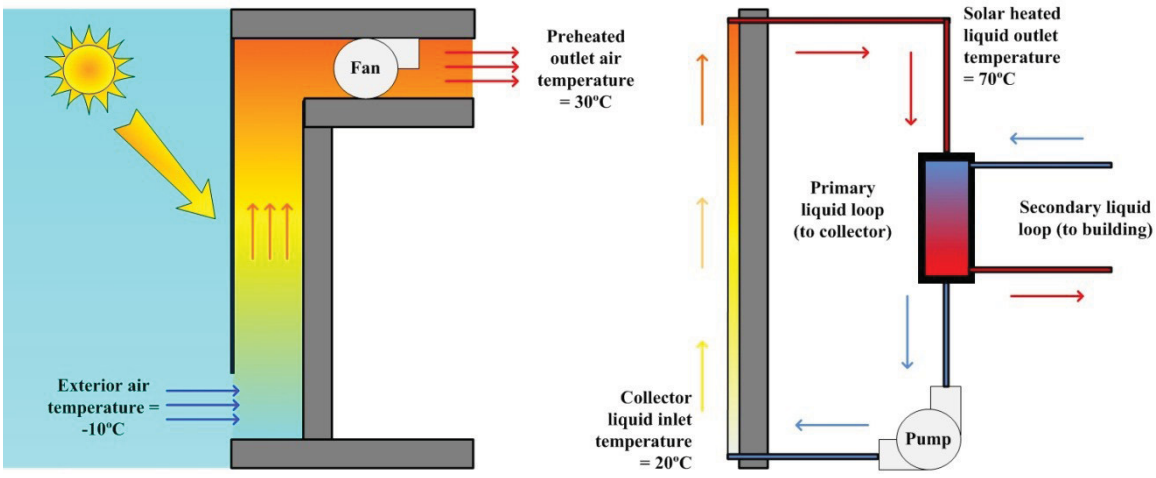

Figure 2.2: Schematics of two types of flat-plate solar collectors**:** open-loop solar air collector (left) and closed-loop solar liquid collector (right).

Typically, solar thermal air collectors operate by moving fluid from a dedicated single inlet, where the ambient air enters and travels through an air cavity to the outlet, where the heated air is collected. This configuration can allow the air temperature to rise nearly as high as the absorber surface temperature (the theoretical upper limit). However, as the air temperature rises, heat loss to the surroundings increases, which negatively affects thermal efficiency, especially in cold climates. The concept of distributed inlets is an alternative to the single-inlet approach, where air enters the air cavity through small holes perforated over the entire collector area. The perforated cladding may be either opaque or transparent (Figure 2.3). Unglazed transpired collectors absorb solar energy on the dark perforated sheets. When the air collection fan is activated, negative pressure is created inside the air cavity, and the colder outside air picks up heat as it is drawn through each perforation of the porous cladding (SolarWall, 2012). Transparent transpired collectors differ from unglazed transpired collectors in that they allow solar radiation to be transmitted inside the air cavity, where it is absorbed by the dark-coloured inner cavity surface and then transferred as heat to the circulating air (Enerconcept, 2012). These two types of distributed air inlet collectors can provide high-efficiency (up to 80%) preheated air collection and may be easily integrated as part of a new building façade or for recladding existing infrastructure.

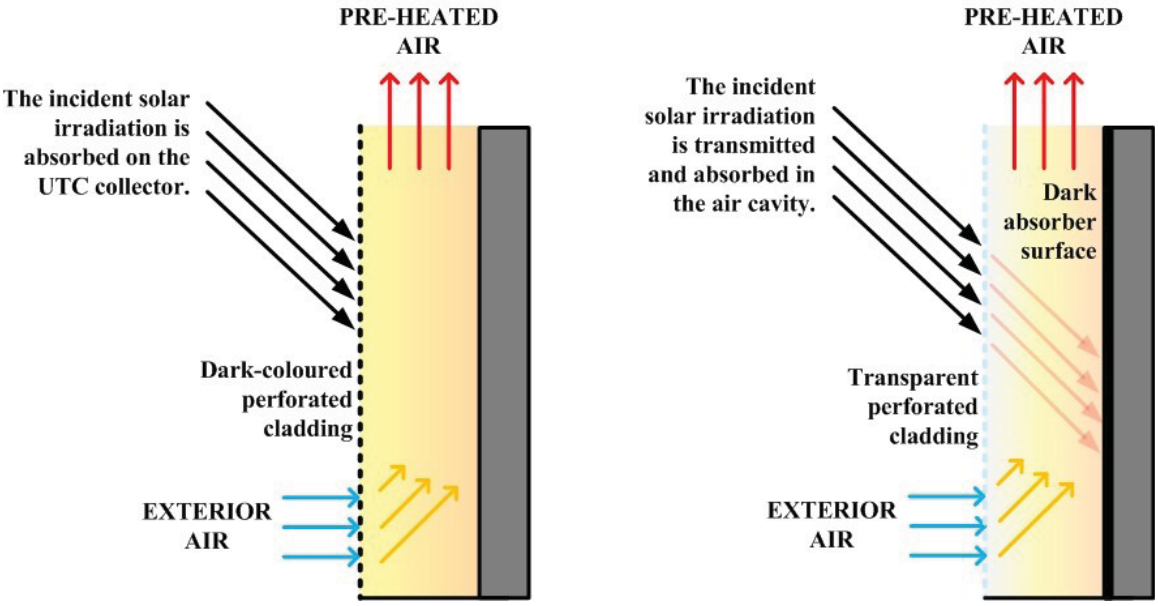

Figure 2.3: Schematics of two types of distributed inlet solar air collectors: unglazed transpired collector (left) and transparent transpired collector (right).

High-performance, solar-optimized buildings should be well insulated, airtight, and have highly efficient windows and heat recovery systems. The heat captured by solar heating systems can cover a significant part of the thermal energy demand of high-performance buildings. The main uses for the heat include space and/or domestic hot water heating (Probst and Roecker, 2007) and air conditioning using desiccants (Pesaran and Wipke, 1992). Because the space heating demand of solar-optimized, energy-efficient buildings is low, the year-round energy demand for domestic hot water becomes relatively important. Solar thermal collectors can be used to cover a large part of this energy demand, often more than 50%, as the demand also occurs in summer (Gajbert, 2008).

2.1.2 Building-integrated solar thermal collectors

Architectural integration is a major issue in the development and spread of solar thermal technologies. Flat-plate collectors can be integrated as a construction element into the building envelope to replace the need for conventional façade and roof materials. When properly integrated from the start, the collector becomes an active energy component whose cost can be similar to that of low-to-medium-end exterior claddings, such as metal sheet and face brick. Currently, the architectural quality of most existing building-integrated solar thermal systems is generally quite poor, which often discourages potential new users. To master all characteristics of the system simultaneously, from the perspectives of both energy production and building design, is not an easy task, especially with the presently available solar collector systems. For new buildings, it is preferable to integrate the collector as much as possible as part of the building skin, in order to save building materials and reduce the labour costs of mounting the collectors. As attractive collector designs continue to emerge, the market for building integrated solar collectors is on the increase, mainly in countries such as Germany and Austria, where proper incentives have advanced the development of energy-generating building envelopes (Gajbert, 2008).

Probst and Roecker (2007) studied the results of a large web survey on architectural integration quality, addressed to more than 170 European architects and other building professionals. The best rating was given to the balcony integration presented in Figure 2.4, where the solar thermal water collector modules occupy the entire spandrel section (the lower portion) of the curtain wall. A clever overhang reflects sunlight onto the façade-integrated solar collectors, increasing their energy output while

protecting the interior space below from overheating during the summer months. For proper integration, the size and shape of the collector modules must be selected to be an integral part of the building. The integration of unglazed transpired collector into a hangar in Canada (Figure 2.4) is considered to be the second best integration. The unglazed system works as both a solar collector and façade cladding.

Regardless of the integration level, the durability of the collector should preferably be as high as that of the rest of the building envelope. In addition, it is important to keep the maintenance requirements as low as possible, in order for the collectors to be attractive to customers. Parts of the collector must be easily replaceable.

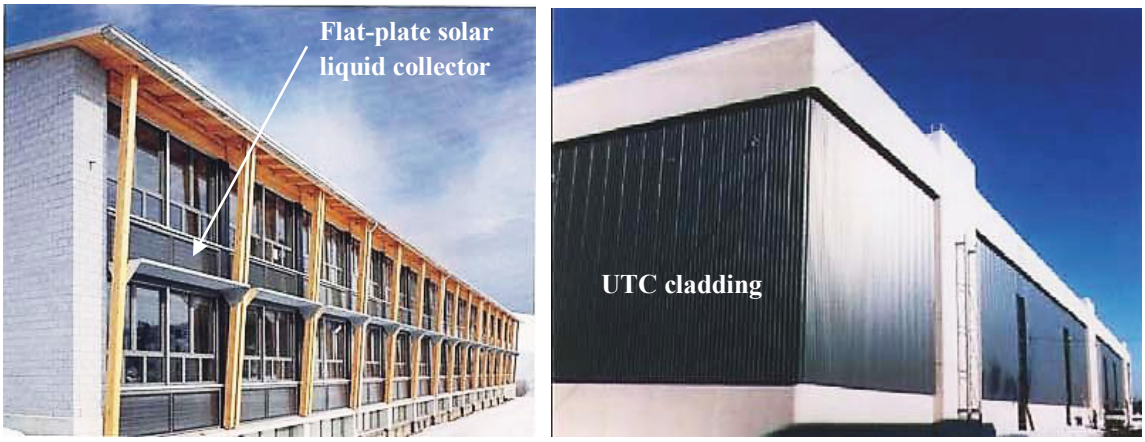

Figure 2.4: Building-integrated, flat-plate solar liquid collector in Sweden (left). Building-integrated solar air collector in Canada (right). (Probst and Roecker, 2007)

Further research, development, and demonstration investment can help to further drive down the cost of solar thermal technology. Cost reductions are expected to stem from the following: direct building integration (façade and roof) of collectors; improved manufacturing processes; and new advanced materials, such as polymers, for collectors (ESTTP, 2008).

2.1.3 Unglazed transpired collector

Unglazed transpired collectors (UTC) are a well-known, highly efficient type of open-loop solar air collector, consisting of dark, porous cladding, through which outdoor air is drawn and heated by absorbed solar radiation. The schematic in Figure 2.5 shows the typical operation of a UTC system, where a fan is used to draw air through small perforations, which generally cover 0.5–2% of the collector (Dymond and Kutscher, 1997). The air that passes through each perforation picks up heat from the dark exterior surface, which is heated by the sun. The characteristics responsible for the high efficiency of UTCs include:

1. High solar absorptance of the dark-coloured collector.

2. Closely spaced perforations that rapidly draw heat from the UTC surface into the air cavity, thereby reducing convective losses, especially at higher air collection rates.

3. Rapid heat removal that lowers the surface temperature and reduces radiative losses.

4. Low exterior air temperature compared to the surface of the UTC, creating an optimal gradient for heat exchange.

Figure 2.5: Schematic of UTC operation (left). UTC corrugated sheets installed as a retrofit over existing cladding (right) (Iron Workers, 2012)**.**

Since the technology was first introduced in the early 1990s (Hollick, 1994), there has been a substantial effort in the research and development of this technology by Conserval Engineering, as well as other research institutes. As a result, Conserval Engineering has produced an UTC, marketed as SolarWall® (Figure 2.6). The SolarWall® UTC system is made from perforating small holes in corrugated galvanized steel sheathing. The UTC sheets can be installed vertically or horizontally as a low-cost substitute for conventional façade cladding. The sheets are installed several inches from an appropriate wall, creating an air cavity.

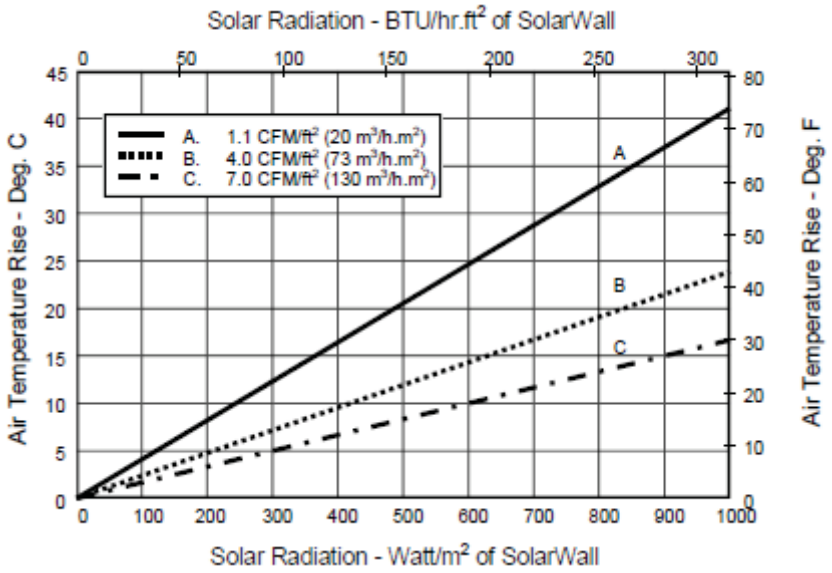

Figure 2.6: Performance of commercially available UTC (SolarWall, 2012).

Heat transfer in a UTC has been modelled assuming uniform air collection by Kutscher *et al.* (1993), who developed a thermal model to predict UTC performance. The study concludes that heat losses due to natural convection are negligible, and that those due to wind should be small for large collectors operated at typical air collection rates. Dymond and Kutscher (1997) also developed an airflow distribution and design model for a UTC. Van Decker *et al.* (2001) developed correlations for the effectiveness of different UTC plates for a number of geometrical patterns of the pores and different porosities and air collection rates. The effectiveness is separated into three parts: heat transfer from the front of the plate, in the hole, and at the back of the plate. A mathematical model was developed by Augustus Leon and Kumar (2007) to predict the thermal performance of UTCs over a wide range of design and operating conditions. The study concludes that solar absorptivity, collector pitch, and air collection rate have the strongest effects on UTC thermal efficiency, and that the effect of thermal emissivity and porosity on heat exchange effectiveness is moderate.

The UTC attains its high efficiency by reducing convective heat losses. Nevertheless, high wind speeds (higher than about 4 m/s) reduce the efficiency of the UTC by increasing turbulence and convection losses, particularly for low air collection rates. Gunnewiek *et al.* (2002) studied the effect of wind flow on UTC performance and made recommendations for air collection to avoid flow reversal. Feck *at al.* (2002) conducted experiments on a building-integrated UTC system, taking wind speed, ambient air temperature, and incident solar irradiance measurements to determine the relation between wind speed and direction, as well as the performance of UTCs. The results showed that maximum performance (collector efficiency) does not occur at zero wind speed, for unknown reasons. Gawlik and Kutscher (2002) performed a numerical and experimental study on wind heat loss from UTCs with sinusoidal corrugations. They report that under certain combinations of wind speed, air collection rate, and plate geometry, the airflow over the plate could be either attached or separated. At low wind speeds, the flow is attached and the wind heat loss is low. The wind heat loss increases significantly when the wind speed is high enough to cause separation.

Gawlik *et al.* (2005) determined the performance of UTCs made from low-conductivity materials, such as styrene and polyethylene, for comparison with conventional UTCs made from high-conductivity steel and aluminum. The numerical and experimental study concluded that the effect of conductivity on the thermal performance of transpired collectors is small, and that low-conductivity materials can be used with minimal thermal performance penalty. The development of new polymers in the future will likely advance the design of UTCs and provide an even lighter and lower cost system.

2.2 Photovoltaic Technology

2.2.1 Overview

The photovoltaic (PV) effect is the basic process by which a PV cell converts sunlight into electricity. When light shines on a PV cell, it may be reflected or absorbed, and a portion of the absorbed light generates electricity. A single PV cell is a thin semiconductor wafer comprised of two layers, generally made of highly purified silicon. PV cells can be made of many different semiconductor materials, such as silicon, gallium arsenide, cadmium telluride, and copper indium. A close-up of a polycrystalline silicone solar cell is shown in Figure 2.7. The two semiconductor layers were doped with boron (p-type semiconductor) on one side and phosphorous (n-type semiconductor) on the other side, producing a surplus of electrons on one side and a deficit of electrons on the other side. When solar energy strikes the wafer, the illuminated photons knock off some of the excess electrons, which causes a voltage difference between the two sides as the excess electrons try to move to the deficit side. Both sides of the semiconductor cell contain metallic contacts. With an external circuit (battery or electrical load) attached to the contacts, the electrons can travel back to where they came from, and current flows through the circuit.

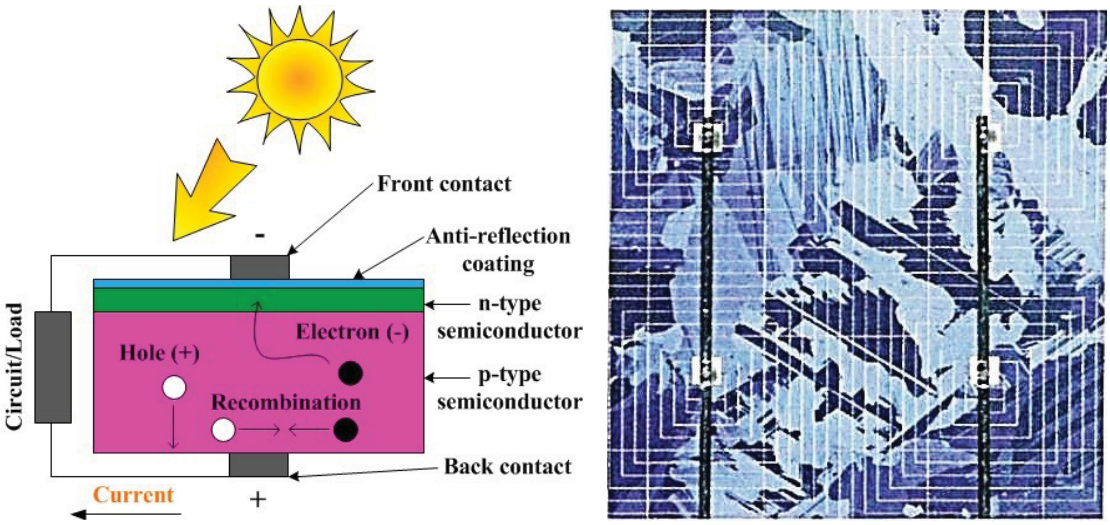

Figure 2.7: Schematic of how photovoltaic effect works (left). Close-up of polycrystalline silicon cell, showing electrical contacts (right). (German Energy Society, 2008)

PV cells are generally made either from crystalline silicon, sliced from ingots, or castings, from grown ribbons or thin film, deposited in thin layers on a low-cost backing (EPIA, 2012). The performance of a solar cell is measured in terms of its efficiency at turning incident solar irradiance into electricity. Improving solar cell efficiencies while holding down the cost per cell is an important goal of the PV industry. A PV module consists of many PV cells wired in parallel to increase current, and in series to produce a higher voltage. Standardization and certification of performance and reliability are well defined for PV technology in European standard IEC 61215. The electrical efficiency that is reported by PV manufacturers is usually measured under standard testing conditions (STC, incident solar irradiance 1000 W/m², cell temperature 20ºC, air mass density 1.5), or more realistically, under normal operating conditions (NOC, incident solar irradiance 800 W/m², ambient air temperature 20ºC, wind speed 1 m/s), to allow users to compare between product types. Since their appearance on the market, the evolution of PV modules can be divided into three distinct generations (Figure 2.8):

1. Crystalline silicon cells are made from thin slices cut from a single crystal of silicon (monocrystalline) or from a block of silicon crystals (polycrystalline). Record conversion efficiencies have been independently verified to be 25.0% for monocrystalline silicon and 20.3% for polycrystalline cells (Green *et al.*, 2010) under STC. To form a PV module, cells are wired together and encapsulated, typically between tempered low-iron glass, and sealed at the edges; there is often an aluminum frame holding everything together, forming a mountable unit. In the back of the PV module there is a junction box, or wire leads, providing electrical connections. Most commercially available crystalline PV modules have an electrical efficiency between 12% and 20%.

2. Thin film modules are constructed by depositing extremely thin layers of photosensitive materials onto a low-cost backing, such as glass, stainless steel, or plastic. Thin film manufacturing processes result in lower production costs compared to the more material-intensive crystalline technology, a price advantage that is counterbalanced by lower efficiency rates (from 4% to 11%) (Benagli *et al.*, 2009).

3. Emerging technologies are those that are still under development and in the laboratory or pre-pilot stages, but which could become commercially viable within the next decade. These third-generation solar cell technologies are based on very low-cost materials and/or processes and include dye-sensitized solar cells, organic solar cells, and low-cost (printed) versions of existing inorganic thin-film technologies.

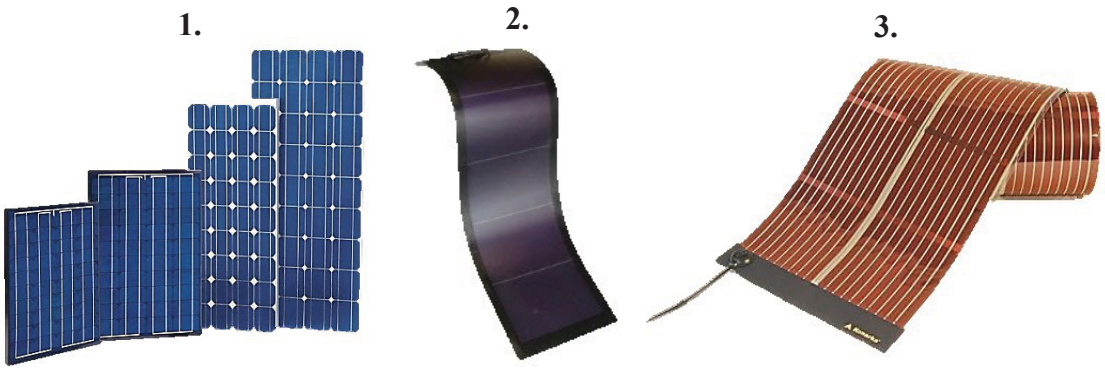

Figure 2.8: Three generations of PV module: Monocrystalline and polycrystalline (left) (PRES, 2012), amorphous thin film (center) (Uni-solar, 2012), and organic thin film (right) (Konarka, 2012).

Crystalline silicon PV is the most common technology, representing nearly 90% of the market today (Solar Generation V, 2008). It is widely favoured for building integration for three major reasons. The first reason is the maturity of this technology and market, which has led to diversification of product offerings, with manufacturer warranties of 10 to 30 years. Secondly, as the crystalline silicon market is mature, the products are becoming a commodity good. The third reason is the higher conversion efficiency of crystalline silicon PV versus the other existing technologies. This element becomes crucial when surface availability is limited.

Usually, a PV system is comprised of individual PV modules wired together to form a typical string of know voltage and current. As shown in Figure 2.9, the strings are then wired together, forming an array of PV modules. The arrangement of PV modules into strings and arrays is generally an iterative process, aimed at maximizing energy delivery from the available surface. The PV array produces direct current (DC), which can be consumed directly by powering DC devices, such as fans and pumps (which operate in proportion to the received solar energy), stored in a battery bank for later use,

or transformed into conventional alternating current (AC) electricity using a solar inverter. When a PV system is grid connected, it delivers AC energy back into the utility's electrical system.

The amount of energy produced by a PV module is a function of the operating current and voltage, which vary with the incident solar irradiance and the PV module surface temperature, respectively. At each solar irradiance level and surface temperature, an I-V curve can be obtained that shows the possible combinations of current and voltage at which the PV module can operate. The PV module generates maximum power (Pmp) when the rectangular area created by the intersection of voltage (Vmp) and current (Imp) is greatest (Figure 2.9). Maximum power point tracking is a technique that solar inverters and battery chargers use to get the maximum possible power from one or more PV modules.

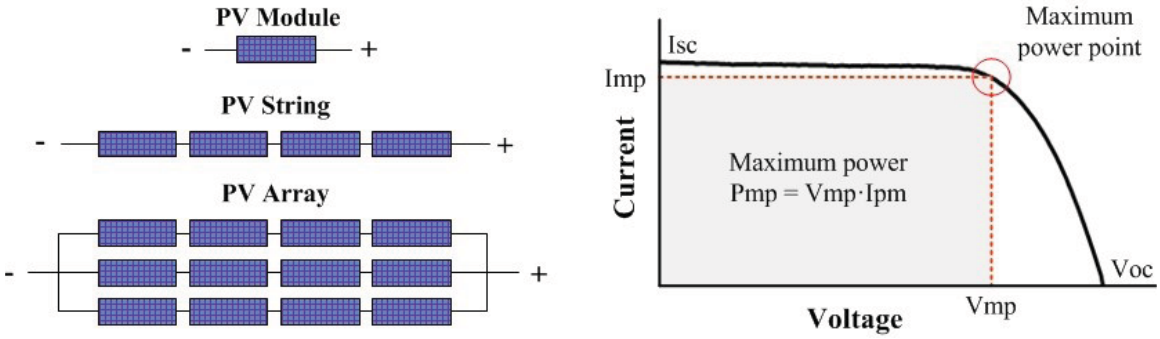

Figure 2.9: Schematic of a PV module, string, and array (left). Typical I-V curve showing the maximum power point (right).

The electrical efficiency of a PV module changes depending on its surface temperature. Each type of solar cell has a specific temperature coefficient, which indicates the decrease in electrical efficiency of the PV module when the average surface temperature rises by 1ºC. Typical temperature coefficients for crystalline and thin film

amorphous are 0.4–0.5%/ºC and 0.1–0.2%/ºC, respectively (Skoplaki and Palyvos, 2009). For example, a 20ºC temperature rise can decrease a monocrystalline PV module by 1% (from 15% to 14%, for example), resulting in nearly a 10% loss in electrical energy generation. Thus, there is an incentive to cool PV modules in order to achieve optimal performance. PV planners typically allow for some form of natural air circulation behind the PV modules to cool them to avoid overheating and reduced lifetime or delamination. The theoretical electrical efficiency of the PV modules, η_{PV_theo} in %, as a function of their temperature, T_{PV} in °C, can be estimated using (Skoplaki and Palyvos, 2009)

$$\eta_{PV\_theo} = \eta_{stc} \cdot \left[1 - \beta_{PV} \cdot \left(T_{PV} - T_{STC}\right)\right] \tag{4}$$

where

β_{PV}, in %/ºC, is the PV module temperature coefficient

η_{stc}, in %, is the PV module efficiency at standard test conditions.

T_{stc} in °C, is the PV module cell temperature at standard test conditions (25°C).

The theoretical electrical power produced by a PV covered surface, E_{PV_theo} in W, as a function of the incident solar irradiance, I_{solar}, in W/m² and the total PV area, A_{PV} in m², is given by

$$E_{PV\_theo} = I_{solar} \cdot A_{PV} \cdot \eta_{PV\_theo} \tag{5}$$

2.2.2 Building-integrated photovoltaics

PV technology can be either installed over existing building surfaces as a retrofit or integrated into the building itself (Figure 2.10). Building-applied photovoltaic refers to concepts where the photovoltaic systems are mounted on top of the building's existing

structure, and therefore, do not add any additional value beside that of producing electricity. Building-integrated photovoltaic (BIPV), on the other hand, means that photovoltaic elements have been present in the project from the very beginning and are a part of a holistic design.

Figure 2.10: Photovoltaics applied onto a roof (left). Semi-transparent PV modules integrated into a greenhouse roof (right). (EPIA Sunrise, 2011)

BIPVs are becoming an increasingly popular system for solar electricity generation, while also serving as a functional building envelope element. When properly integrated into the envelope, several other purposes can be achieved, such as weather protection, thermal insulation, noise protection, or modulation of daylight. Integration also improves the cost effectiveness of PV by providing, in addition to electricity production, a durable building envelope. Architectural and aesthetic integration is a major requirement of BIPV systems. BIPV has a significant advantage over add-on modular systems that often require penetrations of the envelope to be attached.

PV technology may be integrated into the roof, façade, and windows of buildings (Figure 2.11). The latter provides electrical energy and shading, in addition to daylighting. Façade-integrated PV systems can easily replace spandrel sections of a

curtain wall construction. Although vertical exterior walls receive less solar energy compared to roofs, they offer distinct advantages in mid-latitudes, such as providing peak irradiance in the colder months and reduced susceptibility to rainwater penetration and snow accumulation. In addition, they can be designed to provide somewhat equal monthly electrical output during the year. If high-end façade elements, such as stone panels and stainless steel, are replaced with PV, it can lead to only slight additional costs, making the system very interesting from an economic point of view. The possible added prestige value of photovoltaic elements should also not be forgotten.

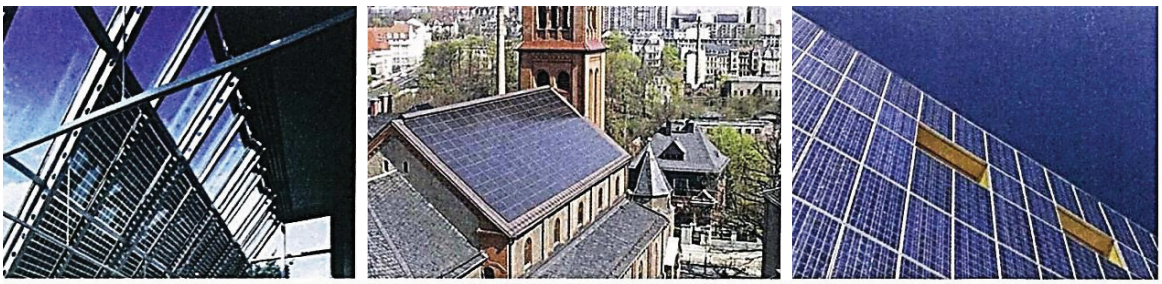

Figure 2.11: Photos of three BIPV applications: semi-transparent PV modules integrated into a façade (left); PV modules integrated into a roof (center); and PV modules integrated into the façade (right). (German Energy Society, 2008)

PV prices have decreased dramatically over the last 30 years. Average global PV module factory prices dropped from about 22 USD/W (2005$) in 1980 to less than 1.5 USD/W (2005$) in 2010 (Bloomberg New Energy Finance, 2010). PV module manufacturing costs are projected to continue to drop. In fact, most projections so far have proven to be too conservative, as the dramatic changes in market conditions could not be foreseen. The average installed cost of a PV system has also decreased significantly over the past couple of decades, and it is projected to continue decreasing rapidly as PV technology and markets mature. However, the system price decrease varies significantly from region to region and depends strongly on the implemented support

schemes and maturity of markets (Wiser *et al.*, 2009). As the cost of PV and BIPV continue to fall, BIPV becomes less costly than high-end building materials and approaches comparability with mid-range materials. This, in turn, will open up a much wider, addressable market (EPIA, 2011).

2.3 Photovoltaic/Thermal Systems

2.3.1 Overview

Photovoltaic/thermal (PV/T) collectors convert solar energy into electricity and heat simultaneously. The overall efficiency of a PV/T collector is higher than the sum of the efficiencies of separate solar thermal and PV collectors. Major advantages of PV/T collectors include greater energy production per unit collector area, lower PV operating temperatures, and enhanced cost effectiveness.

In PV/T systems, a cooling fluid, such as air or water, is used to extract heat from the PV in an open-loop or closed-loop configuration (Figure 2.2). For example, in an open-loop air system, outdoor air circulates behind the solar-heated PV modules, cooling them and recovering useful heat that would otherwise be lost to the outdoor environment. Because PV typically has an electrical efficiency of up to 20%—with the remaining 80% or so of incident solar radiation lost largely as heat—and since it also produces more electricity when cooled, there is a dual benefit to cooling the PV modules: increased electricity production and generation of useful heat. This heat can be used for space or domestic hot water heating, either by direct means or through a heat pump.

Virtually all types of PV technology are suitable for use in PV/T systems. However, PV cells that have a high temperature coefficient, such as polycrystalline silicon, particularly benefit, since notable increases in electrical generation may result from the cooling process. The heat is typically collected by circulating the fluid in front of or behind the PV modules (Figure 2.12). Many different techniques have been developed to optimize heat extraction from PV modules, and improvement continues as research brings new solutions that are more efficient and cost effective. Some of the strategies are the use of extended fins (Tonui and Tripanagnostopoulos, 2007) and phase change materials (Hasan *et al.*, 2010), which can absorb much of the PV heat while maintaining a constant temperature. For homogeneous PV cooling, the length of the airflow path must be carefully considered, in order to avoid large PV module temperature gradients.

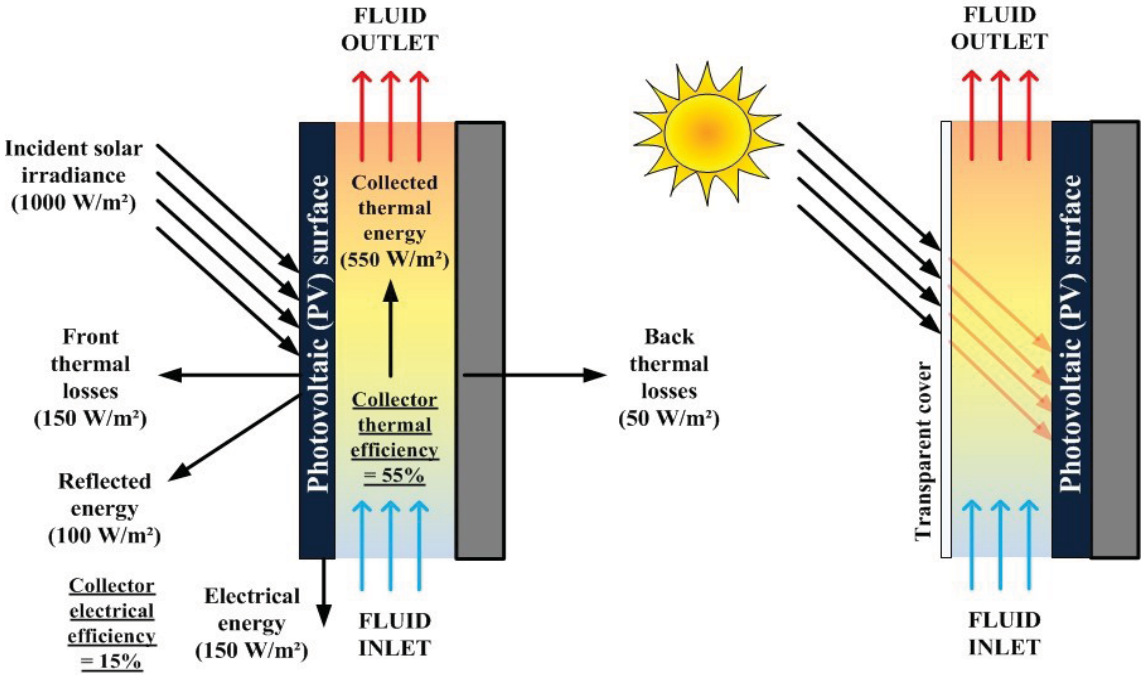

Figure 2.12: Schematic of two common PV/T collector designs: on the left, the working fluid removes heat from behind the PV surface, and on the right, the working fluid collects heat from the front of the PV surface.

The amount of thermal and electrical power produced by a PV/T collector can be estimated using equations 1 and 5. The combined thermal and electrical efficiency of the PV/T system is given by

$$\eta_{PV/T} = 100 \cdot \left(\frac{Q_{thermal} + E_{PV}}{A_{collector} \cdot I_{solar}} \right) \tag{6}$$

In order to compare solar thermal collectors and PV/T collectors, the electricity generated may be converted into its thermal equivalent. The value of the electrical energy can be assumed to be about four times the value of the heat, based on the concept that with one unit of electricity as input to an air source heat pump, one can produce, on average, four units of heat. In general, the ratio between the relative value of electricity and heat ranges from 1 for a simple first law approach, to 17, when a typical exergy analysis is considered (Coventry and Lovegrove, 2003). In the above equation, we may multiply E_{PV} by a factor, COP (heat pump coefficient of performance), representing conversion of electricity to heat, to compute an equivalent PV/T thermal efficiency, as follows:

$$\eta_{thermal\_equivalent} = \frac{Q_{thermal} + COP \cdot E_{PV}}{A_{collector} \cdot I_{solar}} \tag{7}$$

2.3.1 Building-integrated photovoltaic/thermal systems

Considerable work has been done on architecturally integrating solar components into the built environment. Photovoltaic/thermal (PV/T) systems may be integrated into buildings to form a durable exterior skin while generating electricity and heat. Their cost effectiveness is thus improved in comparison with stand-alone systems that need a

separate support structure, particularly when they replace expensive envelope exterior layers, such as stone panel or architectural glazing. The schematics shown in Figure 2.13 illustrate how PV/T systems can be integrated as construction elements into the roofs, façades, and windows of buildings.

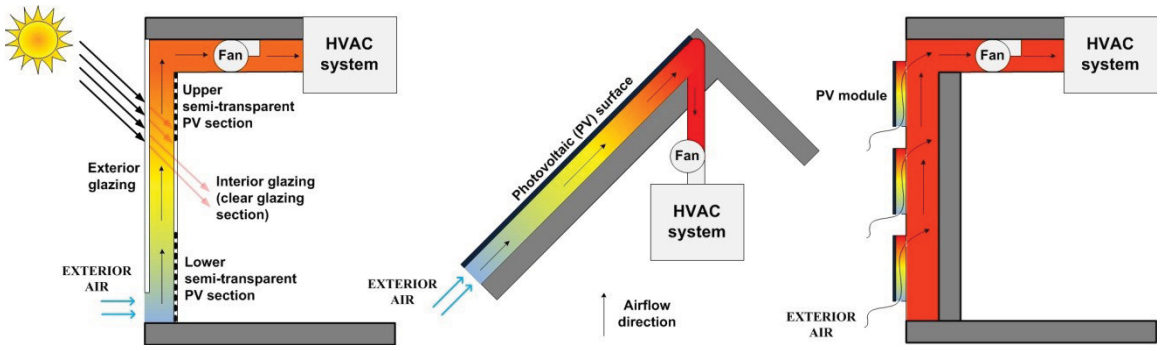

Figure 2.13: Schematic of three BIPV/T system configurations: semi-transparent BIPV/T façade system (left), single-inlet BIPV/T system for a roof (center), and multiple air inlet BIPV/T façade system (right).

Over the past two decades, BIPV/T collectors have garnered great interest in the solar thermal and PV research communities. A considerable amount of research has been conducted on these collectors, particularly on numerical simulation, prototype design, and experimental testing of the commercial development of novel and improved BIPV/T systems. Reviews of recent work in this area are provided by Kumar and Rosen (2011), Chow (2010), and Norton (2010).

Various researchers (Bazilian *et al.*, 2001; Tripanagnostopoulos, 2007; Guiavarch and Peuportier, 2006; Liao *et al.,* 2007) have studied the energy performance of actively cooled PV modules integrated into façades and roofs. Prakash (1994) used a transient simulation model to predict the electrical and thermal behaviors of PV/T collectors with

air and water heat transfer fluids, and found that the thermal efficiencies of BIPV/T water and air collectors were 50–67% and 17–51%, respectively.

Chow *et al.* (2007) presented an experimental study of a BIPV/T water heating system and reported the thermal and combined (thermal plus electrical) efficiency as 39% and 48%, respectively. Corbin and Zhai (2010) experimentally validated a computational fluid dynamics (CFD) model of a novel BIPV/T water collector; the thermal and combined efficiencies obtained were 19% and 35%, respectively.

Only a few studies have been carried out on BIPV/T air collectors, which is probably due to the limited market share of solar air heating. Performance studies for glazed and unglazed BIPV/T air collectors were conducted by Tripanagnostopoulos *et al.* (2002). Candanedo *et al.* (2010) presented a steady-state, transient model for a BIPV/T system, useful for design or control purposes. Unglazed BIPV/T collectors have a lower outlet temperature, and they may be combined with a heat pump (Ito *et al.*, 2004; Bakker *et al.*, 2005; Candanedo and Athienitis, 2011). PV cells have also been developed to be applied to windows to allow daylighting while producing electrical and thermal energy. Charron and Athienits (2006) performed a theoretical study of ventilated double façades with integrated PV to study the effects of different design parameters on thermal and electric system performance.

In recent years, there has been an increase in interest in the idea of the net-zero energy solar building, defined as one that, in an average year, produces as much electrical and thermal energy from renewable energy sources as it consumes. International Energy Agency Task 40 is considering how to achieve this goal (IEA, 2012). Recent examples of

near net-zero energy homes for the Canadian climate are provided by Athienitis *et al.* (2008). Starting from a building that meets the highest levels of conservation, the Ecoterra demonstration project uses a prefabricated modular BIPV/T roof system, where the heated air is used for space heating or as a source for a heat pump (Figure 2.14).

Figure 2.14: Commercially available PV/T water collector modules (left) (Solimpeks, 2012). Ecoterra prefabricated BIPV/T roof (right) (Athienitis et al, 2008).

Smart solar building control strategies may be used to manage the collection, storage, and distribution of locally produced solar electricity and heat to reduce and shift peak electricity demand from the grid. An example of a smart solar building design is provided by Candanedo and Athienitis (2010), where predictive control based on weather forecasts one day ahead and real-time prediction of building response are used to optimize energy performance while reducing peak electricity demand.

Over the past three decades, various designs have been proposed for BIPV/T systems, and some have achieved a degree of market success. Most research and development is related to simulation of new designs, rather than enhancing commercial viability. Several manufacturers have participated in the development, production, and marketing of various BIPV/T collectors. However, the number of commercially available

collectors is still limited, and long-term experiences with the operation of collectors are scarce (PV/T Roadmap, 2004). Further efforts are needed to make BIPV/T collectors a viable alternative to PV and solar thermal collectors. Presently, some companies are attempting to expand product lines for BIPV/T collectors. The use of building surfaces to generate electricity and heat using BIPV/T technology is promising, and its viability will improve further as efficiency increases, costs decrease, and technical design issues associated with this integrated technology are resolved.

2.3.2 Photovoltaic/thermal system integrated with unglazed transpired collector

Over the past thirty years, research on UTCs has focused mainly on the understanding of the heat transfer occurring through perforated plate collectors. The main goals of the different studies were to improve heat transfer and to decrease the cost of the collector. There is little literature available on BIPV/T systems using transpired collectors. A BIPV/T system can be made by mounting PV cells or modules directly over the UTC. The distributed inlets create uniform suction over the collector area, making the UTC a suitable system for excess heat collection off the overlaying PV surface.

Research on the integration of PV cells and UTC started in the late 1990s with Hollick (1998). He combined UTC and PV technologies by partially covering the top of the corrugations of the UTC with encapsulated crystalline silicon PV cells. The UTC area covered by PV cells was approximately 24%. The experiment showed that the temperature of the cells was lower for the PV/T system by 3–7ºC for an irradiation of 900 W/m². It was also found that even if the thermal efficiency of the collector system decreased slightly with the addition of PV cells, the combined efficiency (electrical plus

thermal) was greater than for the stand-alone UTC. Delisle and Collins (2007) also investigated such a system through modelling and a small-scale prototype (Figure 2.15). They reported that the electricity produced might be significantly higher than the reduction in useful thermal energy. However, significant technical challenges remain in the development of a UTC product with PV cells directly integrated on it. Naveed *et al.* (2006) studied the effect of mounting a PV module on the front of a UTC. The electrical performance of this PV/T system was compared to a stand-alone PV module (Figure 2.15). The UTC behind the module was found to decrease the temperature of the PV by 3–9ºC, with a 5% recovery in the electrical power output.

Another option is to integrate custom-designed PV modules onto a UTC using a suitable attachment system. The resulting PV/T system has two portions consisting of exposed UTC and a larger part covered by PV modules. This is the option investigated in this thesis, with the BIPV/T design concept presented in the following chapter.

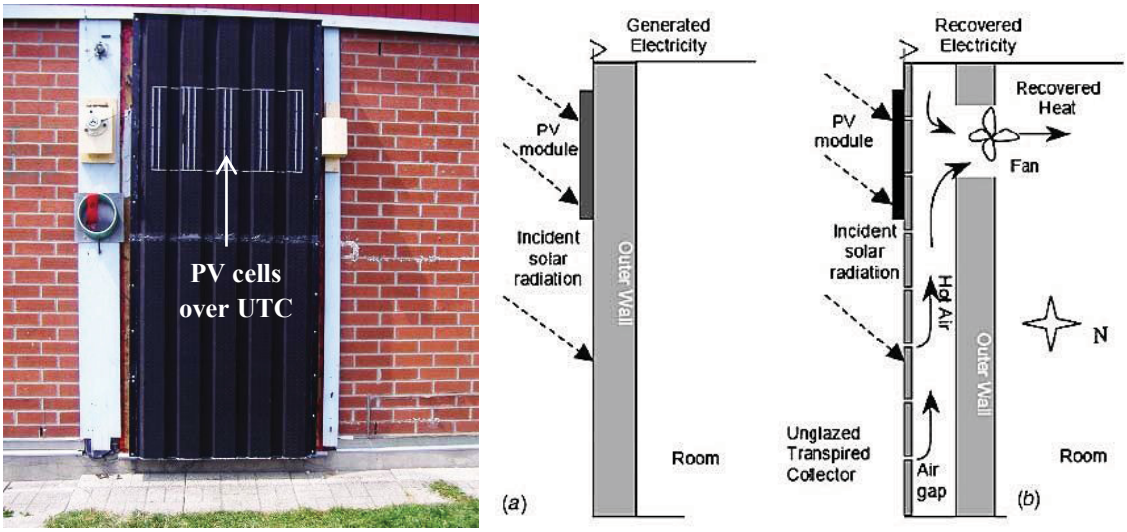

Figure 2.15: Experimental setup of a UTC with overlaying PV cells, developed by Delisle *et al.,* 2008 (left). Schematic of the experimental setup used by Naveed *et al.*, 2006 (right).

3. PHOTOVOLTAIC/THERMAL SYSTEM DESIGN CONCEPT[1]

In 2005, the Natural Sciences and Engineering Research Council (NSERC) approved the creation of the Solar Buildings Research Network (SBRN). The SBRN's long-term goal was the development of the optimized solar building as an integrated, cost-effective technological system that approaches, under Canadian climatic conditions, net-zero annual total energy consumption. An important enabling technology studied by the SBRN is the modelling, design, and control of BIPV/T systems and their integration with the building's energy system. A major task of the SBRN was to develop a BIPV/T system that is optimized for the Canadian climate, and that maximizes energy recovery from a well-situated, solar-exposed building façade. Secondary goals involved the minimization of costs associated with labour and materials, as well as designing a system that is not overly time consuming or complex to install.

The SBRN project investigated the concept of using unglazed transpired collector (UTC) integrated with overlaying PV modules to create an effective BIPV/T system for simple integration into any well-oriented façade. The basic concept for the BIPV/T system with UTC is represented in Figure 3.1. The UTC and overlaying PV modules are installed on a frame that creates an air cavity of approximately 15–20 cm between the building façade and the collector. A variable speed fan creates negative pressure in the air cavity, pulling exterior air through the solar collector and preheating it. The thermal energy recovered by the BIPV/T system is a contribution of two sources. For about 70% of the collector area, air is heated by being circulated behind the relatively warm PV

[1] See related publication in Athienitis A.K., Bambara J., O'Neill B., Faille J., 2011. A prototype

modules, whereas the UTC is used uniquely for PV support and preheated air collection. The other solar heat portion is recovered through direct extraction from the exposed UTC surface. Therefore, solar heat is extracted mainly from the PV modules. The heat lost by the building's facade is also recovered by the air cavity during the air collection process. The system generates heat and electricity at a ratio that depends on the following factors:

1. The portion of the UTC covered by PV modules.
2. The electrical efficiency of the PV modules and their temperature coefficient, which determines how electrical efficiency is reduced by rising PV temperatures.
3. The dimensions, framing, and cell backsheet solar absorptance and thermal properties of the PV module; these affect the energy balance of the PV modules.
4. The PV array design; non-uniform array temperatures, caused by vertical stratification, may affect electrical production, depending on the PV array series and parallel interconnections.
5. The characteristics of the UTC cladding and how the corrugations are oriented—vertical or horizontal.
6. The incidence angle of the solar radiation; at high sun, the PV modules partly shade the area without PV.
7. The air collection rate through the BIPV/T collector, which generally increases heat extraction; however, as it is raised, friction losses and energy consumed by the fan also increase.
8. The wind speed, which generally affects exterior convective heat loss.

9. The fan energy consumption; while it also needs to be considered in designing the system, it is generally much less (less than 5%) than the energy recovered. DC powered fans can operate directly from the generated PV energy and can provide autonomous control.

The outlet air temperature produced by the system is important in deciding air collection rate in addition to thermal efficiency, as well as electrical efficiency increase due to PV cooling. In order to maximize the heat extracted from the integrated PV and UTC technologies, several design strategies were used, and they are discussed further.

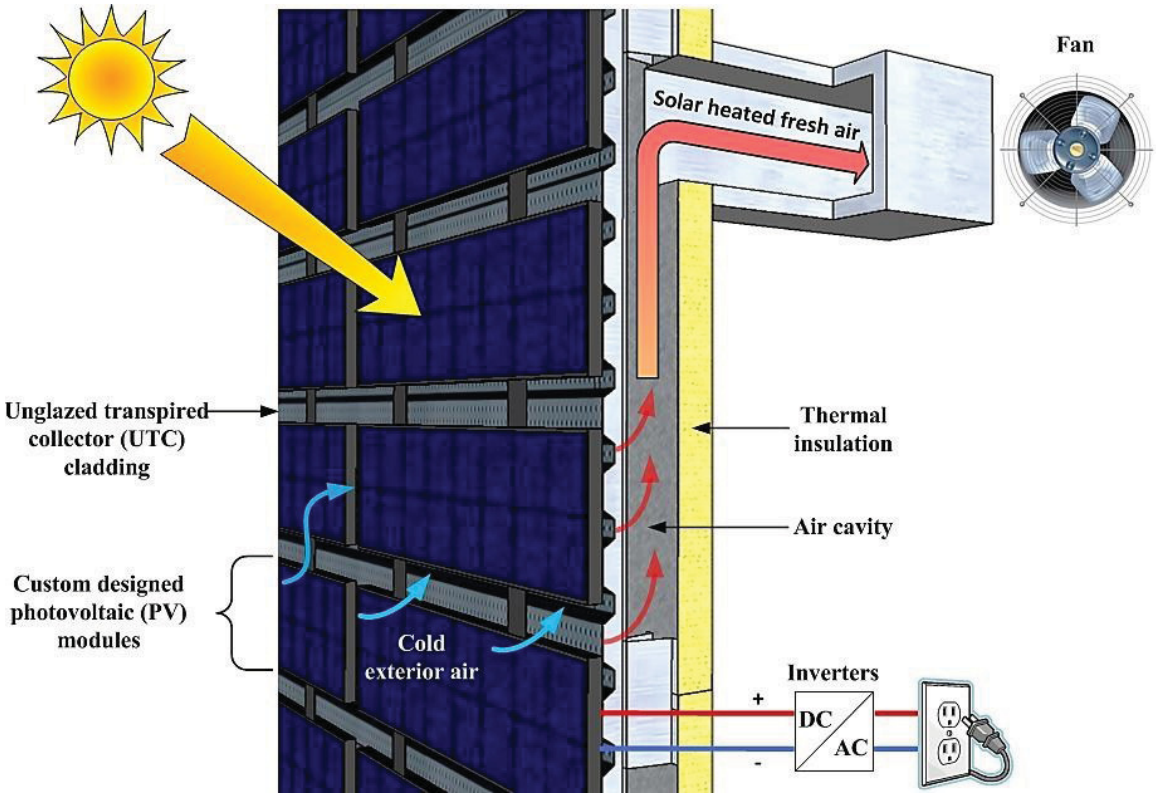

Figure 3.1: Concept schematic of the BIPV/T system consisting of UTC and overlaying PV modules.

3.1 Unglazed Transpired Collector Configuration

The selection of the UTC collector was carried out early in the design process, as dictates the design of the PV attachment system and their alignment. Commercially available SolarWall®, manufactured by Conserval Engineering, was selected for this application. Figure 3.2 gives the dimensions of the SW150 profile, which is made from galvanized steel (26 gauge) and factory painted black (95% solar absorptance). The sheeting is perforated with small holes over 0.6% of its area. Appendix A provides the manufacturer specifications for the SW150 profile.

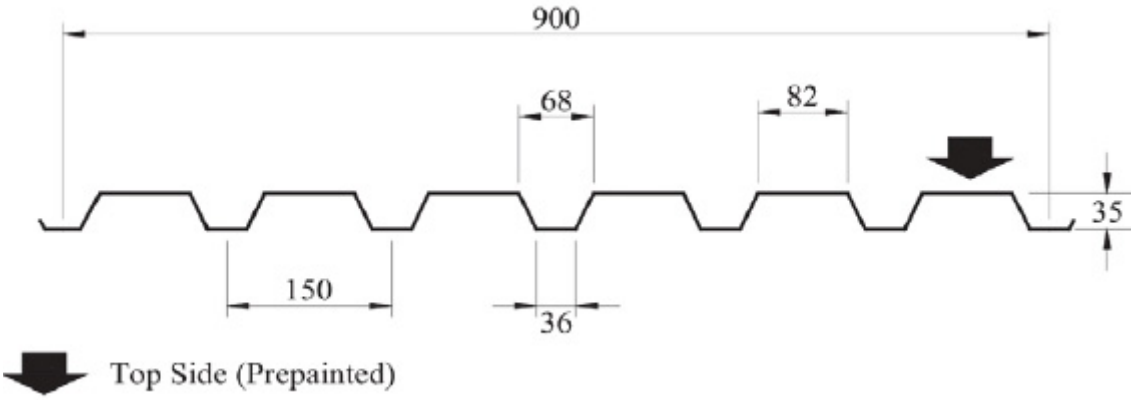

Figure 3.2: Commercially available SolarWall® SW150 sheets.

Unlike most UTC systems, the sheets were installed with the corrugations running horizontally, to facilitate closing a gap between the upper frame of the PV module and the UTC (Figure 3.3). This ensured that warm air could not escape if the natural convention forces were stronger than those of forced air. In addition, the corrugation induces turbulence in the rising air behind the PV modules and increases heat collection, compared to vertically oriented corrugations. Airflow behind the PV modules is possible through the bottom and the sides.

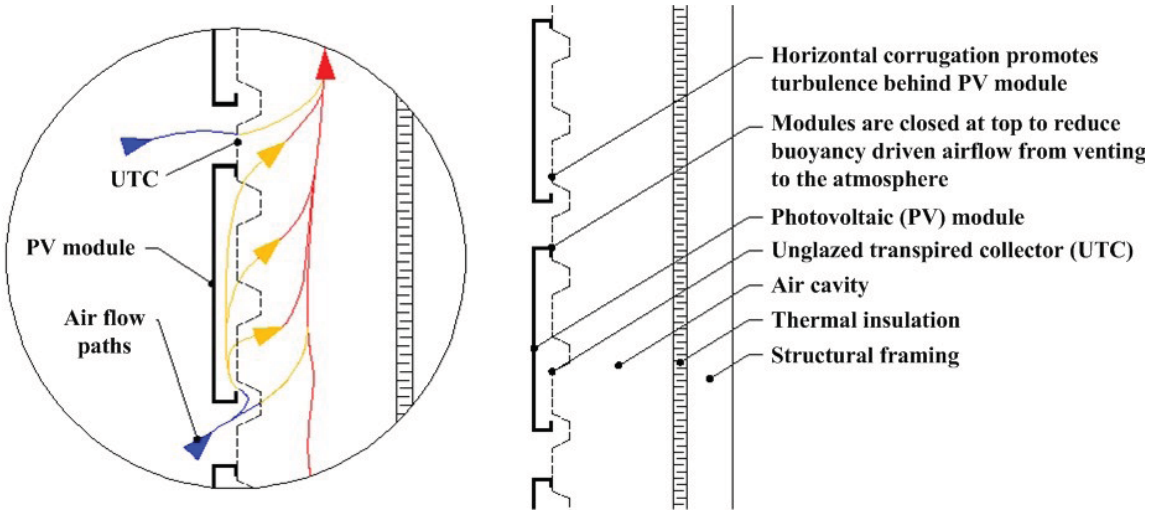

Figure 3.3: Detail showing the attachment of PV modules and airflow paths around the bottom frame of a PV module and into the transpired collector.

3.2 Photovoltaic Module Design Considerations

A major design goal of the BIPV/T system was to maximize the heat recovered from the PV modules, using the following custom designed features:

1. The effective solar absorption of the PV module was increased by selecting a black backsheet (the area between cells). In addition, the anodized aluminum PV frame was factory painted black. Such modifications yielded an area-weighted (including framing) average PV module normal solar absorption of 92%, compared to 85% for the traditional, lighter-coloured counterpart (Figure 4.2). As a consequence, more thermal energy could be recovered from these PV modules.

2. Another important design parameter was the sizing of the PV module. Although greatly dictated by the cell sizes available in the industry, a long, narrow, rectangular module was chosen to reduce vertical temperature stratification of the air in the cavity between the PV module and the UTC. This reduced the PV

operating temperature and facilitated the flow of air from behind the PV into the UTC.

3. The horizontal spacing between the PV modules was mainly dictated by architectural constraints, whereas the vertical spacing was selected based on the criteria of closing the PV module at the top, while maintaining the air inlet from the bottom. In an effort to match the corrugations of commercially available UTC, a vertical spacing of 90 mm between the PV modules was selected.

A 65 Watt PV module, containing two rows of nine polycrystalline solar cells and measuring 1465 mm x 359 mm x 38 mm, was designed for this application (Figure 3.4). The custom-designed MC18 modules were manufactured by Day4 Energy; the electrical specifications, under standard test conditions (STC), are provided in Table 3.1. The proprietary Day4 electrode technology does not use the conventional bus bar and tabbing concept, and the low resistivity associated with interconnection technology provides a high-packing density to the module, with a very uniform-looking surface that is aesthetically pleasing. A special inspection certificate was obtained for the new PV module. Appendix B provides the specifications for the MC 48 module by Day4 Energy which has similar characteristics to that of the MC 18.

Table 3.1: Day4 Energy MC18 PV module specifications under STC

Power [W]	Short Circuit Current [A]	Open Circuit Voltage [V]	Maximum Power Point Current [A]	Maximum Power Point Voltage [V]	Electrical Efficiency [%]	Temperature Coefficient [%/^{o}C]
57–65	7.6–7.7	10.5–10.6	6.89–7.08	8.40–8.47	12.5	-0.46

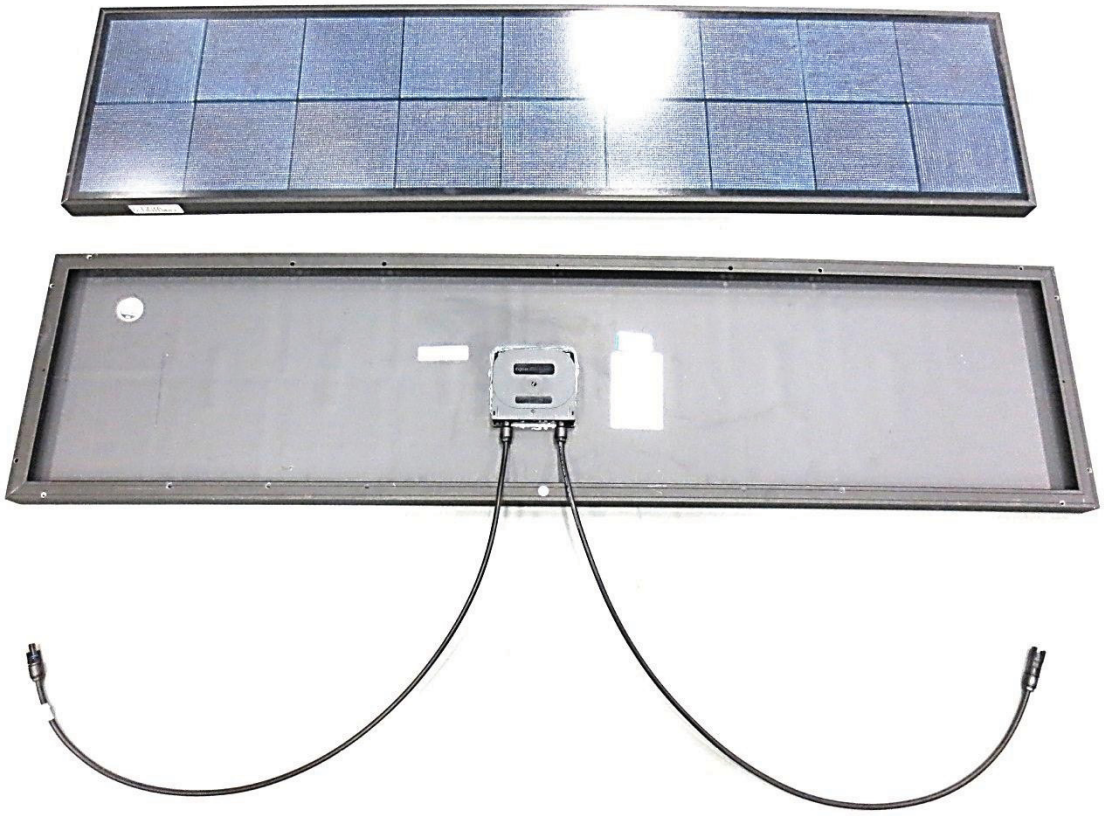

Figure 3.4: MC18 PV modules, custom designed by Day4 Energy.

3.3 Photovoltaic Module Mounting System

The installation of UTC can be performed over new or existing infrastructure; there are several installation techniques for integrating it into the building envelope while creating the required air cavity for preheated air collection. The attachment of PV modules over the UTC demanded a custom-designed mounting system to transfer the excess weight to the appropriate location on the support structure behind the UTC. Figure 3.5 shows a typical installation sequence for retrofitting an existing façade with a BIPV/T system.

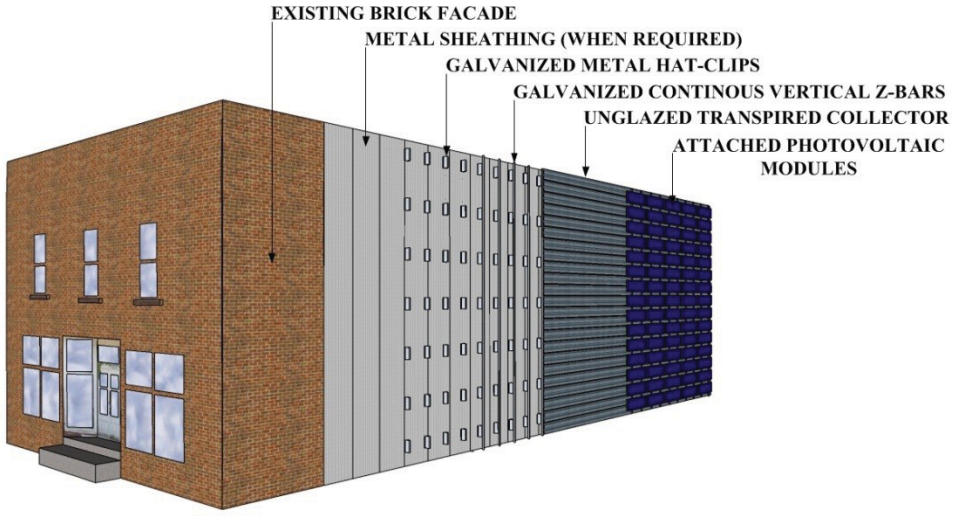

Figure 3.5: Retrofit installation of a PV/T system over an existing façade.

Various iterations for the design of the mounting brackets were conducted by the SBRN design team. The decision to opt for the minimum possible vertical spacing of 90 mm between the PV modules rows allowed for a column of PV modules to be stacked one upon the other. This enabled the brackets themselves to be the reference for spacing the PV modules vertically. In that sense, only the bottom-most row of brackets needed to be aligned, allowing for a quick installation. Figure 3.6 illustrates the mounting system for a typical PV module. The two-piece mounting system consists of brackets that are fastened to the UTC sub-structure and mounting clips that are installed on the PV modules. Each PV module was predrilled with holes spaced 765mm apart for fastening the four mounting clips, which contain a slot for adjustment. The bottom brackets for each row were installed first, followed by the PV modules containing the pre-assembled clips. The brackets and mounting clips were custom manufactured from 16 gauge and 14 gauge stainless steel, respectively and fastened using stainless steel locking bolts. Figure 3.7 displays two sample MC18 PV modules installed over UTC at Concordia University's outdoor solar research facility. In an effort to maintain a dark, uniform

appearance and maximize thermal energy collection, black bracket covers made from black galvanized flashing were installed over each of the bracket clips, using a “clinch” nut, pre-welded to the back of the bracket to ensure ease of installation.

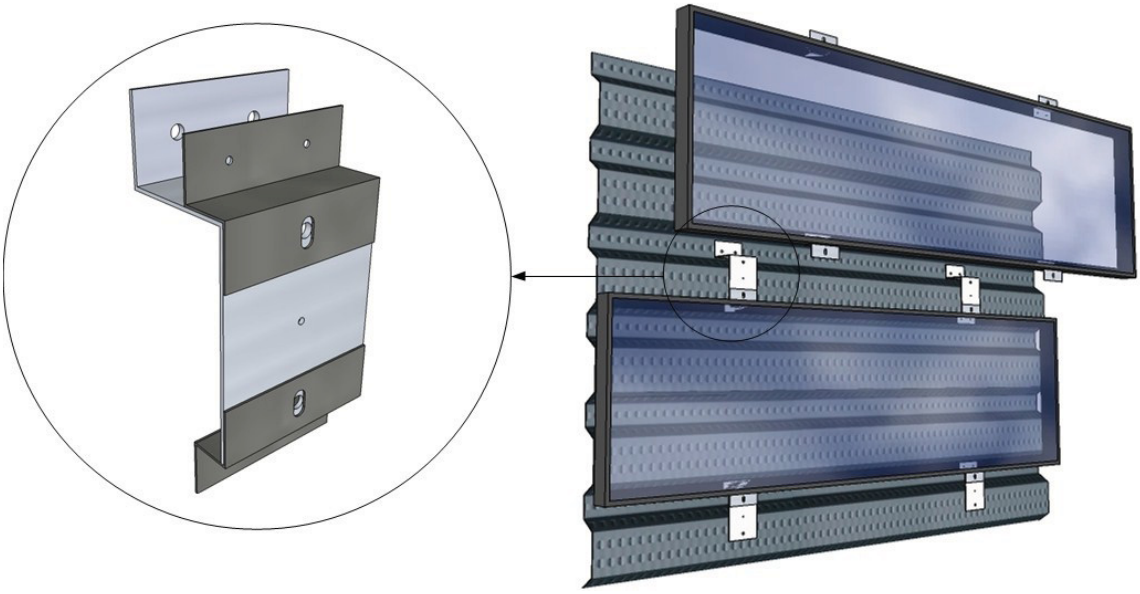

Figure 3.6: Bracket and PV module mounting clips (left). Installation of the second PV module, supported by the upper bracket of the first row (right).

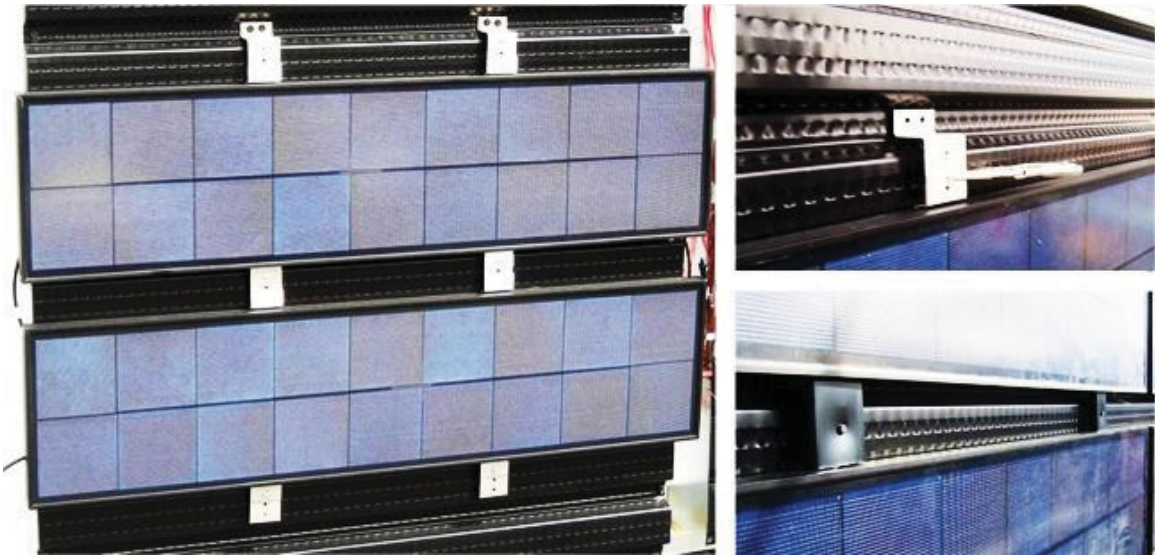

Figure 3.7: MC18 PV modules installed over UTC at Concordia University’s outdoor solar research facility (left). Upper bracket clamped in place, and then bolted (upper right). Black bracket covers fastened to the predrilled hole in the bracket (lower right).

4. EXPERIMENTAL TESTING OUTDOORS

The previous section introduced the project and much of the background for this thesis. This section describes experimental work performed by the author in an outdoor test facility. Located on the roof of a building in downtown Montreal (latitude 45°N), Concordia University's outdoor solar research facility was constructed to evaluate the performance of BIPV/T systems (Figure 4.1). The facility allows for the testing of façade and roof systems (45º tilt angle) facing south. The roof has a test area of about 6 m², and the façade has an open area of 5 m², where various systems can be tested. The weatherized test hut contains all the equipment and controls for fully instrumented, year-round air collector testing.

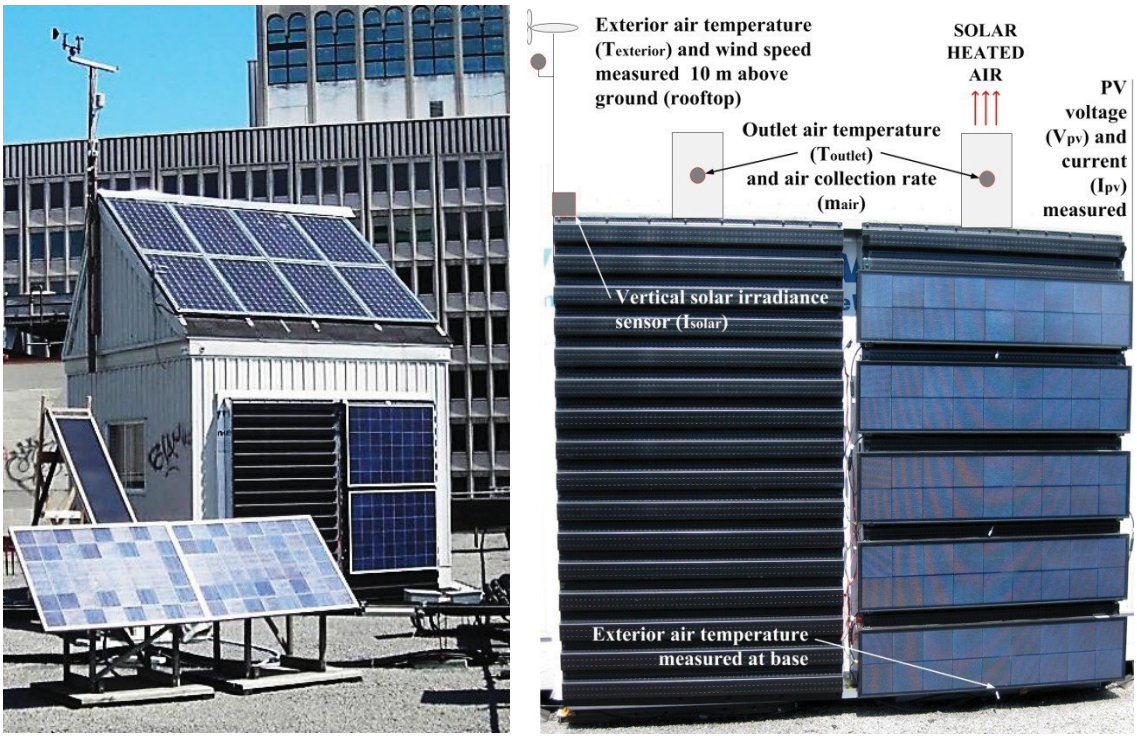

Figure 4.1: BIPV/T test facility at Concordia University (left). Experimental UTC and BIPV/T (addition of PV modules) prototypes (right).

4.1 Experimental Setup

The BIPV/T design concept using UTC collector with overlaying PV modules was put to the test in the outdoor solar testing facility. The façade test section was modified to test a 1.4 m x 2.4 m BIPV/T system side by side with a UTC of equal area (Figure 4.1). The BIPV/T system was fitted with five PV modules (A_{pv} = 2.6m²) wired in series and covering about 75% of the total collector area. Air was drawn through each test section with a centrifugal fan (New York Blower Company – 1406 aluminum) coupled with a variable speed motor (Baldor Electric Company – 3 hp), and airflow was measured by means of a laminar flow element. The thermal insulation was 1.76 °C·m²/W for the vertical wall and collector perimeter.

A weather station was used to determine wind speed and direction, as well as exterior air temperature, about 10 m higher than local ground (rooftop). A pyranometer was mounted on the collector to measure incident solar irradiance. Outlet air temperature sensors were placed at each air collection duct outlet, and the local exterior air temperature was measured at the collector base, using shielded thermocouples. In the BIPV/T section, three of the five PV modules (first, middle, and top) were fitted with six thermocouples each—three distributed along the central vertical axis and three along the outer vertical axis. Electricity produced by the PV modules (operating at their maximum power point) was measured and stored in a battery through a charge controller. The data was collected using multiple Agilent 34970A data acquisition switch units. Table 4.1 presents the details of the important measured parameters.

Table 4.1: Summary of important measured parameters for the prototype experiment

Parameter Measured	Instrument	Unit	Measurement Accuracy
Outlet Air Temperature	T-Type Thermocouples by Omega	°C	± 0.3°C
PV Module Temperature	T-Type Thermocouples by Omega	°C	± 0.3°C
Airflow Collection Rate	Laminar Flow Element by Meriam Instruments (model 50MC2-6-LHL)	kg/hr	± 5% of reading
DC Voltage	Data Acquisition Unit by Agilent (model 34970A)	V	± 1% of reading
DC Current	Shunts by Canadian Shunt Industries (15A, 100mV)	A	± 2% of reading
Exterior Air Temperature	T-Type Thermocouples by Omega	°C	± 0.3°C
Solar Irradiance	Pyranometer by Li-Cor (model LI-200SA)	W/m^2	± 5.0% of reading
Wind Speed	3-cup Type Anemometer	m/s	± 5.0% of reading

The experiment focused on the performance of the two systems under clear low-wind (than 2 m/s), quasi-steady state conditions within one hour from solar noon. A variable speed controller was used to implement four air collection rates in the experiment: 50, 80, 115, and 150 kg/hr/m² (mass flow rate of air per square meter of collector). A 30-minute interval between air collection rates was chosen to maximize the data collected on a clear day, while ensuring that quasi-steady state conditions were achieved (the time constant of each façade section was about 3 minutes). The system was found to be balanced without any need to adjust the balancing dampers, which shows that adding the PV modules to the BIPV/T prototype did not affect the pressure drop in the system (the flow rate was equal in both test sections). Unless specified otherwise, the results reported in this chapter are the average of the 30 minutes of data collected (data was recorded every minute) for each flow rate (excluding initial transient of about 10 minutes), recorded between 11:30 hrs and 13:30 hrs local time. Table 4.2 presents the dates and average environmental conditions that were selected for analysis.

Table 4.2: Dates and average environmental conditions selected for analysis

Date	Local Time [hrs]	Air Collection Rate [kg/hr/m²]	Incident Solar Irradiance [W/m²]	Wind Speed [m/s]	Ambient Temperature [°C]
15/04/2009	13:03–13:28	50	585	2.0	16.6
16/04/2009	11:32–11:57	80	570	1.7	15.8
16/04/2009	12:05–12:30	115	588	1.0	16.8
16/04/2009	12:37–13:02	150	587	1.9	16.3

The thermal energy produced by the UTC and BIPV/T systems is influenced by the air collection rate per unit area of collector surface, m_{air} in kg/h·m², which is generally chosen during the early stages of design. Knowing this air collection rate (generally 50–150 kg/h·m² for typical collectors), the total air collection rate through the collector, $m_{collector}$ in kg/s, is given by

$$m_{collector} = \frac{(A_{collector} \cdot m_{air})}{3600 \frac{s}{hr}} \tag{8}$$

where $A_{collector}$ in m² is the total surface area of the solar collector.

The thermal power produced by the UTC and BIPV/T systems, $Q_{thermal}$ in W, can be calculated as follows:

$$Q_{thermal} = m_{collector} \cdot c_{air\_avg} \cdot (T_{outlet} - T_{exterior}) \tag{9}$$

where the specific heat of air c_{air_avg}, in J/kg·°C, is given by (ASHRAE, 2009).

$$c_{air\_avg} = 1005.7 - 0.066 \cdot \left[\frac{(T_{outlet} + T_{exterior})}{2} - 27 \right] \tag{10}$$

T_{outlet}, in °C, is the measured outlet preheated air temperature of the solar collector.

$T_{exterior}$, in °C, is the measured exterior air temperature.

The thermal efficiency of the system, $\eta_{thermal}$ in %, is given by

$$\eta_{thermal} = 100 \cdot \left(\frac{Q_{thermal}}{A_{collector} \cdot I_{solar}} \right) \tag{11}$$

where I_{solar}, in W/m², is the incident solar irradiance.

Electrical power produced by the PV modules, E_{PV} in W, is given by

$$E_{PV} = I_{PV} \cdot V_{PV} \tag{12}$$

where I_{PV}, in Amps, is the measured current and V_{PV}, in Volts, is the measured voltage across the PV system.

The electrical efficiency of the BIPV/T system, $\eta_{electrical}$ in %, is given by

$$\eta_{electrical} = 100 \cdot \left(\frac{E_{PV}}{A_{PV} \cdot I_{solar}} \right) \tag{13}$$

The combined thermal and electrical efficiency of the BIPV/T system is given by

$$\eta_{BIPV/T} = 100 \cdot \left(\frac{Q_{thermal} + E_{PV}}{A_{collector} \cdot I_{solar}} \right) \tag{14}$$

Again, the measurements were taken under clear-sky, low-wind conditions near solar noon, and they have a margin of error of approximately ± 8%, based on the accuracy of the sensors used in the measurements (Appendix D).

4.2 Experimental Results

4.2.1 Thermal performance and photovoltaic module configuration

A major design goal of the PV/T system is to maximize the heat recovered from the PV modules using the techniques discussed earlier in this paper. Two types of PV modules, covering approximately the same area, were tested, and the thermal energy recovery of the system was calculated for comparison. Figure 4.2 shows how the large PV modules have an aluminum frame with a white module backsheet, whereas their smaller counterparts, made for this project, have a black frame and backsheet. The experiments were conducted between 12:00 and 13:00 hrs on April 17, 2008, for the large PV modules and April 16, 2009, for the small PV modules, under similar environmental conditions. The results indicate that at the high air collection rate (115 kg/hr/m^2), a 33% increase in thermal energy was achieved by using the small, darker PV modules (PV-covered UTC area decreased by 2.5%, and the overall solar absorptance of the PV modules increased by 7%).

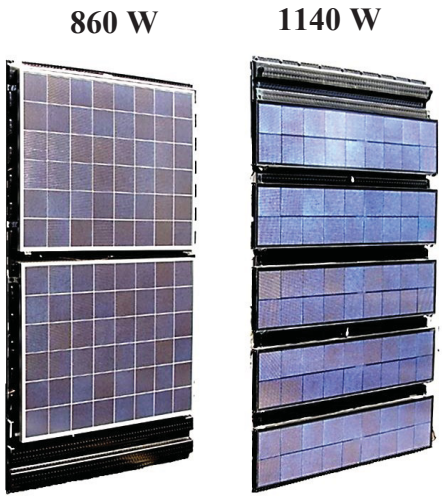

Figure 4.2: Comparison of the BIPV/T system thermal energy production using PV modules with an aluminum frame and white backsheet (left) to that of the custom-designed narrower PV modules with a black frame and backsheet (right).

4.2.2 Thermal performance and location of exterior air temperature

The UTC is an open-loop system in which the heat collected is proportional to the rise in temperature relative to ambient. Therefore, accurately measuring the temperature of the air entering this type of collector is crucial to predicting the efficiency of the system. However, this can be challenging, especially when the exterior air temperature is subjected to local heating by the ground, neighbouring structures, and the collector itself. This was the case for this experimental setup, which was located on a conventional roof, where the exterior air temperature was found to be up to 6°C warmer at the base of the BIPV/T installation than at the weather station located about 10 m above. The effect of both of these exterior temperature sensors on the calculated UTC thermal efficiency is demonstrated in Figure 4.3. An efficiency curve from the UTC manufacturer's published data (SolarWall, 2012) is shown as a reference.

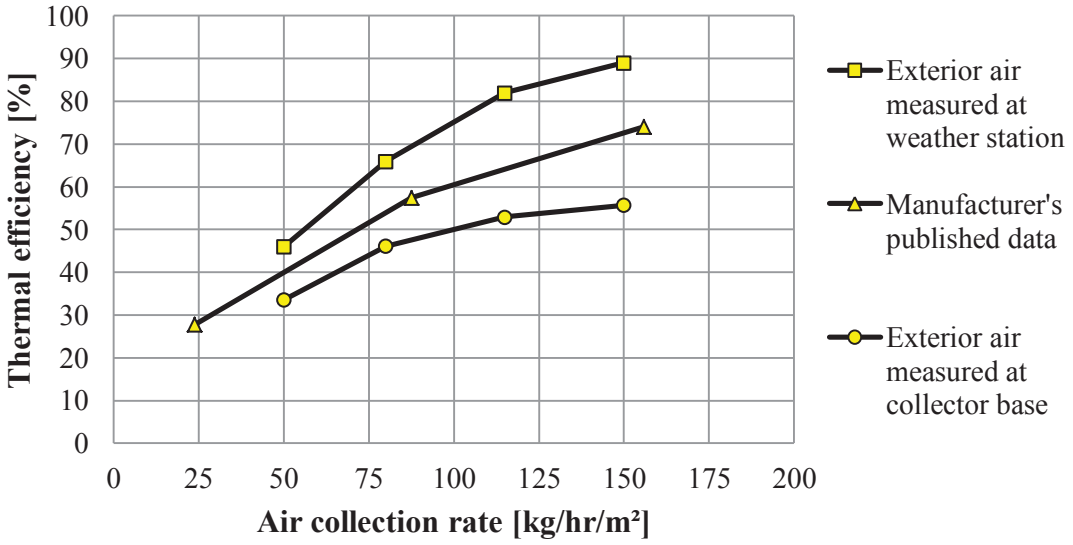

Figure 4.3: Comparison of UTC efficiency using two different exterior air temperature sensor locations and the manufacturer's published data.

Figure 4.4 shows that the BIPV/T combined efficiency (thermal and electrical) obtained using two exterior air temperature sensor locations. The lowest air collection (50 kg/hr/m²) rate yields a combined efficiency between 25% and 40% by taking the exterior air temperature reading at the collector base and the weather station, respectively. As the air collection rate increases to highest flow rate (150 kg/hr/m²), the size of the range increases, and the combined efficiency of the BIPV/T system lies between 35% and 70%. Once again, a range is given, due to the uncertainty of the exterior air temperature entering the collector. In future experiments, wind speed and exterior air temperature should be measured at the collector's mid-height and sufficiently away from the collector, so as not to be affected by the collector's thermal and velocity boundary layers. The results of these experiments prove that the developed BIPV/T system integrated with UTC is an effective way to convert solar energy into heat and electricity.

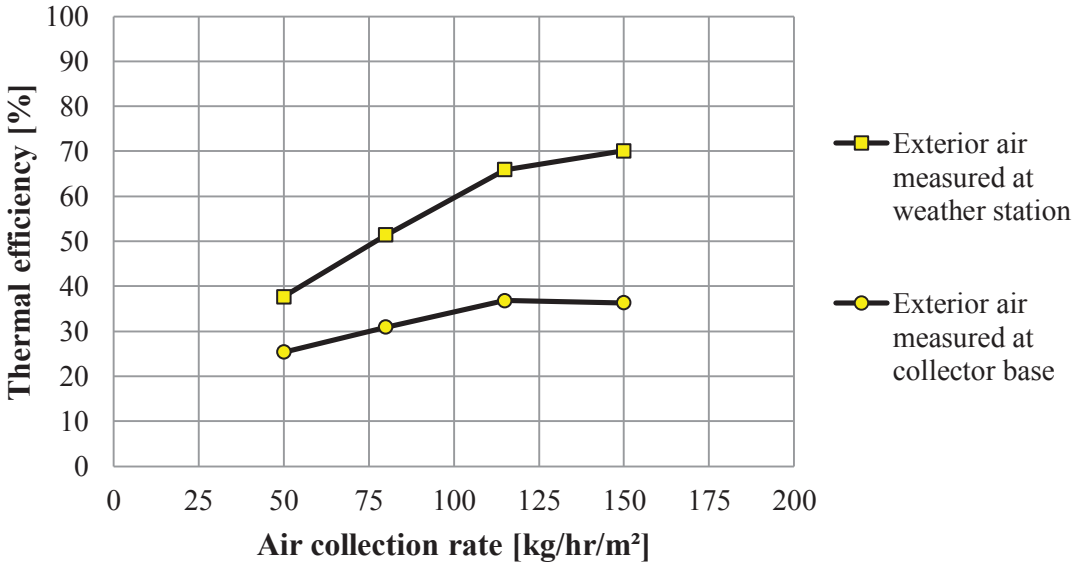

Figure 4.4: Comparison of the combined BIPV/T efficiency range (thermal plus electrical) obtained using two exterior air temperature sensor locations.

4.2.3 Photovoltaic cooling due to active air collection

One of the major goals of a properly designed BIPV/T collector is to have proper heat transfer between the UTC and the PV modules mounted on the surface. The UTC must be capable of extracting significant quantities of heat from the PV modules, in order to maintain a high thermal efficiency, and as a result, keep the core temperatures of the PV modules as low as possible. The infrared thermography images shown in Figure 4.5 demonstrate that the average temperatures of the PV modules were lowered by up to 7°C when the fan was functioning at the higher air collection (115 kg/hr/m²) rate, compared to when the fan was stopped. This indicates that the UTC does have an influence on the temperature of the PV modules and, more importantly, maintains favorable PV operating temperatures.

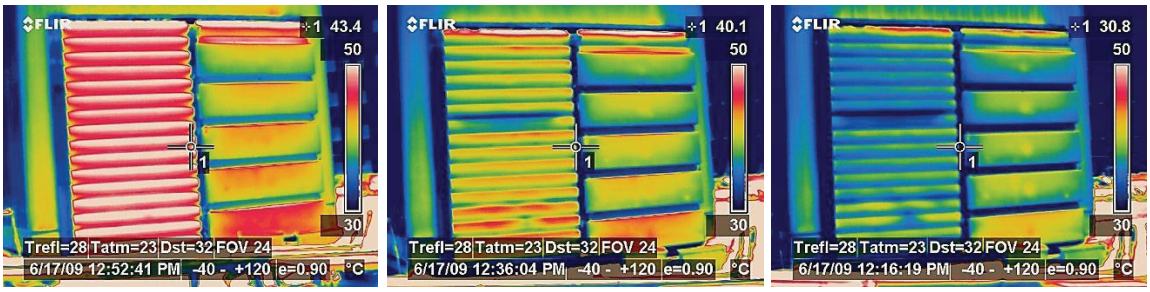

Figure 4.5: Infrared thermography showing the system without air collection (left) and with low (center) and high (right) air collection.

5. MEASUREMENTS AND ANALYSIS WITH DATA FROM A FULL-SCALE DEMONSTRATION PROJECT

5.1 Project Description

The ideas and results of the experimental prototype were used as a basis for the design of a full-scale BIPV/T system for a new office building—that of the John Molson School of Business (JMSB) at Concordia University, located in Montreal (45°N). The JMSB building was designed before the decision was made to install an active BIPV/T façade. A large portion of the Southwest façade (32° West of South) was well oriented for solar exposure, and it had neither windows nor major air intakes. This portion of the façade, 8 m high by 36 m wide, was also the exterior wall of the mechanical room. The fact that the large façade was well oriented, unshaded, and within close proximity to the mechanical system, were strong factors for the selection of this area for the installation of the BIPV/T system.

Essentially, from one vertical building surface with an area of 288 m², the system generates both solar electricity (up to 23.4 kW) which is used within the building, and solar heat (up to 100 kW) for preheating up to one-third (5.6 kg/s or 10000 cfm) of the fresh exterior air for the building occupants. The system replaces the building envelope of the near south-facing façade of the mechanical room, where its proximity to the fresh air intake reduces the need to build long ducts from the façade to the HVAC system. It utilizes 384 PV modules (the same PV modules used in the prototype) connected to five 5kW inverters. As in the experiment above, the UTC area covered by PV is about 70%. The developed mounting system was used to attach the PV modules so as to hinder solar-heated air from escaping from the cavity between a PV module top frame and the UTC.

The aesthetic integration of the solar façade with the building architecture is an important design criterion that was achieved, in part, by designing custom black-framed modules of the same width as the curtain wall sections below. In addition, the integration of BIPV/T systems on a vertical façade inherently eliminates snow accumulation and reduces the risk of water penetration, while receiving its highest solar irradiation during the winter months (up to 1000 W/m²), when heating is most useful. This BIPV/T system may also provide a model for retrofit applications, where a new BIPV/T façade can be constructed over the existing façade.

Figure 5.1: Conceptual drawing of Concordia University's John Molson School of Business building (left). The full scale BIPV/T demonstration project installed on its near-south-facing façade (right).

This BIPV/T demonstration project was partly funded by Natural Resources Canada's Technology Early Action Measures program, within the framework of the NSERC SBRN. It was also supported by L'Agence de l'efficacité énergétique. The project aims to reduce the energy footprint of buildings by turning static building envelopes into dynamic energy conversion systems, seamlessly integrated with the HVAC system of the building. The main project objective is the demonstration of a BIPV/T system, optimized for the Canadian climate, that maximizes energy recovery from a well-positioned building façade. The system's design took into consideration architectural integration, minimization of labour and material costs, ease of installation, and maximization of energy production. During this BIPV/T research project, various participants were involved during the different stages. The author was involved particularly at the early stages of commissioning during the startup of the system to ensured proper operation of all the BIPV/T data acquisition devices and the implementation of a database for the collection and analysis of the presented data.

Key project details:

- 288 m² BIPV/T collector replaces conventional façade
- Unshaded near South facing façade (32° W of S)
- Mechanical room directly behind BIPV/T collector
- Air collection preheats ventilation air (5.6 kg/s or 10000 cfm) by about 20°C
- 384 polycrystalline PV modules (65 W each) and 5 PV arrays
- UTC area covered by PV modules = 70%
- Peak solar electricity = 25 kW
- Peak solar heat = 100 kW
- Combined efficiency = 37-55%
- Annual electricity = 22 MWh
- Annual heat = 55 MWh

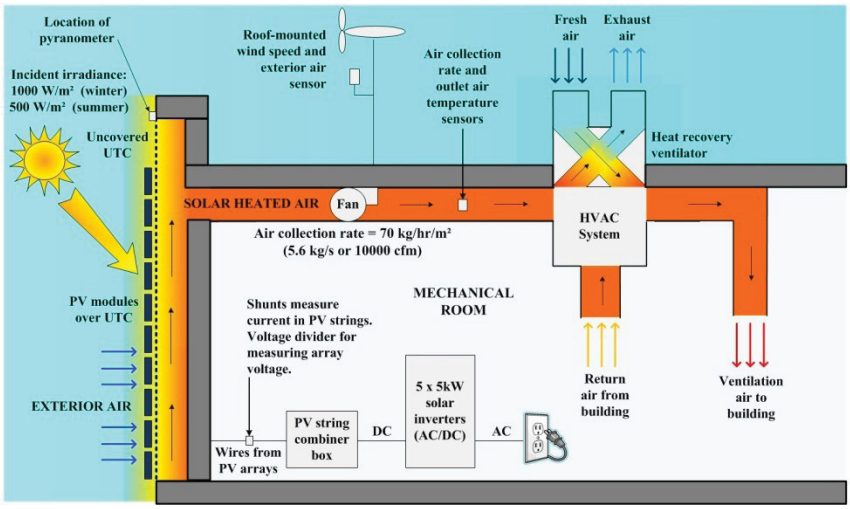

Figure 5.2: Schematic with details of the full-scale BIPV/T demonstration system.

5.2 Project Details

5.2.1 Architectural integration

The recently completed JMSB building site is a 16-story, high-rise commercial construction, located in Montreal in the centre of the downtown campus of Concordia University, at one of its busiest intersections—Guy and St. Catherine Streets. This prominent location is ideal for demonstrating a new concept that aims to change the way engineers and architects design buildings: to convert well-oriented building surfaces into electricity-and-heat-generating surfaces instead of passive components that lose heat in winter and gain it in summer. Indeed, the installed BIPV/T system is actually a part of the building's envelope, and not simply installed on top of it. Building integration of photovoltaic/thermal concepts can be accomplished most optimally during the early design stage, when the form of the building is being decided, along with the location of the mechanical room, with its HVAC and electrical service systems. The two essential elements for an optimal design are optimal orientation, proximity to the HVAC system, and integration with any and other energy systems planned.

The architects were closely involved with the integration work required to ensure the seamless integration of the BIPV/T system with the rest of the envelope and mechanical systems.

1. The PV modules are architecturally coordinated with the design of the façade, on the level of the material colours and texture (Figure 5.3). They were built the same width as the curtain walls, for architectural and aesthetic integration. Again, the PV modules were custom built to be narrow, with black frames and PV cell

backsheet, in order to create a visual integration of the product with the black UTC, while also increasing solar energy absorption and useful heat collection.

2. The mechanical room is behind the façade, which simplifies the technical installation. This is an important fact that architects and engineers have to take into account when designing for solar architecture. When using a BIPV/T façade for active air heating, it is important to reduce the length of ducting required, in order to make the system cost effective; otherwise, the ducting system and fan required may be more expensive than the PV modules. The JMSB BIPV/T system is part of the façade of the mechanical system floor of the building, thus resulting in an optimal, integrated design of the façade and the HVAC system.

Because the exterior cladding was replaced by the BIPV/T façade, costs associated with traditional building materials were avoided through architectural integration. In addition, the design of the system was intended to be such that the installation, due to its lack of complexity, would not be overly time consuming and could be left to existing construction trades, thereby avoiding the need for the costly services of specialists.

Figure 5.3: Street view of JMSB BIPV/T system (left) and close-up of BIPV/T area (right).

5.1.2 Envelope and structural design

Figure 5.4 illustrates the various structural and envelope layers for the BIPV/T system, in their order of installation. The first five layers consist of a typical steel framed wall and include the structural framing, thermal insulation, and interior/exterior cladding (including air and vapor barriers). The thermal resistance for the vertical wall is 4.4 °C·m²/W. The integration of the BIPV/T system requires the addition of "hat-clips" and "Z-bars," which create the air cavity and support structure for the overlaying horizontal UTC sheets. The PV modules are then installed over the UTC, with brackets aligned and fastened to the same vertical sub-structure of the UTC.

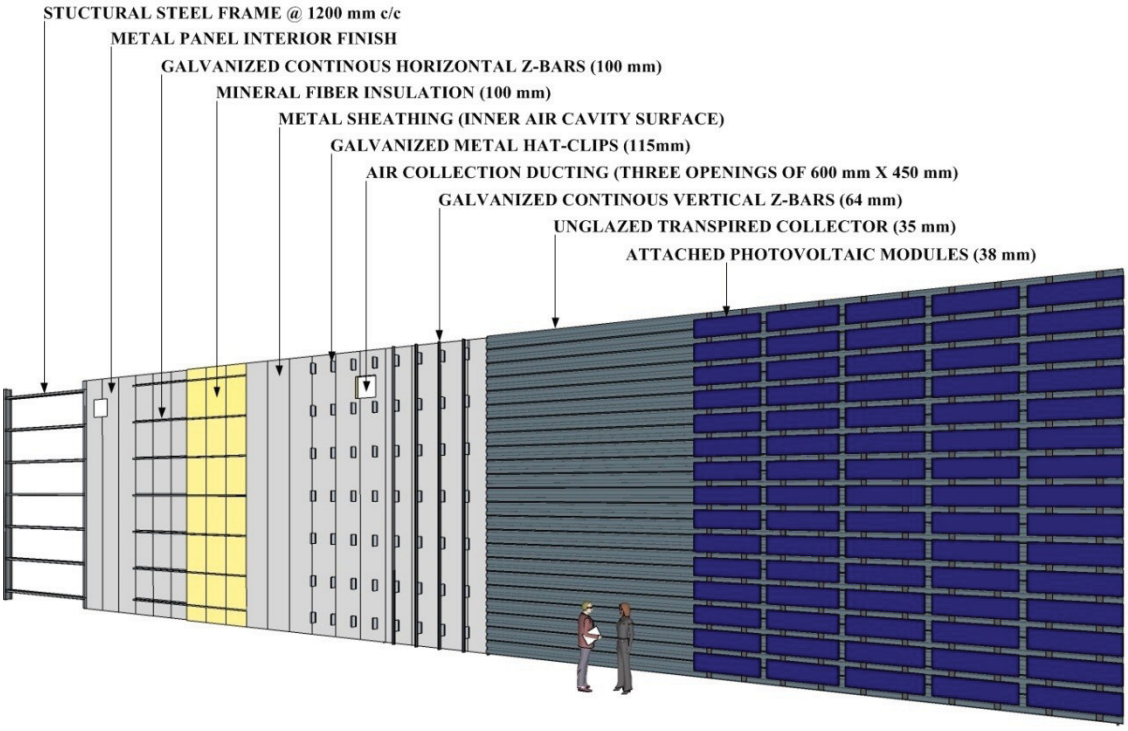

Figure 5.4: Schematic of the construction layers of the BIPV/T demonstration project.

5.2.3 Thermal design

High-efficiency solar heat and electricity generation were achieved by using several techniques explained earlier in the design concept (Chapter 3). Some modifications of the design for the demonstration project include having a top portion of the collector's façade left uncovered to promote buoyancy-driven cooling of both the air cavity and the PV modules in summer (Figure 5.3). Ideally, thermal energy produced in the summer could also be utilized for appropriate applications, such as heating water or for solar cooling systems.

5.2.4 HVAC design and system control

A centrifugal fan (Loren Cook Company – 330 SQN HP) is used to draw fresh outside air behind the relatively warm PV modules, and then through the perforated UTC sheet and into the air cavity. Three air collection ducts (600 mm x 450 mm) carry the preheated air from inside the cavity to the fresh air supply of the building's HVAC system. Figure 5.5 provides the location and details of the ductwork. The operating air collection rate is 70 kg/hr/m², or 5.6 kg/s (10000 cfm), for the entire 288 m² collector. The control system strategy is simple, because the preheated air from the BIPV/T system only represents about 1/5–1/3 of the total ventilation air required for the building. Knowing that preheating this amount of air by about 20°C (current preheating temperature rise) cannot change the total supply air temperature by more than 5°C, the fan can be controlled with the following algorithm: if the difference between the building's supply air set-point temperature and the exterior air temperature is greater than 5°C, draw 5.6 kg/s (10000 cfm) of fresh air through the solar façade; otherwise, turn the

fan off. The current control strategy is independent of the solar irradiation and will draw air through the installation even at night, recovering heat losses from the façade. In a future application, if the system could provide all the fresh air needs of the building by covering a larger surface area, then the air collection rate would be varied to achieve optimum temperature rise of the heated air.

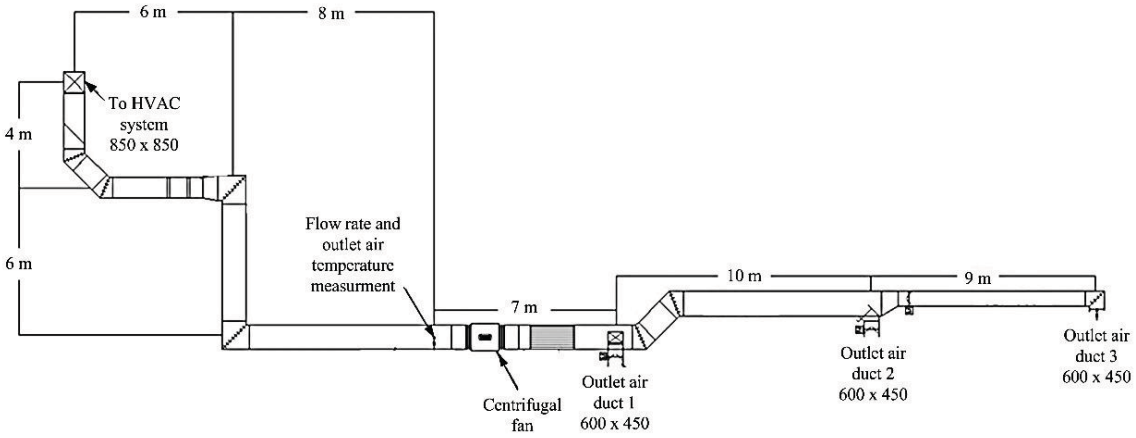

Figure 5.5: Ducting system for the collection of preheated air.

5.2.5 Electrical design

For the full-scale project, priority was given to electrical energy generation, as it can be used within the building all year-round. The collector area was 70% covered by PV, based on architectural and spatial constrains and the desire to have a top portion uncovered for natural cooling. The 288 m² of available façade area allowed for the integration of 384 MC18 polycrystalline PV modules (Figure 3.4) into strings and arrays that maximize electrical production.

Flash reports with electrical performance characteristics of each of the PV modules were sent to the SBRN from Day4 Energy. With this data, the assignment of the PV modules into the optimal string and array configuration was carried out. The SBRN team carefully designed the PV wiring arrangement to maximize the electrical performance. The major considerations include:

- PV modules mismatch losses - caused when PV modules wired in series are dominated by others that have a lower operating current. Strings with only 10 PV modules in connected in series (Figure 5.6) were chosen in order to minimize this effect. The PV modules were manually sorted and selected for each string, based on similar current characteristics.

- The vertical temperature gradient along the façade, which can reach above 10°C under low wind days, can have a notable impact on power output. The arrays were separated into a horizontal arrangement to minimize this effect.

- The inverter's voltage and power at maximum power point tracking. An iterative process was required to determine the optimal number of PV modules in each string, as well as ways to connect the strings together that matched the inverter specifications.

Figure 5.6 shows the wiring for a typical PV string, consisting of ten PV modules wired in series. Figure 5.7 shows the PV string assignment and array configurations for each of the five inverters, which convert the generated direct current (DC) into alternating current (AC) for use within the building. The PV system's electrical production is rated at 23.4kW, under STC (1,000 W/m² irradiance and 25°C cell temperature). Appendix C

provides the electrical characteristics of each string, sub-array, and array created for the project. Four of the five inverters (Inverters A–D) have an identical array configuration, containing 80 PV modules per array. Each of these arrays consists of two sub-arrays wired in parallel (each sub-array consists of four strings wired in series). The fifth inverter (Inverter E) is connected to one array (total of 54 PV modules). Each array consists of two sub-arrays wired in parallel (each sub-array consists of three strings wired in series), and each string consists of nine PV modules wired in series. Finally, ten PV modules are unconnected and used for experimental testing. In order to reduce the number of penetrations through the façade, the strings were "looped" so that both the positive and negative terminals would be near a hole.

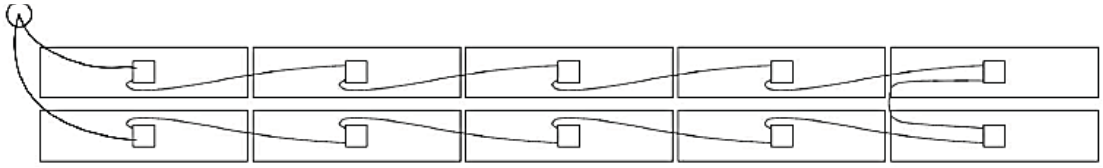

Figure 5.6: Typical string wiring of ten PV modules in series.

A1 A5	O	A2 A6	A3 A7	O	A4 A8	O	E1 E2
B1 B5	O	B2 B6	B3 B7	O	B4 B8	O	E3 E4
C1 C5	O	C2 C6	C3 C7	O	C4 C8	O	E5 E6
D1 D5	O	D2 D6	D3 D7	O	D4 D8	O	Experimental

Figure 5.7: Location of PV strings and arrays connected to each inverter (Note: The hollow circles represent penetrations in the building envelope for electrical wiring).

Schneider-Electric donated five Xantrex GT5.0 grid-tie solar inverters for the project. Table 5.1 provides the inverter manufacturer specifications, which shows they are up to 95% efficient. With a rated capacity of 5kW each, the total installed capacity is 25 kW. Figure 5.8 shows a typical combiner box, with the wires from each of the eight strings connected to each inverter and the installation inside the mechanical room.

Table 5.1: Inverter specifications

Max. AC Power Output	$Voltage_{mppt}$	Maximum Current	AC Output Voltage	Maximum Efficiency
5000 W	240-550 V	22 A	208 V	95.5 %

Figure 5.8: Wiring inside the combiner box (left). Xantrex inverter installation (right).

5.2.6 Project construction

Construction of the BIPV/T system began in 2008 and took approximately one year to complete, followed by a research commissioning stage until 2011. The organizations and companies presented in Table 5.2 worked together with the SBRN team to develop the BIPV/T installation, which is capable of being installed and maintained by traditional building trades. Construction photos of the BIPV/T system are shown in Figure 5.9.

Figure 5.9: Construction sequence for the full-scale BIPV/T demonstration project.

Table 5.2: Organizations and companies involved with the BIPV/T demonstration project

Organization/Company	Description
Solar Buildings Research Network (SBRN)	NSERC Strategic Research Network. Expertise in theoretical and experimental optimization of BIPV/T systems.
Conserval Engineering	Supplier of SolarWall® and mounting hardware.
Day4 Energy	Supplier of custom PV modules MC18.
Schneider-Electric	Donation of Xantrex GT5.0 Grid Tie Solar inverters.
Genivar	Consulting engineers representing Concordia University for the project management of the JMSB building.
KPMB/FSA Architects	Architects for the JMSB and EV building. KPMB architects of Toronto partnered with FSA architecture of Montreal.
Concordia University	Responsible for the operation and maintenance of the BIPV/T system.
Teknika-HBA	Mechanical and electrical engineers. Responsible for ducting, fan, and other equipment downstream of UTC air collection ductwork. Also responsible for AC electrical design after the inverters.
Regulvar	Building controls. Responsible for the sensors, dampers, and connection of research equipment to network.
Revêtement RHR	Installers of the exterior cladding, including UTC and PV modules. Made black bracket covers and modifications to brackets.
Laurentien Electrique	Electricians. Carried out complete electrical installation, including inverters, and connections of PV.
J.P. Lessard	Mechanical installers (ducting).
Matrix Energy	Verification of PV system design. Supplier of combiner boxes and DC breakers.
National Instruments	Supplier of CompactRIO DAQ and LabVIEW software.
Campbell Scientific	Distributors of Kipp and Zone products and their own DAQ hardware and software (used for rooftop weather station).
Tyco Electronics	PV connectors and wire.

5.3 Instrumentation, Measurement, Monitoring, and Analysis

The full-scale BIPV/T installation has a state-of-the-art monitoring system. The collected raw data from over 80 sensors is stored in a database that is accessible remotely via a SBRN web page. In addition, over 20 equations automatically calculate and store quantities of interest, such as the thermal efficiency, and multiple alarms are programmed

to notify the user of any irregular activity. A summary of important measured values for the full-scale project is provided in Table 5.3.

The data acquisition system is made up of three CompactRIOs by National Instruments. Together, the three CompactRIOs collect all the data, except for the weather station data. The CompactRIO chassis uses NI 9205 and NI 9211 modules to convert the analog voltage signal from the sensor into a digital signal that can be stored. The Compact RIOs take data readings every five seconds and store the average for each minute in internal memory.

A weather station, complete with SOLYS 2-Axis Solar Tracker, was installed on the roof of the JMSB building to collect weather data. The data collected by the weather station includes diffused horizontal irradiance, direct beam irradiance, wind speed and direction, exterior air temperature, relative humidity. In addition, a pyranometer was installed on the vertical façade to measure incident solar irradiance. The weather station uses a CR1000 by Campbell Scientific as its DAQ system, which takes data readings every five seconds and stores the minute-average in its internal memory.

The outlet air temperatures are monitored by Regulvar (the building controls contractor) in each of the three air collection duct outlets and just downstream from the fan, where the air collection rate is also monitored (Figure 5.5). Regulvar shares their data readings with the SBRN by feeding the sensor readings to the installed CompactRIO DAQ. The ducting is covered by standard 50 mm mineral wool insulation to reduce heat transfer to or from the pre-heated air. The air cavity, which has a depth of 175 mm, was fitted with nine air cavity sensors located in the center of the cavity and equally spaced

along the collector, in order to monitor air collection uniformity. The average PV temperature was taken as the average of the temperatures of six PV modules, spaced equally along the vertical centerline of the BIPV/T façade. The PV module thermocouples are located in the vertical centerline of each PV backsheet, about one-quarter of the length from the side-frame. Again, the measurements were taken under clear-sky days near solar noon, and they have a margin of error of approximately ± 8%, based on the accuracy of the sensors used in the measurements (Appendix D).

The current of each string and the voltages of each of the five inverter arrays are also monitored. Shunt resistors supplied by Canadian Shunt Industries are used to accurately and unobtrusively measure the string currents. The shunts are installed on every array extension wire and located before the combiner boxes. The PV array voltage was measured at the string combiner box using voltage dividers, which step-down the voltage by 60 times, so that it can be read by the 0–10V voltage input of the CompactRIOs.

Every five minutes, the Monitored Site Data Manager (MSDM) fetches new data from the three CompactRIOs and from the CR1000, and stores it on the SBRN server. As a result, the data is stored on the SBRN server and in the internal memories of the CR1000 and of the CompactRIOs, which is limited. Some of the variables in the database are not measured, but are calculated using equations based on raw data. The SBRN created the MSDM as a means of enabling users to access the data collected at the JMSB and at its other demonstration project sites.

Table 5.3: Summary of important measured values for the demonstration project

Parameter Measured	Instrument	Unit	Accuracy
Outlet Air Temperature	T-Type Thermocouples by Omega	°C	± 0.3°C
Air Cavity Temperature	T-Type Thermocouples by Omega	°C	± 0.3°C
PV Module Temperature	T-Type Thermocouples by Omega	°C	± 0.3°C
Air Collection Rate	GTA 116 Analog Transmitter by Ebtron	kg/hr	± 5% of reading
DC Voltage	Voltage divider (60x array voltage step-down)	V	± 1% of reading
DC Current	Shunts by Canadian Shunt Industries (10A, 100mV)	A	± 2% of reading
Exterior Air Temperature	T-Type Thermocouples by Omega	°C	± 0.3°C
Solar Irradiance	Pyranometer by Li-Cor (model LI-200SA)	W/m^2	± 5% of reading
Wind Speed	R.M Young Wind Monitor by Campbell Scientific	m/s	± 5% of reading
Wind Direction	R.M Young Wind Monitor by Campbell Scientific	° (0° North)	± 5% of reading

In the lobby of the JMSB, a display screen allows the public to see the operating conditions, current energy output, and accumulated energy output of the BIPV/T demonstration project. Real-time data is taken from the SBRN database, and then processed by a computer on Concordia's server, to create an XML file that is suitable for input to the public display. In addition, commemorative plaques have been installed in the JMSB lobby and mechanical room to educate the general public on how the façade integrated solar system works and to honor the contribution of the individuals and organizations involved in its design and construction.

The thermal, electrical, and combined efficiency of the full-scale BIPV/T system was calculated using the collected raw data and equations 8–14, where the collector and PV areas are taken as 288 m² and 196.7 m², respectively. The actual electrical efficiency of the PV system was measured, but it also can be estimated for comparison using

theoretical equations. The theoretical electrical efficiency of the PV modules, η_{PV_theo} in %, as a function of their temperature, T_{PV} in °C, is given by (Skoplaki and Palyvos, 2009)

$$\eta_{PV\_theo} = \eta_{stc} \cdot [1 - \beta_{PV} \cdot (T_{PV} - T_{STC})] \tag{15}$$

where

β_{PV} = 0.46%/ºC (PV module temperature coefficient)
η_{stc} = 12.5% (PV module efficiency at standard test conditions)
T_{stc} = 25 °C (PV module cell temperature at standard test conditions)

The theoretical electrical power produced by the PV modules, E_{PV_theo} in W, as a function incident of solar irradiance, I_{solar}, in W/m², and the total PV area, A_{PV} in m², is given by

$$E_{PV\_theo} = I_{solar} \cdot A_{PV} \cdot \eta_{PV\_theo} \tag{16}$$

As discussed earlier, wind speed and direction on open-loop solar collectors is known to affect thermal efficiency, and it is investigated further in this chapter. Figure 5.10 shows the location of the anemometer sensor, which measures wind speed and direction, on the JMSB rooftop. When winds blow normal to the façade (direction about 210º, where 0° is North), there is generally a stagnation point at around 2/3 of the building height, where the top portion of the air flow moves upward along the upper section of the façade and produces a wind that is more or less parallel to the BIPV/T system. Generally, when the upward airflow rises above the top of the collector and travels above the roof, a recirculation region is created, which causes the readings of the rooftop anemometer to be erroneous. Thus, the wind data measured by the rooftop anemometer are seldom representative of the "freestream" airflow, which assumes no building interference. In addition, there is a wall located about 3 m North of the

anemometer that is taller than the height of the anemometer; as a result, wind directions between about 300º and 120º cannot be measured. Instead, the wind speed and direction on the BIPV/T façade is estimated using hourly averaged data collected by Environment Canada at the Montreal-Pierre Elliott Trudeau international airport (National Climate Data and Information Archive, 2012).

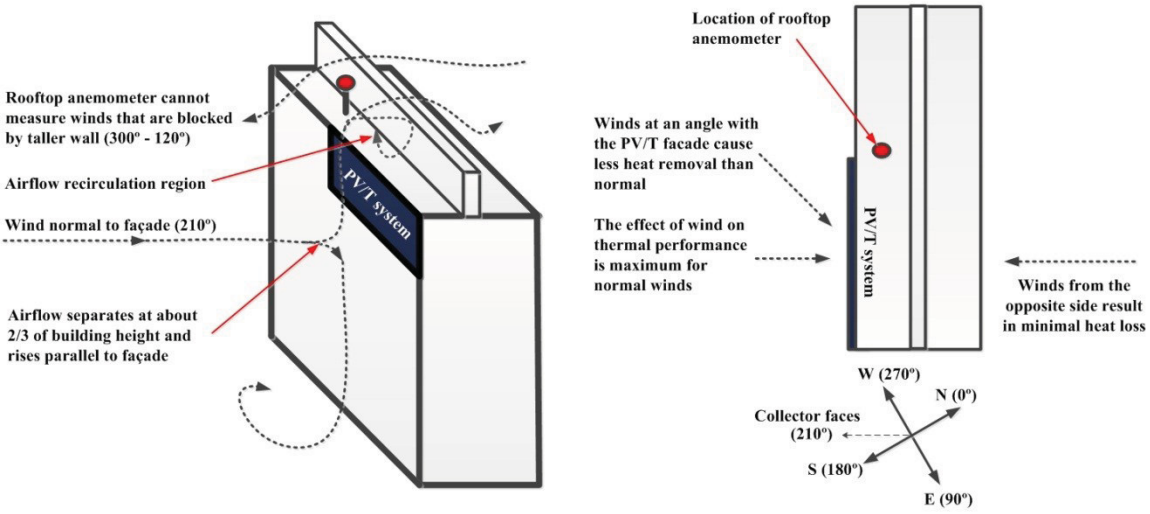

Figure 5.10: Schematic showing airflow around the JMSB building (left); Aerial view of the JMSB roof and the airflow directions.

The anemometer used at the Montreal airport is located 36 m above the ground, whereas the JMSB collector's mid-height is located about 50 m above the ground. The following equations are common in wind engineering and were used to find the adjusted wind speed on the collector mid-height for an approximate comparison with that measured by the JMSB anemometer. The wind speed measured at the Montreal airport, $V_{airport}$ in m/s, is first adjusted to the atmospheric gradient level, $V_{gradient}$ in m/s, using the wind profile power law relationship:

$$V_{gradient} = \frac{V_{airport}}{\left(\frac{Z_{airport}}{Z_{gradient}}\right)^{\alpha_{flat\_open}}} \tag{17}$$

where

$V_{gradient}$, in m/s, is the wind speed at the atmospheric gradient height.

$V_{airport}$, in m/s, is the wind speed measured at Montreal international airport.

$Z_{airport}$, in m, is the height above ground for airport wind speed measurement (36 m).

$Z_{gradient}$, in m, is the atmospheric gradient height for flat, open terrain (275 m).

α_{flat_open} is the exponential coefficient for neutral air around flat, open terrain (0.15).

Solving for wind speed at gradient height ($V_{gradient}$), the power law is reused now for Montreal downtown conditions:

$$V_{anemometer} = V_{gradient} \cdot \left(\frac{Z_{freestream}}{Z_{gradient}}\right)^{\alpha_{city}} \tag{18}$$

where

$V_{anemometer}$, in m/s, is the "freestream" wind speed measured by an anemometer located at collector mid-height.

$V_{gradient}$, in m/s, is the previously calculated wind speed at the atmospheric gradient.

$Z_{anemometer}$, in m, is the height for anemometer wind speed measurements (50 m).

$Z_{gradient}$, in m, is the atmospheric gradient height for cities (400 m).

α_{city} is the exponential coefficient near the JMSB building in the city of Montreal (experimentally determined in Concordia's Aerodynamics Laboratory to be 0.31).

The results presented further use the adjusted wind speed, $V_{anemometer}$, in order to be representative of an anemometer measuring "freestream" winds at the collector's mid-height. Wind direction measured at the airport was found to have sufficiently good agreement with downtown and is reported unadjusted throughout.

5.4 System Performance

5.4.1 Thermal performance

The temperature inside the air cavity provides insight on the airflow uniformity that can be achieved across the large surface of the BIPV/T collector. Figure 5.11 presents the air cavity and outlet air temperatures for both low (2.3 m/s) and high (7.3 m/s) wind speed conditions. The rightmost duct outlet air temperature is higher compared to the two others, indicating that less air is being drawn inside by this particular duct. This is most likely due to the unequal friction losses within the duct design (the right duct is the farthest from the fan). Despite this, the air cavity temperatures show that a more or less equal air cavity temperature distribution exists, and thus, it is assumed for analysis that uniform airflow conditions exist across the BIPV/T system.

Table 5.4 presents data taken when the BIPV/T system experiences sunny, clear-sky conditions and low wind conditions around solar noon. The first four days present conditions where the wind is blowing at a normal angle to the collector, whereas the three bottom days show the typical effects observed for other wind directions of interest. The first two days show an example of when there is good agreement between wind direction measured on the roof and that of the airport. This suggests that wind directions taken at the airport and adjusted for the JMSB building in downtown Montreal can correctly represent actual conditions when the recirculating effect is minimal. The third and fourth days show a situation where the façade is again experiencing normal winds, but the rooftop-mounted anemometer does not measure the correct wind direction. This effect is likely due to the recirculating region explained earlier (Figure 5.10). Based on the

presented typical data, the thermal efficiency of the BIPV/T system, operating at the air collection rate of 70kg/h/m², is 40–45% when low winds blow normal to the collector.

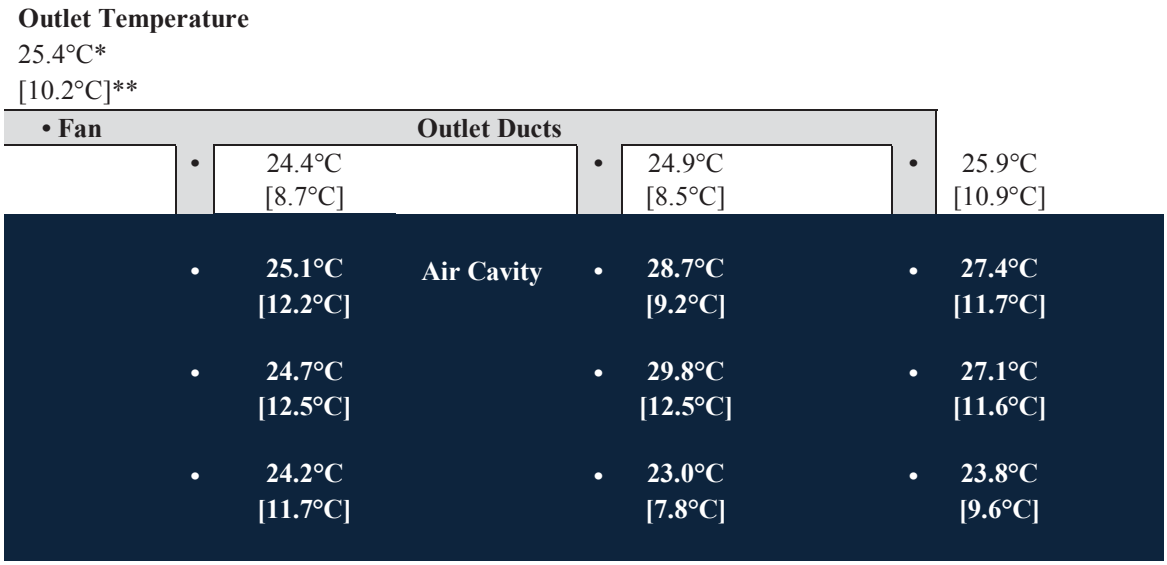

Hourly average of data collected at 13:00–14:00 hrs.
*07/04/2011, Wind speed (direction): 2.6 m/s (210º), $T_{exterior}$: 8ºC, I_{solar}: 753 W/m², m_{air}: 70 kg/hr/m².
**27/03/2011, Wind speed (direction): 7.3 m/s (260º), $T_{exterior}$: -3.2ºC, I_{solar}: 853 W/m², m_{air}: 67 kg/hr/m².

Figure 5.11: Conceptual elevation view of the BIPV/T collector showing the temperature distribution within the air cavity and the ducting system during low* and high** wind conditions.

From a thermal perspective, normal winds (collector faces 210º) provoke the highest heat removal for the BIPV/T system. As the angle of attack increases by shifting west or east, the lessened effect of the wind on heat removal effect can be observed. For example, on March 30 and December 18, off-normal winds yielded thermal efficiencies up to 50%, representing at least a 5% increase, compared to the first four days, when winds were normal to the collector (Table 5.4). Directions between about 300º and 120º approach the building from behind, which generally results in higher thermal efficiencies than during the critical normal direction. The last day presented in Table 5.4 demonstrates this case, where a thermal efficiency of 47% is found for winds blowing at an angle of 350º.

Table 5.4: Effect of wind direction on thermal performance

Date	Wind Direction* Measured at Airport [º]	Wind Direction* Measured on Roof [º]	Thermal Efficiency [%]	Adjusted Wind Speed Measured at Airport* [m/s]	Wind Speed Measured on Roof [m/s]	Incident Solar Irradiance [W/m²]
22/04/2011	210	210	41.3	1.2	0.8	705
19/04/2011	190	189	42.8	1.2	1.2	718
15/03/2011	210	145	39.9	1.4	0.8	879
07/04/2011	200	135	45.1	3.4	1.0	759
30/03/2011	270	103	48.5	3.0	1.0	818
18/12/2011	120	211	51.1	1.2	0.6	812
15/04/2011	350	152	47.2	1.8	0.8	756

Hourly average of data collected during 12:00–15:00 hrs, m_{air} range: 67-71 kg/hr/m².
*Wind direction: 0º is North and clockwise, positive (collector faces 210º)

In general, the thermal energy collected by BIPV/T systems is strongly influenced by the air collection rate (typical range is 50–150 kg/hr·m²). As shown in table 5.5, the BIPV/T demonstration project preheats fresh air by up to 20°C, at an operating air collection rate of 70 kg/h·m² (about 5.6 kg/s). The exterior wind conditions have a significant influence on the amount of heat collected by the BIPV/T system. In order to quantify this effect, days with different wind speeds (and when the wind was blowing normal to the collector) were selected and presented in Table 5.5 for analysis. It was found that when wind conditions change from low to high, the thermal efficiency can decrease by up to 15% (from 30% to 45%). Thus, wind can reduce the amount of heat collected by up to 33%, and therefore, must be considered by designers in order to accurately predict BIPV/T energy production.

Table 5.5: Effect of wind speed on thermal performance

Date	Thermal Efficiency [%]	Wind Speed [m/s]	Incident solar Irradiance [W/m²]	Exterior Air Temperature [°C]	Preheated Air Temperature Rise [°C]
27/03/2011	29.5	7.3	853	-3.2	13.4
20/01/2012	35.9	5.9	894	-14.9	15.8
12/12/2011	37.2	4	789	5.3	14.8
29/03/2011	37.8	3.8	798	3.7	15.6
15/03/2011	39.9	1.4	879	6.1	17.7
15/01/2012	41.6	4	892	-15.5	18.5
07/04/2011	45.2	2.4	753	8	17.4
20/12/2011	45.7	3.7	843	-4.2	19.6

Hourly average of data collected during 13:00–14:00 hrs, Wind direction: 210-280º, m_{air} range: 67-72 kg/hr/m².

5.4.2 Electrical performance

The PV system's electrical performance depends mainly on available solar radiation and the exterior air temperature. In winter, colder air temperatures allow the system to operate at a higher electrical efficiency. Meanwhile, the solar altitude is also at its lowest during the cold months, providing higher incident solar irradiance on the system (about 1000W/m² in winter, compared to 500W/m² in summer). The combined effect of colder operating temperatures and high insolation allows peak production on vertical façades to occur in winter.

Table 5.6 provides the PV surface temperature gradient along the collector's vertical centerline. The first two days (June 1 and June 15) have almost identical wind direction, exterior air temperature, and incident solar irradiance, which allows for a fair comparison of the impact of higher winds. Both days have almost uniform PV temperatures, inferring that wind speed does not cause significant PV temperature gradients for near-normal winds. However, the higher wind does reduce the average PV temperature by about 10°C (from 51°C to 39.9°C). The third day (September 26) has low

winds blowing from the North (winds approaching from the opposite side of the collector). As discussed earlier, this direction provokes minimal heat loss on the façade, which is confirmed by noticing a gradient of the PV module temperature of almost 10°C. The temperatures of the PV modules reached their recorded maximum of up to 70°C on this day, when the fan was turned off. This confirms that distributed inlet BIPV/T technology is a suitable design for preventing PV module overheating. Due to this vertical temperature gradient, an electrical production difference of 100 W (from 3247 W to 3342 W) was observed between the top and bottom arrays.

Table 5.6: PV temperature distribution for warm days when the fan is turned off

Date*	**15/06/2011**	**01/06/2011**	**26/09/2011**
Wind Speed [m/s]	3.4	9.9	1.8
Wind Direction [°]	230	230	340
Ambient Temperature [°C]	30.1	29.1	25.9
Incident Solar Irradiance [W/m²]	456	453	771
Height from Collector Base [m]	**PV Temperature along Collector Height [°C]**		
7.0	51.4	39.3	69.3
5.6	51.9	39.1	66.3
4.3	51.9	39.7	65.1
3.0	50.9	39.6	62.1
1.6	50.5	39.9	60.4
0.3	49.7	41.8	60.7
Average PV Temperature [°C]	51.0	39.9	64.0

*Hourly average of data collected during 12:00–16:00 hrs

The effect of PV operating temperature on electrical performance was assessed by comparing production on extreme cold and warm days. As shown in Table 5.7, electrical energy production increases by nearly 30% (net electrical efficiency from 10.2% to 13.1%) when the average PV temperature decreases by 50ºC (from 64ºC to 13ºC). The electrical efficiency obtained using equation 15 compares well with the measured data and, therefore, can be used for predicting the PV system's performance.

Table 5.7: Electrical efficiency of the PV system

Date	Electrical Efficiency (Eq. 15)** [%]	Typical Array Power [W]	Typical Array Current [V]	Typical Array Voltage [A]	Incident Solar Irradiance [W/m²]	Ambient Air Temp. [°C]	Average PV Temp. [°C]
26/09/2011*	10.2 (10.3)	3295	11.3	292	771	25.9	64.0
06/06/2011	11.2 (11.3)	2016	6.4	315	457	26.6	46.5
22/12/2011	12.1 (12.1)	3998	11.8	339	780	2.9	32.3
20/01/2012	13.0 (13.2)	4900	13.3	368	894	-14.9	13.2

Hourly average of data collected during 12:00–15:00 hrs, Wind speed (direction): 1.8-5.9 m/s (190-240º), m_{air} range: 67-72 kg/hr/m².
*Fan is off and wind direction is 0º (North)
**Estimated electrical efficiency using equation 15 (for comparison)

Table 5.8 presents the initial electrical production, measured from each of the five 5 kW inverters. The 95% inverter efficiency reported by the manufacturer is confirmed.

Table 5.8: Inverter performance

Inverter #	Voltage [V]	Current [A]	DC Power [W]	AC Power [W]	Inverter Efficiency [%]	DC Efficiency [%]	AC Efficiency [%]	Average PV Temp. [°C]
Inverter A	341.3	13.0	4432	4199	94.7%	11.2%	10.7%	36.3
Inverter B	340.1	13.0	4404	4187	95.1%	11.2%	10.6%	34.9
Inverter C	338.6	13.0	4414	4187	94.9%	11.2%	10.6%	34.4
Inverter D	339.2	13.1	4427	4208	95.1%	11.2%	10.7%	35.2
Inverter E*	465.2	6.6	3062	2916	95.2%	11.5%	11.0%	34.6
	Total/Average		**20738**	**19697**	**95.0%**	**11.3%**	**10.7%**	**35.1**

Date: 24/11/2010, 15-minute average of data collected every three minutes during 13:00–13:15 hrs, Wind speed (direction): 6.3 m/s (280º), $T_{exterior}$: 1.0ºC, I_{solar}: 937 W/m², m_{air}: 55 kg/hr/m²
*During this period, this inverter was connected to six strings in series containing seven PV modules each. The design was later changed to a parallel connection, reducing the voltage.

Figure 5.12 shows the electrical energy produced by the PV system during clear, sunny days that are representative of each season. Peak electrical production of 23 kW is recorded on cold winter days, when solar irradiation levels reach nearly 900 W/m². Electrical output is lowest in the summer months, when the warmer exterior air temperatures and the high solar altitude limit production on the near-south-facing BIPV/T

façade (32º West of South). The data presented in Table 5.9 indicates how daily electrical energy generated in winter (up to 130 kWh) can be as much as double that of summer, while simultaneously collecting up to 700 kWh of heat per day for preheating the building's ventilation air. The power required to operate the centrifugal fan was determined, from the manufacturer's fan curve, to be about 1.1 kW (daily operating consumption under 30 kWh) and, therefore, represents only a small fraction (under 5%) of the total energy collected during the day.

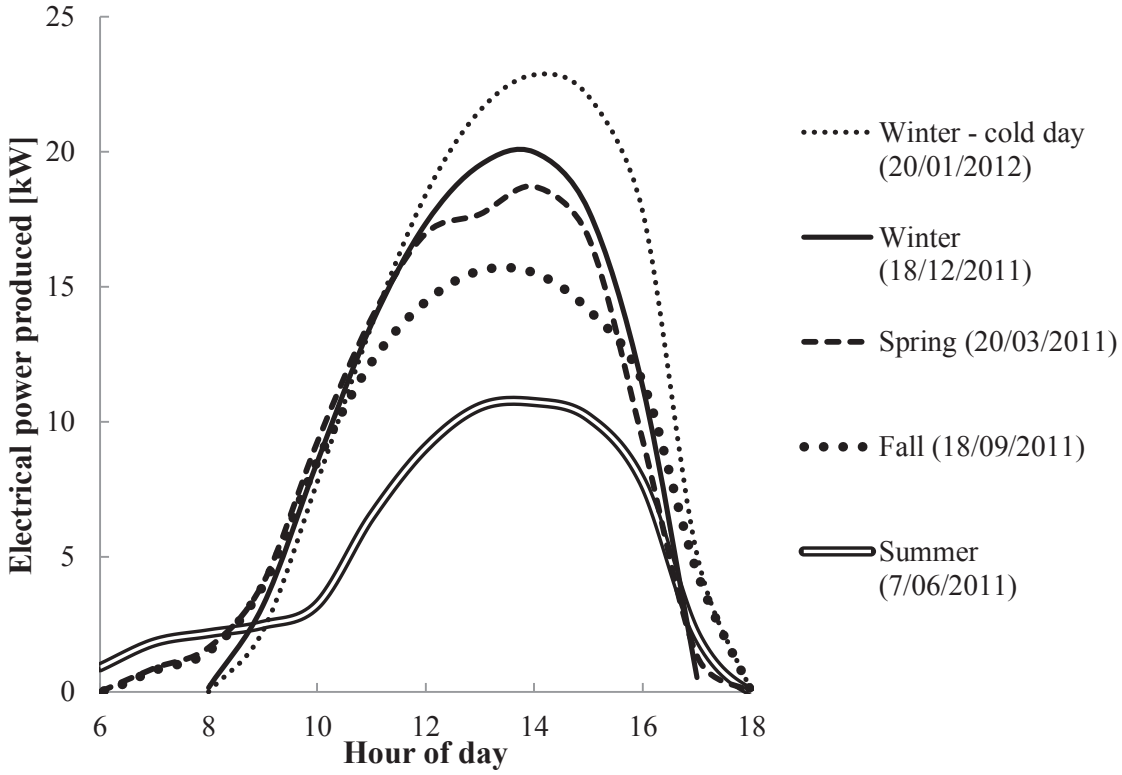

Figure 5.12: Clear-sky daily electrical energy production for each season of the year.

Table 5.9: Daily energy production of the BIPV/T system in various seasons

Representative Season	Date	Peak Solar Irradiance [W/m²]	Ambient Temp.* [°C]	PV Temp.* [°C]	Wind Speed (Dir.)* [m/s]	Electrical Energy Generation [kWh/day]	Thermal Energy Collection [kWh/day]
Spring	20/03/2011	853	4.9	36.8	3 (190°)	110	563
Summer	10/06/2011	523	23.3	49	0.8 (360°)	68	fan off
Fall	18/09/2011	761	20.3	53.7	1.4 (110°)	103	fan off
Winter	18/12/2011	841	-6	29.3	4 (250°)	112	734
Winter (cold day)	20/01/2012	894	-14.9	13.2	5.9 (270°)	131	589

*At peak solar irradiation occurring during 13:00–15:00 hrs.

5.4.3 Annual thermal and electrical energy production

The demonstration project was monitored beginning January 1, 2010. However, during the project start-up and commissioning process, different monitoring devices were out of service, and some data is missing. A full year's data was successfully recorded for every minute of the year from March 31, 2011, until April 1, 2012.

Figure 5.13 shows the monthly energy produced by the full-scale system during this one-year period. The monthly electrical production varies between 1200 and 2000 kWh and remains relatively constant during the year, whereas thermal energy production varies according to the building's fresh air demand, and peaks at about 12000 kWh in February. From the 288 m² BIV/T collector, the annual production of solar electricity and useful heat was 20 MWh and 55 MWh, respectively.

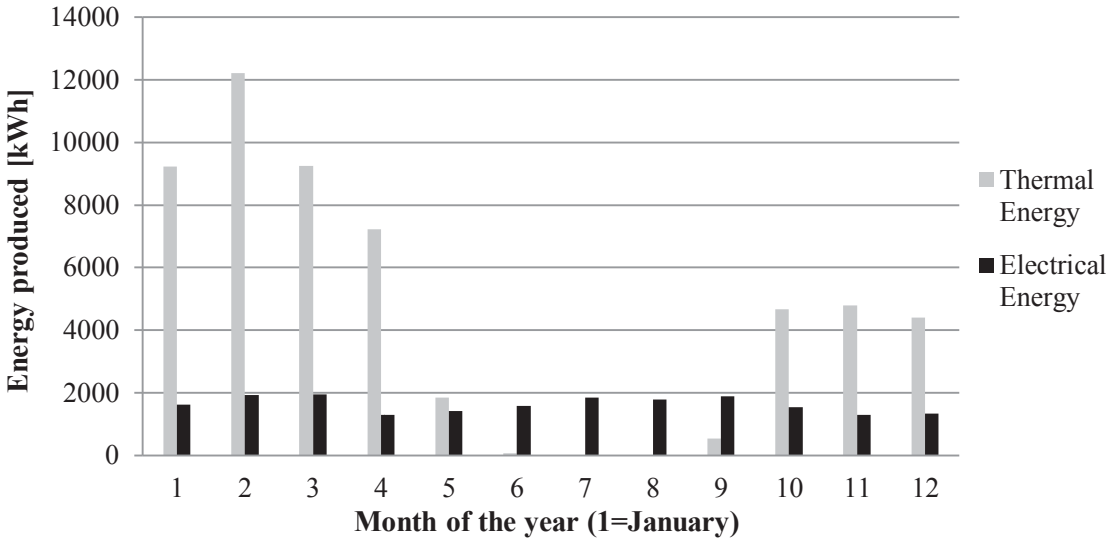

Figure 5.13: Monthly thermal and electrical energy generation (01/04/2011 – 31/03/2012).

5.4.4 Overall system efficiency

Table 5.10 summarizes the combined (thermal plus) electrical efficiency range measured for the BIPV/T demonstration project. Combined efficiencies of 37–55% demonstrate the potential for this technology to generate significant energy onsite, from well-oriented building façades.

Table 5.10: Efficiency range of the BIPV/T demonstration project

Efficiency*	Low Wind/Cold Day	High Winds/Warm Day
Thermal	46%	30%
Electrical	13%	10%
Combined	**55%**	**37%**

Data was extracted from Tables 5.5 and 5.7.
*At the operating air collection rate of approximately 70kg/hr/m²

6. EXPERIMENTAL TESTING IN A SOLAR SIMULATOR

The Concordia University solar simulator - environmental chamber (SSEC) laboratory (Figure 6.1) is an indoor research facility designed to emulate outdoor weather conditions (solar radiation, exterior air temperature, wind, etc.) in order to provide a fully controlled and monitored environment for research, development, and testing of solar energy applications and advanced building envelopes.

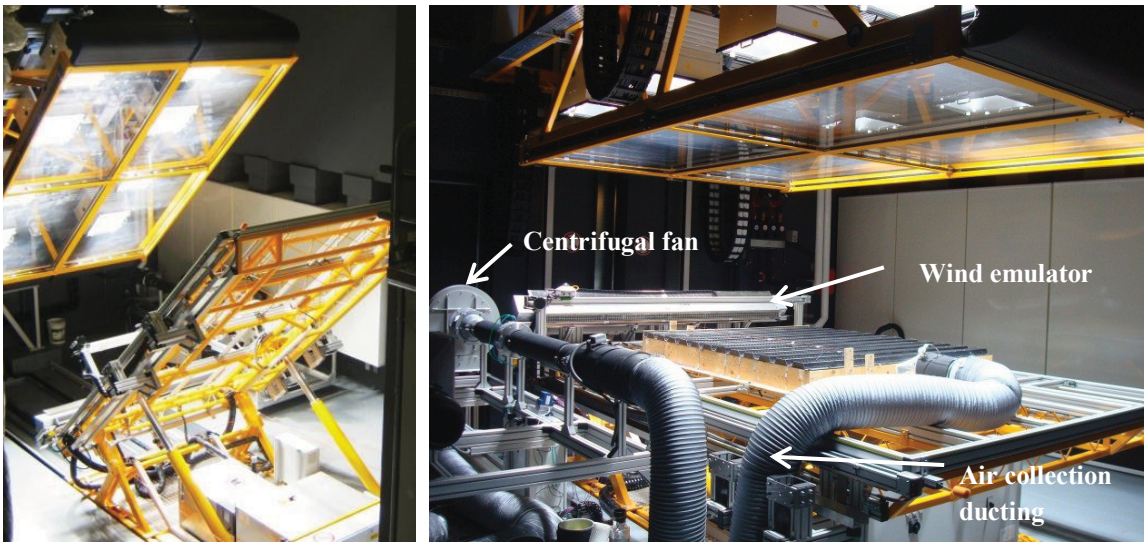

Figure 6.1: Solar simulator lampfield and test platform under 45° angle (left). Horizontal testing of the UTC system in the solar simulator (right).

The solar simulator is designed to emulate sunlight and wind conditions under room ambient temperatures (20–25°C) in order to test various solar systems, such as PV modules, solar air and liquid collectors, BIPV/T systems, building envelope systems, and more. The solar systems tested can be mounted on a 1-axis rotational test platform that can be tilted at any angle between horizontal (0°) and vertical (90°) position within accuracy of 1°, while maintaining constant irradiance levels and uniformity. Depending on the test conditions required, the dimensions of solar systems tested under the solar

simulator can be up to 2.4 m x 3.2 m. The solar simulator consists of two main components: 1) the test platform, where the solar system is mounted, and 2) the lampfield, which emulates sunlight and under which the test platform is exposed. The solar simulator can be used for steady-state as well as cycling (temperature, wind, and irradiance) test conditions.

The lampfield uses a set of eight metal halide global (MHG) lamps, with a total peak power output of 36.8 kW. The MHG lampfield produces a dense multiline spectrum of rare earth metals similar to the air mass 1.5 spectrum defined by EN 60904-3. This provides a spectral distribution very close to natural sunlight and fulfils the specifications of relevant standards EN 12975:2006 and ISO 9806-1:1994 (PSE, 2009). The lamps can be individually moved on 2 axes and dimmed, offering the possibility to illuminate test surfaces of different sizes with variable degrees of irradiance intensity and uniformity. Depending on the size of the solar system tested, the irradiance intensity can vary from 700 W/m^2 to 1100 W/m^2, while the uniformity can be up to ± 5%.

As the glass in front of the MHG lamps can reach temperatures of over 100°C during operation, an artificial sky is installed in front of the lampfield in order to eliminate long-wave infrared radiation emitted by the hot lamps to the solar system tested, while emulating sky temperatures. The artificial sky consists of two panes of low-iron glass with an anti-reflection coating, positioned parallel to the lampfield, creating a cavity in between where cold air is circulated in a closed loop and it is cooled down by a water-air heat exchanger.

Convection heat transfer due to wind is an important factor that has to be taken into account every time a solar system is tested. Therefore, a wind emulator unit is mounted on the lower edge of the test platform, creating a uniform airflow, parallel to the surface of the test. Depending on the size of the solar system tested, the air speed can be up to 10 m/s. Finally, a solar air collector testing unit is available to test the performance of PV/T and solar air collectors, under controlled conditions. The unit is equipped with a variable speed centrifugal fan that can be used to test open-loop and closed-loop systems with adjustable (shape and size) inlet and outlet orifices. The air collection rate is controlled automatically for volume flows of up to 900 kg/hr at a 400 Pa pressure drop. The inlet (ambient air) and outlet air temperatures, air collection rate, and pressure drop are measured.

6.1 Experiment Description

A 1.50 m x 1.75 m prototype BIPV/T (Figure 6.2) was built, similar to the JMSB building system, using the same type of UTC and PV modules and tested in the solar simulator under high irradiation and ambient room temperature maintained constant at around 20 ºC. A variable-speed centrifugal fan heats the ambient room air by drawing it through the collector. The irradiated PV modules produce electrical energy, which is measured along with their operating temperatures. Because the only difference between the two setups is the addition of PV modules on the BIPV/T side, their influence can be directly evaluated.

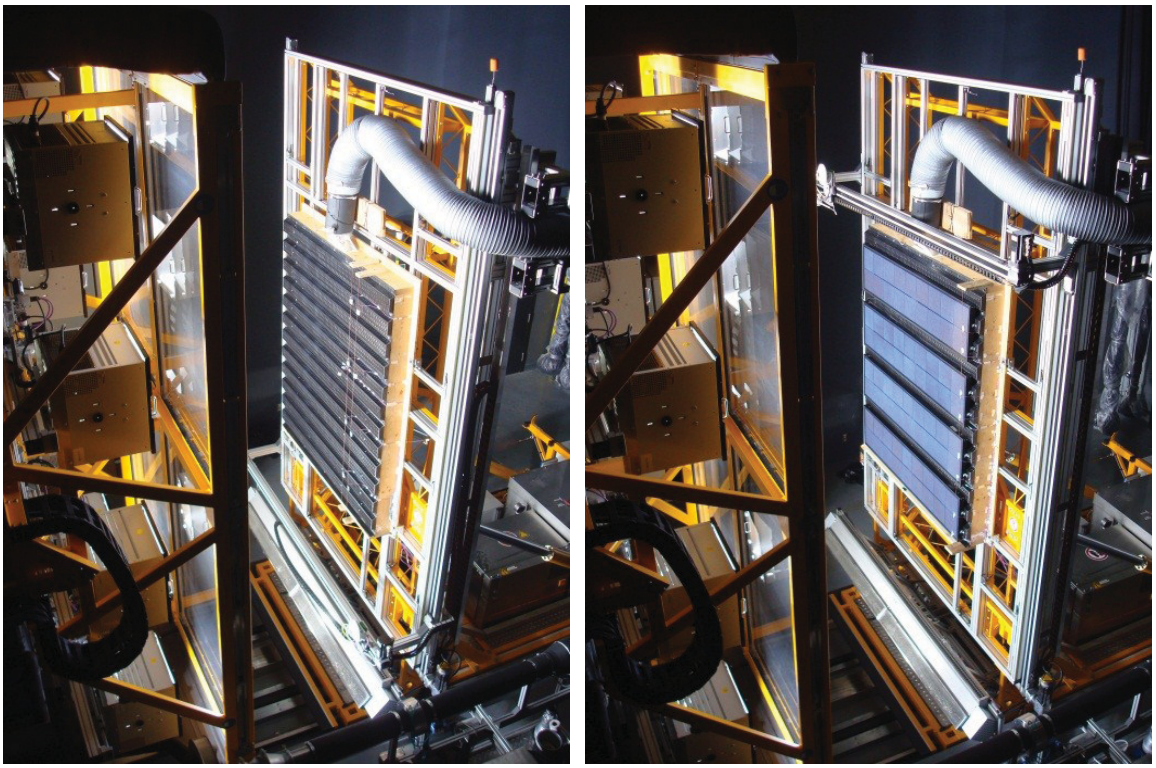

Figure 6.2: Vertical testing of the UTC system in the solar simulator (left). Vertical testing of the BIPV/T system (addition of PV modules) in the solar simulator (right).

The experiment focused on the performance of the two systems under high irradiance and low and high wind conditions (Figure 6.3). A variable-speed controller was used to implement five air collection rates in the experiment: 50, 75, 100, 125, and 150 kg/hr/m². The collector was tested first for the UTC, then four PV modules covering 80% of the UTC area (Apv = 2.1 m²) were added, and the tests were repeated under the same conditions. A 30-minute interval between air collection rates was chosen to ensure that quasi-steady-state conditions were achieved (the time constant of each façade section is about 3 minutes). Unless specified otherwise, the results presented in this chapter are the average of five minutes of data collected (data was recorded every 20 seconds) for each air collection rate, under steady-state conditions.

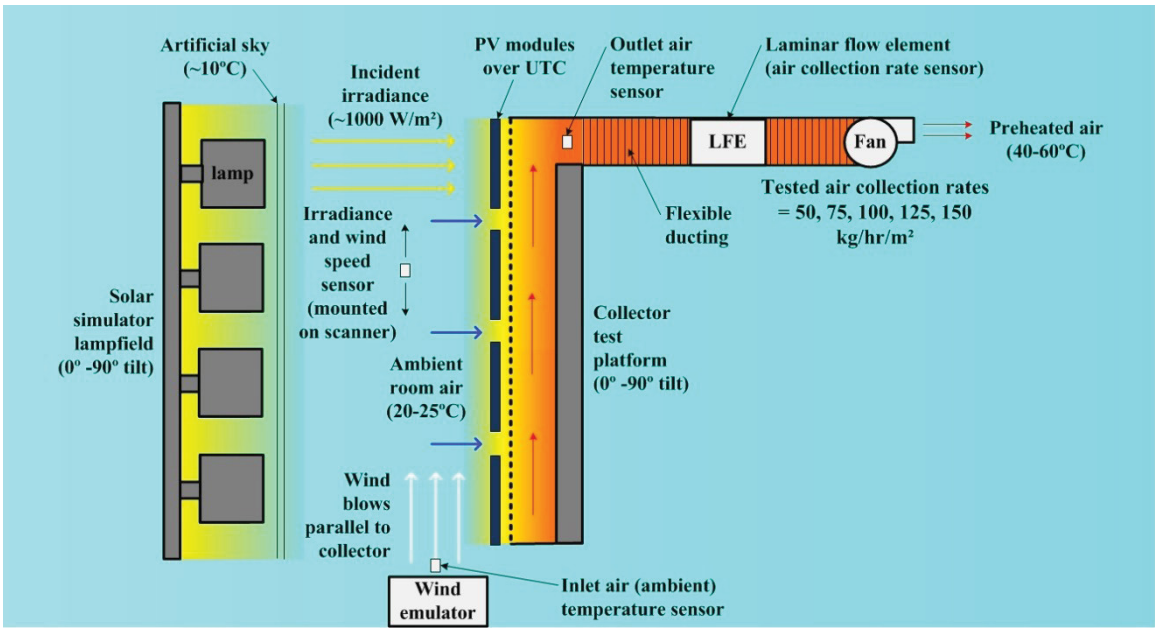

Figure 6.3: Schematic of the experimental BIPV/T system tested in the solar simulator.

The ambient air temperature was measured at the wind emulator outlet. The outlet air temperature was measured using thermocouples placed inside the collector's 150mm-diameter round duct outlet. The thermal resistance of the vertical wall and collector perimeter was 1.76°C·m²/W. In the BIPV/T section, each of the four modules was fitted with two thermocouples distributed along the vertical centerline of each PV backsheet, about one-quarter of the length from the side-frame. As the PV modules are centrally located with respect to the test façade, symmetric temperature distribution about the vertical central axis can be assumed (this was confirmed through infrared thermography). Table 6.1 presents the details of the important measured parameters. The collector area was scanned with an automated pyranometer that was programmed to measure irradiance on a 150 mm grid. The distribution of solar irradiation has 5.5% uniformity, and the average irradiance measured was 1029 W/m² for the UTC experiment and 1034 W/m² for the BIPV/T experiment. The minimum measured irradiance of 984 W/m² was used for

PV energy calculations, as that would likely dictate the string's energy production. The data acquisition system is made up of one CompactRIO by National Instruments. The CompactRIO chassis uses NI 9211 thermocouple input modules to convert the analog voltage signal from the sensor into a digital signal that can be stored. The CompactRIO device was connected to a desktop computer running National Instruments' LabVIEW software. A program running inside LabVIEW was designed to provide a real-time graphical display, to ensure that the experiment was running correctly and to record data on the computer's hard drive.

The electrical energy produced by the four PV modules (wired in series) was consumed by resistors while voltage and current were recorded manually at the end of each test (before the wind speed or air collection rate was changed). The wind emulator blows ambient air upwards and parallel to the collector surface. The height of the wind emulator was adjusted by the PV thickness (38mm) for the PV/T experiment to ensure similar approaching winds. The average parallel winds measured over each collector are provided in Table 6.2, and reported hereafter to be approximately 1 m/s and 3 m/s for the low and high wind conditions, respectively (average of twelve readings taken along the collector height, using a hot wire anemometer located 50 mm away from the surface of the collector). Again, the measurements were taken under high irradiance and they have a margin of error of approximately ± 8%, based on the accuracy of the sensors used in the measurements (Appendix D).

Table 6.1: Summary of important measured values for the solar simulator experiment

Parameter Measured	Instrument	Unit	Accuracy
Outlet Air Temperature	T-Type Thermocouples by Omega	°C	± 0.3°C
PV Module Temperature	T-Type Thermocouples by Omega	°C	± 0.3°C
Airflow Collection Rate	Laminar Flow Element by PSE	kg/hr	± 5% of reading
DC Voltage	Multimeter by Agilent (model U1241B)	V	± 1% of reading
DC Current	Multimeter with clamps by Kyoritsu (model Kew Mate 2000)	A	± 2% of reading
Ambient Air Temperature	T-Type Thermocouples by Omega	°C	± 0.3°C
Solar Irradiance	Pyranometer by PSE mounted on X-Y collector scanner	W/m^2	± 5% of reading
Wind Speed	Hot Wire Anemometer	m/s	± 0.1 m/s + 2% of reading

Table 6.2: Average wind speed measured in the solar simulator

Tested wind conditions	UTC Experiment	BIPV/T Experiment
Low	1.06 m/s	0.83 m/s
High	3.18 m/s	2.69 m/s

6.2 Experimental Results

6.2.1 Thermal performance

Figure 6.4 presents the thermal efficiency obtained in the solar simulator for the UTC collector for the five tested air collection rates and for low wind conditions. The manufacturer's published data is shown for comparison (SolarWall, 2012). The agreement between these separate experiments is reasonable (less than 5%), which demonstrates that experimental testing in the solar simulator laboratory yields precise results that are repeatable, due to the controlled conditions.

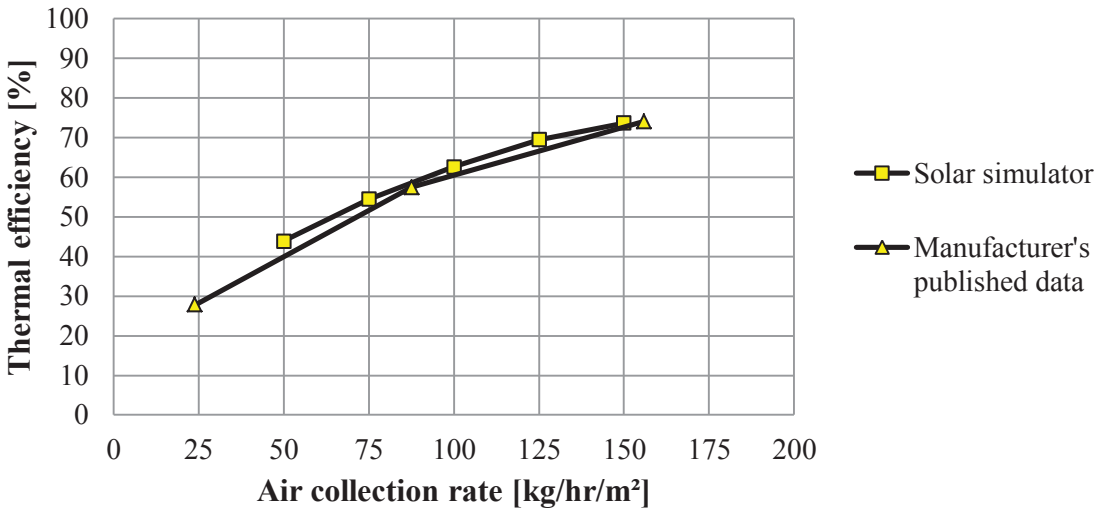

Figure 6.4: Comparison between UTC efficiency and manufacturer's published data.

Unlike experiments conducted outdoors, testing inside the solar simulator laboratory allows one parameter to be changed at a time while the others remain constant, with the same experiment repeated under identical conditions. For example, the solar radiation, wind speed, and ambient air temperature were maintained constant while the air collection rate was gradually decreased from high (150 kg/hr/m²) to low (50 kg/hr/m²). These controlled conditions allowed a straightforward comparison of various collector designs and the selection of optimal configurations. In this study, it was desirable to compare the heat collection capabilities of both the UTC and BIPV/T collectors, so that the impact of the additional PV could be evaluated. In order to compare accurately the heat collected by each solar collector, it was necessary to consider only the solar radiation that could be effectively converted to heat. In the case of the BIPV/T collector, some of the incident solar irradiation was converted into electricity. Therefore, to determine the net energy available for conversion into heat, it was necessary to subtract the electrical

portion from the total. The following equation was used to calculate the adjusted thermal efficiency for the BIPV/T system.

$$\eta_{thermal\_adjusted} = 100 \cdot \left(\frac{Q_{thermal}}{A_{collector} \cdot I_{solar} - E_{PV}} \right) \tag{19}$$

Figure 6.5 presents the thermal efficiency (adjusted for BIPV/T) obtained for both collectors under low (about 1 m/s) and high (about 3 m/s) wind conditions. During low wind conditions, the BIPV/T's thermal efficiency was typically about 5% lower than that of the UTC. For high wind conditions, the difference in thermal performance between both collectors grew from 5% to 10% as the air collection rate increased. This was likely caused by the characteristic heat transfer paths of each collector. In the UTC, increasing the air collection rate breaks up the thermal boundary layer and draws preheated air inside the cavity before the wind can remove it. In the BIPV/T collector, heat is removed from behind the PV modules, which is not as effective as the perforations of the UTC, thus making it more susceptible to heat loss under high winds. The experimental results show that incorporating PV modules onto UTC decreases thermal efficiency by 4–10%. However, the PV modules convert about 12% of the incident solar energy into electricity. The thermal deficit can surely be justified for most applications, as electrical energy carries a higher value than heated air.

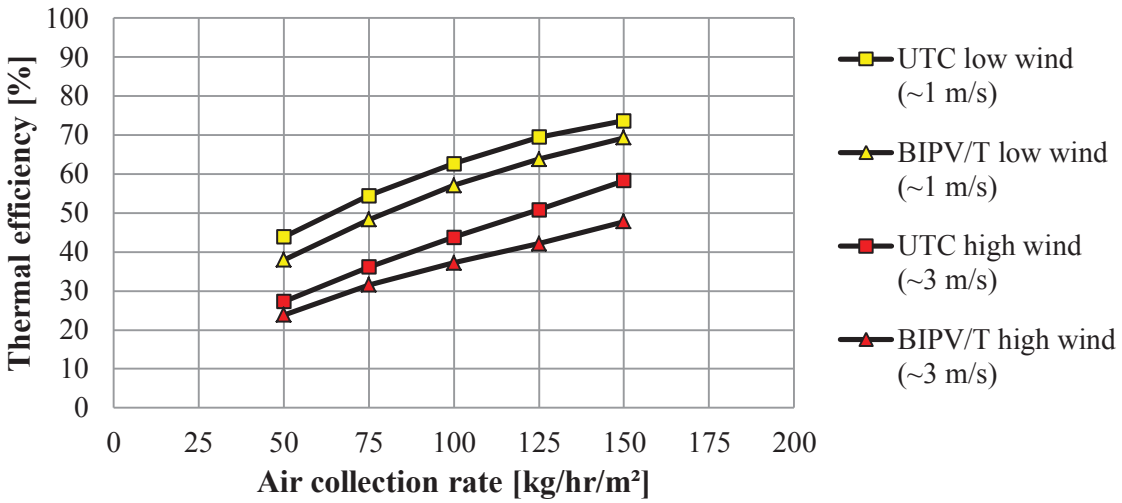

Figure 6.5: Comparison between UTC and adjusted BIPV/T thermal efficiency under low and high wind conditions.

The performance results provided in Figure 6.5 indicate that up to a 30% increase in thermal efficiency can be achieved by increasing the BIPV/T air collection rate from low (50 kg/hr/m²) to high (150 kg/hr/m²). The effect of wind on the collector's performance can be assessed by comparing the efficiency curves for low and high wind conditions at a specific air collection rate. Based on the results, the wind is capable of reducing the BIPV/T system's thermal efficiency by up to 20%. Thus, wind conditions and air collection rate play key roles in predicting system efficiency.

As explained above, the outlet air temperature of the BIPV/T collector is reduced with increasing air collection rate, while thermal efficiency increases. Depending on the application, there is an optimal air collection rate and optimal outlet air temperature. It is often convenient to be able to predict the outlet air temperatures and operating surface temperature of a solar collector, given the combination of incident solar irradiance and exterior air temperature. These parameters can be useful for various purposes, such as selecting optimal fan control strategies to achieve the desired outlet temperature and

estimating energy generation. Because the outlet temperature of BIPV/T collectors is mainly influenced by wind speed, incident solar irradiance, and exterior air temperature, normalization of the results can be achieved by studying the parameter $(T_{outlet}-T_{exterior})/I_{solar}$ as a function of the air collection rate (Figure 6.6).

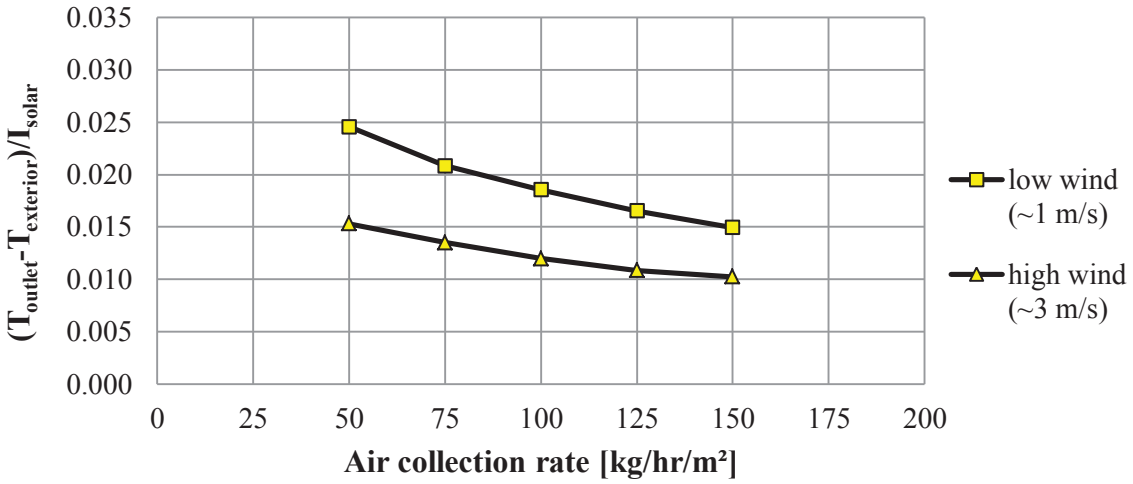

Figure 6.6: BIPV/T system normalized parameter $(T_{outlet}-T_{exterior})/I_{solar}$ as a function of air collection rate under low and high wind conditions.

The BIPV/T collector's outlet temperature, T_{outlet} in ºC, can be estimated using the following equations, which were derived from a second-order polynomial curve fit to the experimental data, presented in Figure 6.6. Note that these equations may be used to estimate the outlet air temperature of the BIPV/T system for low and high winds that are parallel to the collector.

$$T_{outlet\_low\_wind} = T_{exterior} + I_{solar} \cdot \left(5.26 \cdot 10^{-7} \cdot \left(m_{air}\right)^2 - 2 \cdot 10^{-4} \cdot \left(m_{air}\right) + 3.31 \cdot 10^{-2}\right) \quad (20)$$

$$T_{outlet\_high\_wind} = T_{exterior} + I_{solar} \cdot \left(3.22 \cdot 10^{-7} \cdot \left(m_{air}\right)^2 - 1.16 \cdot 10^{-4} \cdot \left(m_{air}\right) + 2.03 \cdot 10^{-2}\right) \quad (21)$$

where

m_{air}, in kg/h·m², is the air collection rate per unit area of collector (50-150 kg/h·m²).

$T_{exterior}$, in °C, is the measured ambient air temperature.

I_{solar}, in W/m², is the incident solar irradiance.

The estimated outlet temperature can be used to find the thermal energy collected and thermal efficiency for the BIPV/T collector by using equations 9 and 11. Such relationships may be obtained from a few measurements for any BIPV/T system during commissioning and used to optimally control the air collection rate.

6.2.2 Electrical performance

The solar simulator experimental setup contains four PV modules wired in series. Figure 6.7 shows how the I–V curve of the PV array is continuous and smooth, and therefore, a proper irradiation distribution was achieved over the collector area. The air collection removes excess heat from the PV modules, and their average surface temperature decreases, resulting in improved electrical performance. This cooling effect was observed to lower the average PV temperature by up to 3ºC and 5ºC at the low (1 m/s) and high (3 m/s) wind speed conditions, respectively. These lower temperatures increase electrical energy production by up to about 5%. The effect of wind on the PV module has a larger cooling effect and is responsible for reducing the PV temperature by up to 15ºC, resulting in a 10% increase in electrical energy production.

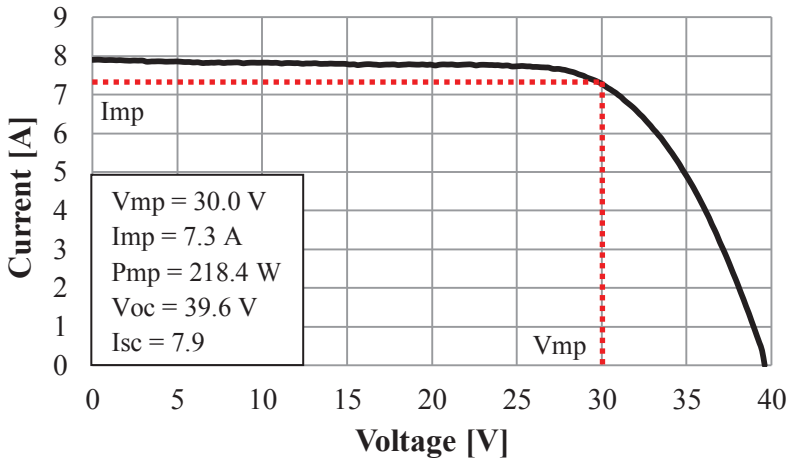

Figure 6.7: I–V curve for the PV array consisting of four PV modules wired in series.

The electrical energy generation of a BIPV/T system is mainly influenced by incident solar irradiance, exterior air temperature, and wind conditions. Normalization of the PV temperature for incident solar irradiance and exterior air temperature can be achieved by studying the parameter $(T_{PV}-T_{exterior})/I_{solar}$ as a function of the air collection rate (Figure 6.8). A second-order polynomial curve fit to normalized data yields the following correlations, which may be used to predict the average PV temperature, T_{PV} in ºC, for low and high winds that are parallel to the collector.

$$T_{PV\_low\_wind} = T_{exterior} + I_{solar} \cdot \left(3.57 \cdot 10^{-7} \cdot (m_{air})^2 - 1.22 \cdot 10^{-4} \cdot (m_{air}) + 5.3 \cdot 10^{-2}\right) \quad (22)$$

$$T_{PV\_high\_wind} = T_{exterior} + I_{solar} \cdot \left(2.51 \cdot 10^{-7} \cdot (m_{air})^2 - 8.09 \cdot 10^{-5} \cdot (m_{air}) + 3.32 \cdot 10^{-2}\right) \quad (23)$$

where

m_{air}, in kg/h·m², is the air collection rate per unit area of collector (50-150 kg/h·m²).

$T_{exterior}$, in °C, is the measured ambient air temperature.

I_{solar}, in W/m², is the incident solar irradiance.

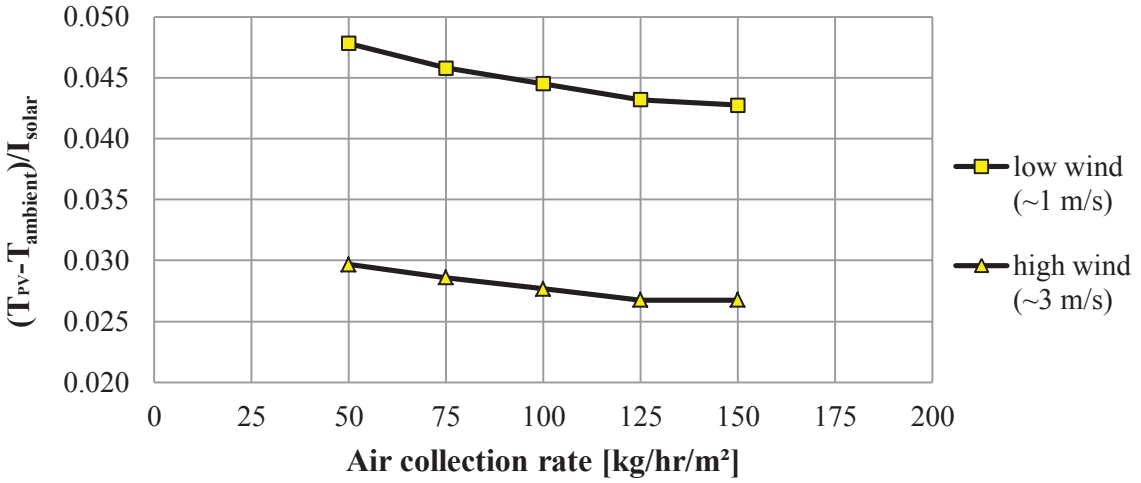

Figure 6.8: BIPV/T system normalized parameter $(T_{PV}-T_{exterior})/I_{solar}$ as a function of air collection rate under high and low wind conditions. (Note: The minimum solar irradiation in distribution and maximum temperature were used; therefore, results are conservative.)

Having calculated the approximate PV operating temperature, the electrical efficiency and energy generated by the PV system can be estimated using equations 15 and 16. Once thermal and electrical energy production of the BIPV/T system has been estimated, the combined efficiency of the BIPV/T collector may be calculated using equation 14.

6.2.3 BIPV/T and UTC comparison

Figure 6.9 compares UTC thermal efficiency and BIPV/T combined (electrical plus thermal) efficiency. Interestingly, it was found that UTC thermal efficiency was almost the same as the combined efficiency of the BIPV/T. For both systems, efficiency varies between 30% and 70%, depending on the combination of air collection rate and wind speed. The lower limit (30%) occurs when the collector experiences high winds (3 m/s) and operates at a low air collection rate (50 kg/h·m²), whereas the upper limit (70%) is achieved with the combination of low winds (1 m/s) and a high air collection rate (150 kg/h·m²). These results indicate that the BIPV/T system has an overall efficiency that is close to that of the UTC, with the added benefit of electrical energy generation.

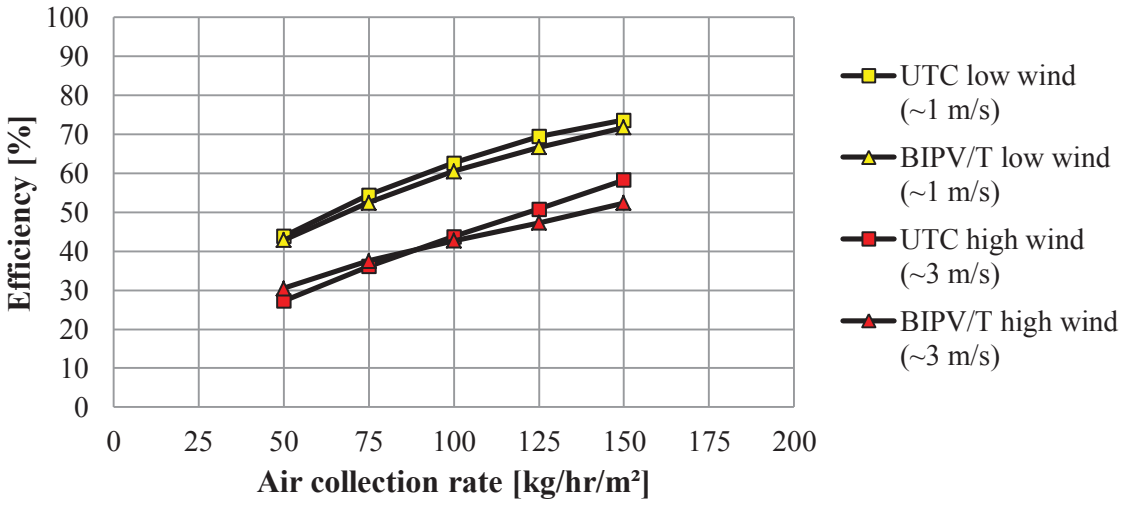

Figure 6.9: UTC thermal and BIPV/T combined efficiency (electrical and thermal) as a function of air collection rate under low and high wind conditions.

7. CONCLUSION

7.1 Summary

The present research aims to reduce the energy footprint of the built environment by turning static building skins into dynamic energy conversion systems. In 2005, the Canadian Natural Sciences and Engineering Research Council approved the creation of the Solar Buildings Research Network (SBRN). A major goal of the SBRN was to develop a building-integrated photovoltaic/thermal (BIPV/T) system that maximizes solar energy conversion and can be easily integrated onto well-oriented building façades and roofs. As the exterior cladding is replaced by the BIPV/T façade, costs associated with traditional building materials can be avoided through architectural integration. The SBRN's team designed a novel BIPV/T system using custom-designed PV modules installed over unglazed transpired collector (UTC), with a suitable mounting system. The main objective of this thesis is to investigate the performance of the developed BIPV/T system with UTC and its integration with the building's envelope and energy systems. Experimental data was collected and analyzed for the following three BIPV/T research projects:

1. Experimental testing of the prototype BIPV/T system in an outdoor research facility. The work of the author consisted mainly of modifying and instrumenting the experimental façade for testing of the prototype BIPV/T system.
2. The developed BIPV/T design concept was applied to a Concordia building as a demonstration project. Large amounts of data have been collected since the construction of the demonstration project, and significant work has been done as

part of this thesis to structure and organize the data into usable forms, in support of this thesis as well as the work of future researchers.

3. Experimental testing of the BIPV/T system under controlled conditions in a new solar simulator- environmental chamber laboratory. The author participated in the commissioning of the new research laboratory and the instrumentation and setup of data acquisition devices for the analysis of the experimental data.

Photovoltaic/thermal systems may be integrated into buildings to form a durable exterior skin while generating significant amounts of renewable electricity and heat onsite. The presented BIPV/T system uses custom-designed PV modules which are installed over the UTC, using an appropriate mounting system. A variable-speed fan creates negative pressure in the air cavity, pulling exterior air through the solar-heated collector and preheating it. The heat may be used within the building for space heating, fed into an air source heat pump to preheat domestic hot water, and/or provide cooling using desiccants. In order to maximize the heat extracted by the integrated PV and UTC technologies, several design strategies were used:

1. Unlike most transpired collector installations, the sheets were installed with the corrugations running horizontally, in order to achieve the following:

    a) Facilitate closing the gap between the upper frame of the PV module and the UTC.

    b) Induce turbulence in the rising air behind the PV modules and increase heat collection compared to vertically oriented UTC corrugations.

2. A major design goal of the PV/T system was to maximize the heat recovered from the PV modules, using the following custom-designed features:

    a) The effective solar absorption of the PV module (including the area between cells) was increased by selecting a black backsheet and frame.

    b) A long and narrow PV module design was selected to reduce the vertical temperature gradient.

The BIPV/T design concept was tested in an outdoor solar testing facility. Two types of PV module configurations were tested, and it was demonstrated that a 33% increase in thermal energy production was achieved by using the custom-designed, narrower, darker modules. The measurement location of the exterior air temperature affects the reported thermal efficiency considerably; therefore, it should be selected carefully for this type of distributed inlet solar collector. The results of the experiments indicate that combined efficiencies of 25–70% (depending on air collection rate) can be achieved using the proposed BIPV/T design. Infrared thermography shows that the UTC effectively cools the PV modules by up to 7°C and, more importantly, maintains favorable PV operating temperatures.

The concept was applied to a full-scale institutional building in Montreal (45°N). The recently completed BIPV/T system demonstrates how a building façade with good solar exposure in a densely built-up urban centre can be constructed as an active energy-generating component of the building envelope. The 288 m² system replaces the building envelope of the near-south-facing façade of the mechanical room, where proximity to the fresh air intake reduces the need to build long ducts from the façade to the HVAC

system. It utilizes 384 building-integrated PV modules (the same modules used in the prototype) connected to five inverters. The aesthetic integration of the solar façade with the building architecture is an important design criterion, and it was achieved, in part, by designing custom dark-coloured PV modules of the same width as the glazed curtain wall sections below. Measured combined efficiencies (thermal plus electrical) between 37% and 55% (varies mainly with the wind speed) show the potential of this technology for converting incident solar energy into high-grade electricity and thermal heat for use within the building. In addition, it provides engineers and architects with a working example of what can be achieved. Moreover, it stimulates a shift in the way we design buildings, converting the walls and roofs of buildings into electricity-and-heat-generating surfaces instead of passive components that lose heat in winter and gain heat in summer. The active façade collects 55 MWh of renewable solar heat as preheated fresh air during times of peak demand, ideal for applications where there is a significant need for heating in winter. In addition, 20 MWh of solar electricity are generated and consumed onsite annually.

An experimental mock-up UTC and BIPV/T system was built and tested in a solar simulator under high irradiation and ambient room temperature maintained constant at around 20ºC. As the only difference between the two setups was the addition of PV modules on the BIPV/T side, their influence could be directly evaluated. The experimental results show that incorporating PV modules onto UTC decreased the thermal efficiency by 4–10%. However, the polycrystalline silicone PV modules also converted about 12% of the incident solar energy into electrical energy. The thermal deficit can surely be justified for most applications, as electrical power carries a higher

value than heated air. The combined efficiency of the experimental BIPV/T system was found to be in the range of 30–70% for the tested conditions. The lower limit (30%) occurs when the collector experiences high winds and operates under low air collection (50 kg/hr·m²), whereas the upper limit (70%) is achieved when there are low winds and high air collection (150 kg/hr·m²). It was found that the effect of wind on these open-loop collectors possibly reduces net overall system efficiency by up to 20%. Design correlations developed for predicting the performance of the BIPV/T system may be used for the design of similar systems in new buildings or for retrofit.

7.2 Recommendations for Future Work

This research has advanced the design and development of innovative BIPV/T technology and demonstrated its use as a fully integrated, active component of the building envelope. Significant potential exists for improving the design and integrated energy concepts of BIPV/T systems. One possibility of increasing the efficiency of the transpired collector in removing the excess PV module heat is to lower the profile of the module. A lower profile would decrease the space between the PV module and the UTC, effectively increasing the convective heat transfer, due to higher air velocities in the airspace. Another solution, which would eliminate the need for low profile modules, is to construct PV modules (or PV sheets of cladding) that are porous, making the PV module a transpired collector. This would surely improve the efficiency of the collector; however, the increased cost of developing such a collector, weighed against the benefits, would have to be considered. Collaboration with Dr. Panagiota Karava from Purdue University has provided significant insights into the wind effects on BIPV/T collectors. Further investigation through modelling using computational fluid dynamics would provide

valuable information for the optimization of future systems, including wind effects. Moreover, the integration of BIPV/T technology with other building energy systems can provide significantly higher overall energy output by using, for example, heat pumps to upgrade the solar-heated air for domestic hot water uses.

Significant lessons have been learned throughout the design, construction, and operation of these projects. It is certain that future projects will be less expensive, for this reason alone. BIPV/T concepts can be optimally incorporated during the early design stage, when the form of the building is being decided on, along with the location of the mechanical room, with its HVAC and electrical system. The essential elements for an optimal design are optimal orientation, proximity to the mechanical room, and proper integration with the HVAC and other energy systems. However, retrofit applications are also possible, with a new, active façade constructed over an existing one.

Approaches such as prefabrication will also help to reduce costs, by taking advantage of economies of scale, standardization, and optimization of manufacturing processes. For example, major reductions in costs may be achieved by adopting curtain wall technology, where two-to-three-storey-high modular BIPV/T sections come with whole PV strings installed and prewired in a factory environment, similar to the one used to build the ÉcoTerra BIPV/T roof module. Figure 7.1 illustrates this concept, wherein prefabricated modules can be installed vertically or horizontally. Furthermore, technologies are continuously advancing, and prices are dropping. As more industry partners become experienced in supplying and installing these systems, labour costs will also drop.

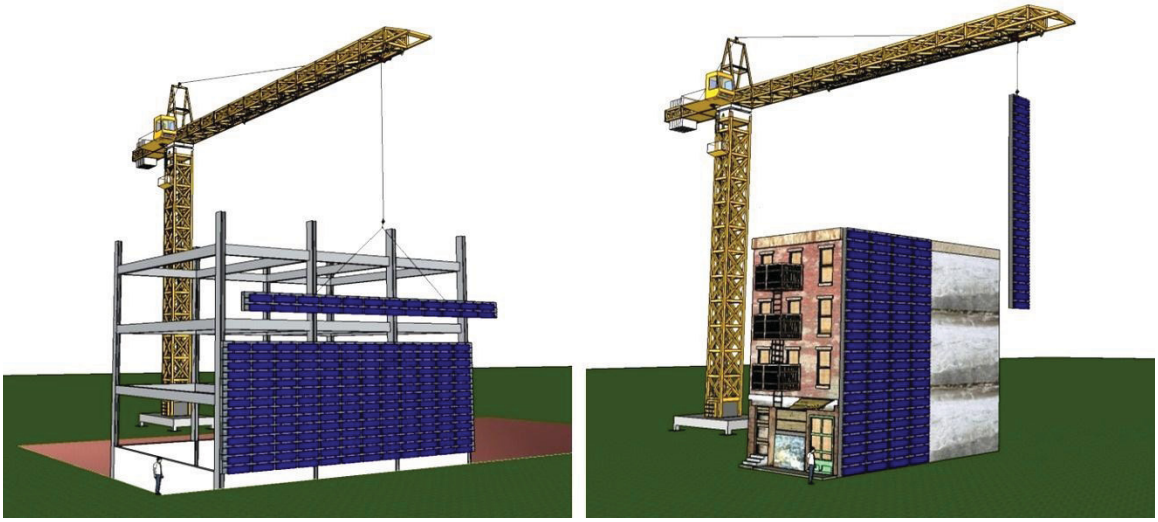

Figure 7.1: Installation of horizontal prefabricated BIPV/T modules for new construction (left). Retrofit of an old building façade using vertical prefabricated BIPV/T modules (right).

The results of this research show that BIPV/T collectors can effectively reduce the energy needs of the built environment, while providing a durable building façade. The full-scale BIPV/T demonstration project is a good example of how well-oriented building façades can be used to convert about 50% of incident solar energy into large amounts of renewable electricity (55 MWh) and heat (22 MWh) for use within the building annually. The BIPV/T system integrates two existing solar technologies and is not overly time consuming or complex to install, making it an appropriate design for use on the energy efficient infrastructure of tomorrow. Some challenges that were faced in the research and demonstration of the project include the fragmentation of the building industry and the need to educate architects and engineers regarding the new technologies. The design of appropriate incentives and policies should help accelerate the deployment of building-integrated solar collectors and contribute to the long-term reduction in costs by helping the industry grow.

REFERENCES

ASHRAE, 2009. ASHRAE Handbook of Fundamentals, American Society of Heating, Refrigerating and Air-Conditioning Engineers, Atlanta, GA, USA.

Athienitis, A.K., 2008. Design of Advanced Solar Homes Aimed at Net-Zero Annual Energy Consumption in Canada. ISES-AP – 3rd International Solar Energy Society Conference – Asia Pacific Region. Incorporating the 46th ANZSES Conference. November 2008. Sydney, Australia.

Athienitis A.K., Bambara J., O'Neill B., Faille J., 2011. A prototype photovoltaic/thermal system integrated with transpired collector. Solar Energy, 85(1), 139–153.

Augustus Leon, M. and Kumar, S., 2007. Mathematical modeling and thermal performance analysis of unglazed transpired solar collectors. Solar Energy 81:62–75.

Bakker, M., Zondag, H.A., Elswijk, M.J., Strootman, K.J., Jong, M.J.M., 2005. Performance and costs of a roof-sized PV/thermal array combined with a ground coupled heat pump, ISES Solar World Congress. Solar Energy 78(2), 331–339.

Bazilian M.D., Leenders F., Van Der Ree B. and Prasad D., 2001. Photovoltaic cogeneration in the built environment. Solar Energy 71(1), 57-69.

Benagli, S., Borrello, D., Vallat-Sauvain, E., Meier, J., Kroll, U., Hoetzel, J. Bailat, J., Steinhauser, J., Marmelo, M., and Castens, L., 2009. High-Efficiency Amorphous Silicon Devices on LPCVD-ZnO40 TCO Prepared in Industrial KaiTM-M R&D Reactor. In: Proceedings of the 24th European Photovoltaic Solar Energy Conference, Hamburg, Germany, p. 2293.

Bloomberg New Energy Finance - Renewable Energy Data. Available at: http://bnef.com/, viewed August, 2012.

Candanedo L.M., Athienitis A.K, Candanedo J.A., O'Brien W., Chen Y., 2010. Transient and Steady State Models for Open-Loop Air-Based BIPV/T Systems. American Society of Heating, Refrigerating and Air-Conditioning Engineers. Transactions 2010, Vol. 116, Part 1, 600–612.

Candanedo, J. A. and Athienitis, A.K., 2010. A simulation study of anticipatory control strategies in a net zero energy solar-optimized house. ASHRAE Trans., 116(1), 246–260.

Candanedo, J.A. and Athienitis, A.K., 2011. Predictive control of radiant floor heating and solar-source heat pump operation in a solar house. HVAC & R Research 17(3), 235–256.

Charron R. and Athienitis A.K., 2006. Optimization of the performance of double-façades with integrated photovoltaic panels and motorized blinds. Solar Energy 80(5), 482–491.

Chow T.T., He W., Ji J., 2007.An experimental study of facade-integrated photovoltaic/ water-heating system. Applied Thermal Engineering, 27, 37–45.

Chow T.T., 2010. A review on photovoltaic/thermal hybrid solar technology. Applied Energy 87(2), 365–379.

Corbin C.D. and Zhai Z.J., 2010. Experimental and numerical investigation on thermal and electrical performance of a building integrated photovoltaic–thermal collector system. Energy and Buildings 42: 76–82.

Coventry J.S. and Lovegrove K., 2003. Development of an approach to compare the 'value' of electric and thermal output from a domestic PV/thermal system. Solar Energy, 75(1), 63–72.

Enerconcept. Available at: http://www.enerconcept.com/en/solar-air-heating-products/lubi/, viewed August 2012.

EPIA (the European Photovoltaic Industry Association), Available at: http://www.epia.org/solar-pv/pv-technologies-cells-and-modules.html, viewed August, 2012.

EPIA (the European Photovoltaic Industry Association) Sunrise project, Montoro D. F., Vanbuggenhout P., Ciesielska J., Building integrated Photovoltaics: An overview of the existing products and their fields of application, March 2011.

ESTTP (European Solar Thermal Technology Platform), 2008. Solar Heating and Cooling for a Sustainable Energy Future in Europe - Strategic Research Agenda. European Solar Thermal Technology Platform (ESTTP) Secretariat, Brussels, Belgium.

Delisle V. and Collins, M.R., 2007. PVT unglazed corrugated transpired solar collector model. Canadian Solar Buildings Conference, June 2007, Calgary, Canada.

Duffie, J.A. and Beckman, W.A., 2006. Solar Engineering of Thermal Processes. John Wiley & Sons, Hoboken, New Jersey.

Dymond, C. and Kutscher C.F., 1997. Development of a flow distribution and design model for transpired solar collectors, Solar Energy, 60(5), 291–300.

Fleck, B.A., Meier, R.M., Matovic, M.D., 2002. A Field Study of the Wind Effects on the Performance of an Unglazed Transpired Solar Collector. Solar Energy, 73(3), 209–216.

Gajbert H., 2008. Solar thermal energy systems for building integration, Licentiate thesis, Lund University, Faculty of Engineering LTH, Report EBD-T-08/10.

Gawlik, K.M., and Kutscher C., 2002. Wind Heat Loss from Corrugated, Transpired Solar Collectors. Transactions of the ASME 124(3), 256–261.

Gawlik, G., Christensen C., and Kutscher C., 2005. A Numerical and Experimental Investigation of Low-Conductivity Unglazed, Transpired Solar Air Heaters. Journal of Solar Energy Engineering Transactions of the ASME, 127(1), 153–155.

German Energy Society, 2008. Planning and installing photovoltaic systems: A guide for installers, architects, and engineers.

Green, M.A., Emery, K., Hishikawa, Y., and Warta, W., 2010: Solar efficiency tables.

Guiavarch A. and Peuportier B., 2006. Photovoltaic collectors efficiency according to their integration in buildings. Solar Energy, 80(1), 65–77.

Gunnewiek, L.H., Hollands, K.G.T., and Brundrett, E., 2002. Effect of Wind on Flow Distribution in Unglazed Transpired-Plate Collectors. Solar Energy, 72(4), 317–325.

Hasan A., McCormack, S.J., Huang, M.J., and Norton, B., 2010. Evaluation of phase change materials for thermal regulation enhancement of building integrated photovoltaics. Solar Energy, 84(9), 1601–1612.

IEA (International Energy Agency). Available at: http://www.iea-shc.org/task40/, viewed August, 2012.

Hollick J. C., 1994. Unglazed solar wall air heaters. Renewable Energy 5, 415–421.

Hollick, J.C., 1998. Solar Cogeneration Panels. Renewable Energy 15 (1-4), 195-200.

Iron workers local. Available at: http://www.ironworkerslocal404.org/sub/solarwall_1, viewed August, 2012.

Ito, S., Matsubayashi, T., Miura, N., 2004, Studies of a heat pump using dual heat sources of solar heat and ambient air, Eurosun 2004, Freiburg.

Konarka. Available at: http://www.konarka.com/, viewed August, 2012.

Kumar R. and Rosen M.A., 2011. A critical review of photovoltaic–thermal solar collectors for air heating. Applied Energy, 88, 3603–3614.

Kutscher, C.F., Christensen, C., and Barker, G., 1993. Unglazed transpired solar collectors: heat loss theory. ASME Journal of Solar Engineering, 115(3), 182–188.

Liao L., Athienitis A.K., Candanedo L. and Park K.W., 2007. Numerical and experimental study of heat transfer in a BIPV-thermal system. ASME Journal of Solar Engineering, 129(4), 423–430.

National Climate Data and Information Archive. Available at: http://climate.weatheroffice.gc.ca/climateData/StationResults_e.html?timeframe=1&Prov=XX&StationID=5415&Year=2012&Month=7&Day=28, viewed August 2012.

Natural Resources Canada, Office of Energy Efficiency. Comprehensive Energy Use Database. Available at: http://oee.nrcan.gc.ca/corporate/statistics/neud/dpa/comprehensive_tables/list.cfm, viewed August, 2012.

Naveed, A.T., Kang, E.C., and Lee, E.J., 2006. Effect of Unglazed Transpired Collector on the Performance of a Polycrystalline Silicon Photovoltaic Module. Journal of Solar Engineering, Transactions of the ASME 128, 349–353.

Norton, B., Eames, P.C., Mallick, T.K, Huang, M.J., McCormack, S.J., Mondol, J.D., Yigzaw, G., Yohanis, Y.G., 2010. Enhancing the performance of building integrated photovoltaics. Solar Energy, 85(8), 1629–1664.

Pesaran A.A and Wipke K., 1992, Desiccant Cooling using unglazed transpired solar collectors, National Renewable Energy Laboratory (NREL/TP-432-4827).

Prakash J., 1994.Transient analysis of a photovoltaic-thermal solar collector for cogenerationof electricity and hot/air water. Energy Convers Manage, 35, 967–972.

PRES (Pakistan Renewable Energy Society). Available at: http://www.pres.org.pk/category/re-technologies/solar-energy/, viewed August, 2012.

Probst M.M. and Roecker, C., 2007. Towards an improved architectural quality of building integrated solar thermal systems. Solar Energy, 81(9), 1104–1116.

PSE (Projects in Solar Energy), 2009. Indoor Test Stand for Solar Thermal Collectors – Technical Description. Freiburg, Germany.

PV/T Roadmap, 2004. Available at: http://www.pvtforum.org/pvtroadmap.pdf, viewed August, 2012.

Skoplaki E. and Palyvos J.A., 2009. On the temperature dependence of photovoltaic module electrical performance. A review of efficiency/power correlations. Solar Energy, 83(5), 614–624.

Solar Generation V - Solar electricity for over one billion people and two million jobs by 2020, European Photovoltaic Industry Association/Greenpeace, 2008. The Netherlands/Belgium.

SolarWall. Available at: http://solarwall.com/en/home.php, viewed August, 2012.

Solimpeks. Available at: http://solimpeks.com, viewed August, 2012.

Tiwari, G.N. and Ghosal, M.K. Renewable energy resources, basic principle and applications. Middlesex: Alpha Science International; 2005.

Tonui, J. K. and Tripanagnostopoulos, Y., 2007. Improved PV/T solar collectors with heat extraction by forced or natural air circulation. Renewable Energy, 32(4), 623–637.

Tripanagnostopoulos, Y., Nousia, T., Souliotis, M. and Yianoulis, P., 2002. Hybrid Photovoltaic/Thermal solar systems, Solar Energy, 72(3), 217–234.

Van Decker, G.W.E., Hollands, K.G.T., Brunger, A.P., 2001. Heat-exchange relations for unglazed transpired solar collectors with circular holes on a square or triangular pitch. Solar Energy, 71(1), 33–45.

Visionwall. Available at: http://www.visionwall.com/res/pdf/GOCB.pdf, viewed August, 2012.

Uni-Solar. Available at: http://www.uni-solar.com/, viewed August, 2012.

Wiser, R., Barbose, G., Peterman, C., 2009. Tracking the Sun: The Installed Cost of Photovoltaics in the U.S. from 1998-2007. Lawrence Berkeley National Laboratory, 42pp.

APPENDIX A: UTC Manufacturer's Specifications

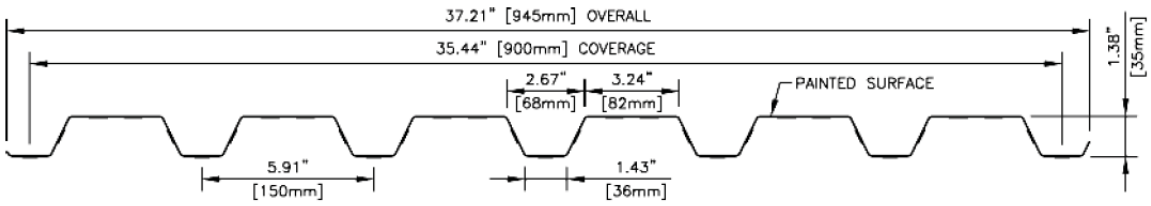

SW150

COLOR OPTIONS AND SOLAR ABSORPTIVITY VALUES

Color name	Absorptivity	Color name	Absorptivity
Black	0.95	Tile Red	0.69
LSR Dark Brown	0.94	Tan	0.67
Dark Green	0.91	Bright Red	0.67
Heron Blue	0.90	Regent Grey	0.64
Royal Blue	0.78	Stone Grey	0.58
Deep Water Green	0.78	Bone White	0.52
Dark Brown	0.76	White White	0.45
Green	0.75	Antique Linen	0.44
Metro Brown	0.74	Ivory	0.42
Slate Blue	0.73	Cambridge White	0.38
Pacific Turquoise	0.73	Gold	N/A
Charcoal	0.72	Navy Blue	N/A

1. Product Name

SolarWall® Solar Air Heating System

E-mail: info@solarwall.com
www.solarwall.com

2. Manufacturer

Conserval Systems, Inc.
4242 Ridge Lea Road, Suite 28
Buffalo, NY 14226
(716) 835-4903
Fax: (716) 835-4904

For Canada:
Conserval Engineering, Inc.
200 Wildcat Road
Toronto, Ontario M3J 2N5
Canada
(416) 661-7057
Fax: (416) 661-7146

APPENDIX B: PV Manufacturer's Specifications

Day4 Energy Inc.
www.day4energy.com

Anodized Aluminum Frame

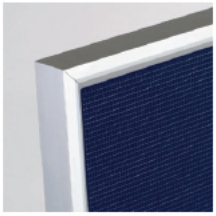

- Water drainage holes to reduce frame breakage due to freezing temperatures
- Multiple grounding holes for ease of installation
- Beveled top profile to reduce dirt and water trapping
- Deep glass frame slot for increased strength and durability

Short Circuit Current Temp. Coefficient (175W)	2.67mA/K
Open Circuit Voltage Temp. Coefficient (175W)	-0.10V/K
Max. Power Temp. Coefficient (175W)	-0.44%/K
Module Power Tolerance	± 3.5%
Module Maximum Fuse Series Amps	15A
Reduction of Efficiency (from 1000 W/m² to 200 W/m²)	<4%
Normal Operating Cell Temperature (NOCT)	46.9°C
Maximum System Voltage	UL: 600V, IEC: 1000V

Mechanical Specifications	
Cells	48 cells, multicrystalline silicon, 156mm square (6+ inches)
Glass	Solar glass (tempered)
Junction Box	Tyco Solarlok Interconnection, output cables, male and female locking cable couplers, other connectors upon request (subject to certification)
Back Sheet	Multi-layer water resistant film compound

Typical Electrical Performance at STC (1000 W/m², AM 1.5 Spectrum, cell temperature 25°C)

Peak Power (Wp)	Watts	160	165	170	175	180	185	190
Max. Power Voltage (Vmp)	Volts	22.60	22.95	23.04	23.40	23.70	23.82	24.00
Max. Power Current (Imp)	Amps	7.08	7.19	7.38	7.48	7.60	7.77	7.92
Open Circuit Voltage (Voc)	Volts	28.30	28.6	28.80	29.20	29.40	29.51	29.70
Short Circuit Current (Isc)	Amps	7.70	7.80	7.90	8.05	8.10	8.20	8.30

Typical Electrical Performance (800 W/m², AM 1.5 Spectrum, cell temperature 25°C)

Peak Power (Wp)	Watts	160	165	170	175	180	185	190
Max. Power Voltage (Vmp)	Volts	22.46	23.02	23.39	23.58	23.84	23.71	23.89
Max. Power Current (Imp)	Amps	5.84	5.77	5.92	6.01	6.09	6.29	6.41
Open Circuit Voltage (Voc)	Volts	28.04	28.25	28.58	28.97	29.10	29.22	29.41
Short Circuit Current (Isc)	Amps	6.23	6.27	6.36	6.48	6.52	6.59	6.67

Day4 48MC 175W

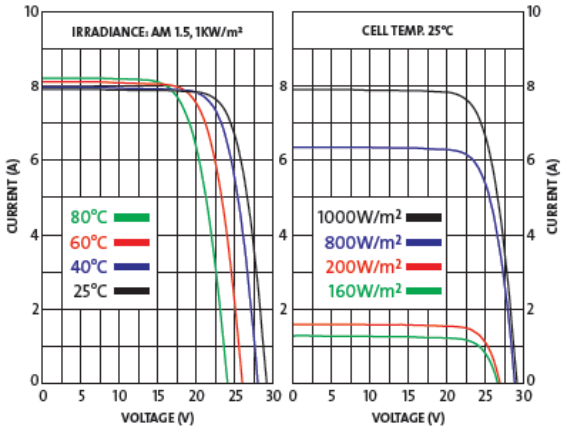

Module Diagram

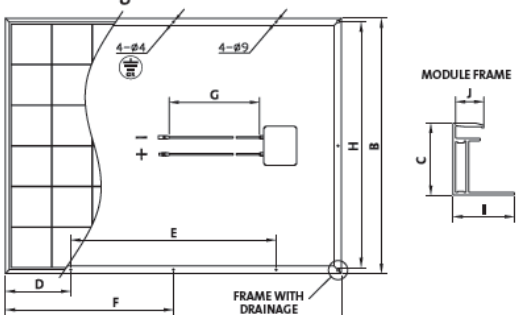

Qualification Test Parameters	
Temperature Cycling Range	-40°C to +90°C (-40°F to 194°F)
Humidity Freeze	85% rH, -40°C to +85°C (-40°F to 185°F)
Static Load Front And Back	UL: 1436pa (30lbs/ft²), IEC: 2400N/m²
Front Loading (eg. Snow)	UL: 1436pa (30lbs/ft²), IEC: 5400N/m²
Fire Class	C
Corrosive Atmosphere Test	pass
Protection Classification	IP 65

APPENDIX C: PV String and Array Electrical Details

Array	String	String Vmp* [V]	String Imp* [A]	Sub-array Vmp [V]	Sub-array Imp [A]	Array Vmp [V]	Array Imp [A]	Array Pmp [W]
A	1	85.80	7.3	344.0	7.0	344.0	14.1	**4850**
	2	86.26	7.3					
	3	85.80	7.3					
	4	86.13	7.0					
	5	86.32	7.2	346.4	7.1			
	6	86.62	7.3					
	7	86.81	7.1					
	8	86.69	7.1					
B	1	87.34	7.2	349.9	7.2	349.9	14.3	**5004**
	2	87.45	7.2					
	3	87.53	7.2					
	4	87.61	7.3					
	5	87.58	7.2	350.8	7.2			
	6	87.65	7.2					
	7	87.69	7.2					
	8	87.87	7.2					
C	1	87.02	7.3	346.9	7.2	346.9	14.4	**4995**
	2	86.32	7.3					
	3	87.18	7.2					
	4	86.38	7.4					
	5	87.03	7.3	349.1	7.1			
	6	87.34	7.1					
	7	87.37	7.2					
	8	87.37	7.2					
D	1	87.63	7.2	351.1	7.2	351.1	14.3	**5021**
	2	87.72	7.2					
	3	87.88	7.2					
	4	87.89	7.3					
	5	87.86	7.2	351.7	7.1			
	6	87.82	7.3					
	7	88.06	7.3					
	8	87.95	7.1					
E	1	79.68	7.5	236.9	7.4	236.9	14.8	**3506**
	2	78.78	7.6					
	3	78.40	7.4					
	4	79.09	7.4	236.9	7.4			
	5	79.21	7.4					
	6	78.62	7.4					
	7	78.56	7.4	Only used by experimental inverter				
*mp = maximum power and occurs under standard test conditions (i.e., solar irradiation = 1000 W/m², PV temperature = 25°C)						**Total Pmp [W]**		**23376**

APPENDIX D: Measurement Uncertainty Calculations

The main parameters affecting the uncertainty of thermal, electrical and combined efficiency are the air collection rate, air temperature and solar irradiance sensors. Assuming that the collector area and the specific heat of air are constant and measured more accurately, the uncertainty of thermal energy production is given by

$$\Delta Q_{thermal} = \sqrt{\left(\left(\frac{\Delta T}{\Delta T_{rise}}\right)^2 + (\Delta m_{air})^2\right)} = \sqrt{\left(\left(\frac{\sqrt{0.3^2 + 0.3^2}}{20}\right)^2 + (0.05)^2\right)} = 5.4\%$$

Where ΔT_{rise} is the typical temperature rise of 20ºC.

The uncertainty of thermal efficiency is given by

$$\Delta \eta_{thermal} = \sqrt{\left((\Delta Q_{thermsl})^2 + (\Delta I_{solar})^2\right)} = \sqrt{\left((0.054)^2 + (0.05)^2\right)} = 7.4\%$$

The uncertainty of the reported thermal efficiency is approximately 8%.

The uncertainty for the PV electrical power production is given by

$$\Delta E_{PV} = \sqrt{\left((\Delta I_{PV})^2 \cdot (\Delta V_{PV})^2\right)} = \sqrt{\left((0.02)^2 \cdot (0.01)^2\right)} = 2.2\%$$

The uncertainty for the PV electrical efficiency, $\Delta\eta_{electrical}$, is given by

$$\Delta \eta_{electrical} = \sqrt{\left((\Delta E_{PV})^2 + (\Delta I_{solar})^2\right)} = \sqrt{\left((0.022)^2 + (0.05)^2\right)} = 5.5\%$$

The uncertainty of the reported PV electrical efficiency is approximately 6%.

The uncertainty for the combined thermal and electrical production is given by

$$\Delta Combined = \sqrt{\left((\Delta Q_{thermal})^2 + (\Delta E_{PV})^2\right)} = \sqrt{\left((0.054)^2 + (0.022)^2\right)} = 5.8\%$$

The uncertainly of the combined efficiency, $\Delta\eta_{combined}$, is given by

$$\Delta \eta_{combined} = \sqrt{\left((\Delta Combined)^2 + (\Delta I_{solar})^2\right)} = \sqrt{\left((0.058)^2 + (0.05)^2\right)} = 7.7\%$$

The uncertainty of the reported combined efficiency is approximately 8%.